Roskilde University,
Department of Science, Systems and Models, IMFUFA
P.O. Box 260, DK - 4000 Roskilde
Tel: 4674 2263 Fax: 4674 3020

Testing predictions of the isomorph theory by experiment

By: Ditte Gundermann
IMFUFA tekst nr. 491/ 2013 – 106 sider – ISSN: 0106-6242

The overall theme of the present PhD thesis is an experimental approach to the concept of strongly correlating liquids and isomorphs. Three theoretical predictions are treated:

1) The identity between the density scaling exponent γ_{scale} and the fluctuation exponent γ_{isom} (chapter 6). It is shown how the fluctuation exponent can be determined through linear-response measurements. By such measurements on a van der Waals bonded liquid, tetramethyl-tetraphenyl-trisiloxane (DC704), the resulting value of γ_{isom} is compared to the value of γ_{scale} found from high-pressure dielectric measurements. The results show that the two values for the exponent agrees well, which implies that strongly correlating liquids exist. These liquids can be viewed as a class of simple liquids.

2) The state-point dependence of the density-scaling exponent (chapter 7). Data sets for two liquids, DC704 and polyphenylether (5PPE), are examined with respect to the temperature and density dependence of the density-scaling exponent. The density range for the data turns out to be too small to draw a conclusion on the matter.

3) The aging properties of strongly correlating liquids (chapter 8). An idea for testing the predicted and in computer simulations observed aging properties of strongly correlating liquids is presented (chapter 8), along with some experimental challenges involved with the experiment. The experiment is to be carried out in a new setup for high-pressure dielectric spectroscopy. A detailed description of the setup is given and the main challenges involved with the implementation, in particular in relation to the proposed experiment, are described.

Furhtermore, a set of data on the frequency dependent adiabatic bulk modulus for two molecular liquids, trimethyl-pentaphenyl-trisiloxane (DC705) and dibuthyl phtalate (DBP), are presented and analyzed in terms of relaxation time, time-temperature-superposition (TTS) and high-frequency slope of the alpha relaxation (chapter 3). The bulk modulus measurements are one of the four frequency-dependent response functions used to calculate γ_{isom}.

Testing predictions of the isomorph theory by experiment

Revised PhD thesis

Ditte Gundermann

Supervisor: Kristine Niss

Danish National Research Foundation Centre "Glass and Time",
IMFUFA, Department of Science, Systems, and Models,
Roskilde University, Denmark
January 2013

Acknowledgements

This work has benefited from the help and support from a number of people whom I wish to thank.

First of all I am extremely greatful for the help and encouragement, both mentally and scientific, I have recieved from my supervisor Kristine Niss. I also want to thank Tage Christensen as my supervisor in the first part of my PhD period, and for his willingness and ability to engage in various both theoretical and experimental issues. Next I wish to thank Jeppe Dyre for giving me the opportunity to be a PhD student in the "Glass and Time". It has been a great pleasure being part of such a big group of inspiring people. In particular I would like to thank Tina Hecksher for help in many aspects and good company, and Ulf Pedersen for our fruitful collaboration on the $\gamma_{isom} = \gamma_{scale}$ project.

The technical staff at IMFUFA, Ebbe H. Larsen, Torben Rasmussen, Preben Olsen, Ib Høst Pedersen has made a significant contribution to the implementation and setup of the high pressure dielectric equipment. In particular I wish to thank Ib Høst Pedersen for saving me a lot of time and trouble on many occasions. I also wish to thank Heine Larsen for valuable IT-support. In addition I would like to thank Dorthe Vedel for always being available and for help with various practical issues.

My visit at Mike Rolands group at the Naval Research laboratory made a great impact on me, and I am greatful for the hospitality I met, and for the experience with high pressure measurements that I gained. I enjoyed the company of Riccardo Casalini and Daniel Fragiadakis and our discussions on both science and politics.

During both the implementation of the high pressure setup and the development of the idea for the aging-experiment, I have benefited from several discussions with Simone Capaccioli. Moreover I would like to thank the committee for valuable comments and critique.

Finally I am greatful to my family for their moral support and understanding.

Dedicated to my father Jesper Gundermann

Dansk abstract

Det overordnede tema for denne Ph.D.-afhandling er en eksperimentel tilgang til "stærkt korrelerede væsker" (strongly correlating liquids) og deres "isomorfer". Tre teoretiske forudsigelser er behandlet:

1) Ækvivalensen mellem densitetsskalleingseksponenten γ_{scale} og fluktuationseksponenten γ_{isom} (kapitel 6). Det vises hvorledes fluktuationseksponenten kan bestemmes ved hjælp af lineær response-målinger. Ved hjælp af disse målinger på en van der Waals væske, tetramethyl-tetraphenyl-trisiloxane (DC704), sammenlignes værdien for γ_{isom} med værdien for γ_{scale} opnået ved hjælp af dielektriske målinger under højt tryk. Resultatet viser at de to værdier for eksponenten stemmer godt overens, hvilket indebærer at stærkt korrelerede væsker eksisterer and kan betragtes som en klasse af særligt simple væsker.

2) Tilstandspunktsafhængigheden af densitetsskalleingseksponenten γ_{scale} (kapitel 7). Data for to væsker, DC704 og polyphenylether (5PPE), undersøges med hensyn til temperatur- og densitetsafhængigheden af γ_{scale}. Det viser sig at densitetsvariationen er for lille til at drage en konklusion angående γ_{scale}.

3) "Aging"-opførselen for stærkt korrelerede væsker (kapitel 8). En ide til at teste den forudsagte og gennem computersimuleringer viste "aging"-opførsel for stærkt korrelerede væsker præsenteres (kapitel 8) og de eksperimentelle udfordringer forbundet med eksperimentet diskuteres. Eksperimentet skal udføres på en ny opstilling til dielektriske målinger under tryk. En detaljeret beskrivelse af opstillingen gives og hovedudfordringerne forbundet med implementeringen og især i forbindelse med udførslen af det foreslåede eksperiment beskrives.

Endelig præsenteres data for det frekvensafhængige adiabatiske bulkmodul for to væsker, trimethyl-pentaphenyl-trisiloxane (DC705) and dibuthyl phtalate (DBP). Data analyseres med hensyn til relaxationstid, tid-temperatur-superponering (TTS) og højfrekvenshældning for alpha-relaksationen (kapitel 3). Det frekvensafhængige bulkmodul en af de fire frekvensafhængige responsefunktioner som benyttes til at bestemme γ_{isom}.

Contents

1 Introduction

This text is a revised version of the PhD thesis of January 2012 by the same title.

The PhD thesis is the result of work carried out in the period from March 2008 till January 2012, interrupted by a maternity leave in 2010. During this period, a whole new concept developed in the glass community, with the Glass and Time group as a main generator. This concept of "strongly correlating liquids", which came out of computer simulations, emerged in the beginning of 2008 and a substantial amount of theory and computer simulation results developed in the following years.

Computer simulations provide means for fast investigation of theoretical predictions and ideas and are a very powerful tool for understanding molecular behavior, but due to the heavy demands for processing power, only relatively small systems can be studied and only on very short time scales. Moreover, the systems that are simulated are to a large extend idealized models of real molecules. Therefore it is (still) crucial to have experimental evidence for computer simulation findings.

The initial goal of this phd project was to buy and implement a new setup for high pressure measurements and PVT measurements. High pressure measurements provide new possibilities for studying not only the temperature dependence of the relaxation time, but also the pressure or density dependence. It turned out that high pressure measurements was also suited for investigating many of the isomorph predictions. For different reasons such experiments are not always straight forward though. Computer simulations are for instance often done at constant volume while experiments are done at constant pressure. For this reason among others, it required 6 different measurements of linear response functions and a set of high pressure dielectric measurements with associated PVT measurements to test the first isomorph prediction (chapter 6). In the attempt to develop experimental pendents to computer simulations, a central theme of this PhD thesis is the link between experiments and computer simulations.

1.0.1 Reading guide

First an introduction to the field of viscous liquids is given in chapter 2, including a somewhat extended outline of linear response and the fluctuation dissipation theorem. This serves as a definition of different terms and physical parameters that will be used in the rest of the thesis. The thesis then has a chapter about measurements of the frequency dependent bulk modulus measured by the piezo electric bulk modulus gauge technique. This falls maybe a little outside the general theme of the thesis, but can be viewed as an example of measurement of one of the linear response functions that is used to calculate γ in chapter 6 (although on a different substance). The chapter also gives a relatively thorough description of the experimental technique and the somewhat

involved data analysis. Chapter 4 describes the new high pressure setup, and (some of) the challenges involved in the implementation. Furthermore it discusses potential challenges related to the experiment described in chapter 8. Chapter 5 goes through the relevant theory and findings related to strongly correlating liquids isomorphs, which is the basis of chapters 6, 7 and 8. Chapter 6 describes the results of an experimentel test of one of the isomorph predictions, namely that the density scaling exponent can be measured from linear response at a single state point. An interpretation of the result is given in terms of the Prigogine Defay ratio and single parameter liquids. Chapter 7 investigates the density dependence of γ, as predicted from the isomorph theory. The analysis is based on high pressure dielectric data for two substances. Finally chapter 8 discusses ideas for an experimental test of the aging behavior of strongly correlating liquids as found in computer simulations. Some potential experimental challenges involved with such an experiment are also discussed.

Although the chapter on the high pressure setup constitutes a relatively small part of this thesis, the implementation of the high pressure setup has taken up a significant amount of time and effort during my PhD. This has partly been due to various practical and technical problems on the way, and partly because I wanted to utilize the setup for a different type of measurements than it is usually used for.

2 Viscous liquids and the glass transition

This chapter introduces the most relevant subjects and phenomena of viscous liquids and the glass transition. Furthermore, it gives a somewhat extended introduction to linear response and the fluctuation dissipation theorem. This may seem redundant considering that such an introduction can be found in many text books (eg. [Doi & Edwards 1986]). The motivation for the repetition here is twofold: First of all, a central theme in this thesis is the connection between computer simulations and experiments. Computer simulations are mostly done in the time domain, while experiments are often done in the frequency domain. In addition, computer simulations provide knowledge of thermal fluctuations, while experiments give information on average macroscopic properties. Hence the connection between the different domains and timescales and the connection between response functions and thermal fluctuations is central. Second, different notation and formulations exist in the literature, and in order to be clear about the definitions, the relation between the most common formulations is discussed.

2.1 Producing a glass

When we speak about glasses, we most often think of it as the result of super cooling a liquid below its melting point without crystallization. Figure 2.1 shows a schematic of the volume or enthalpy as a function of temperature for a typical liquid. When the liquid is cooled from high temperatures, the volume and enthalpy of the liquid generally decreases. The rate with which for instance the volume decreases (the slope of the curve) is given by the liquids thermal expansion coefficient. The liquid is in equilibrium, meaning that any property of the liquid is uniquely determined by the thermodynamic state (temperature and pressure) of the liquid. By lowering the temperature of the liquid at a constant cooling rate, the liquid will at some point reach its melting temperature T_m, where it may go through a phase transition to become a crystal. The volume then goes through a discontinuous change at T_m. By further cooling, the volume of the crystal will keep decreasing, but at a smaller rate than in the liquid, reflecting the fact that the thermal expansion coefficient of the crystal is smaller than that of the liquid.

If the cooling rate is sufficiently fast, the phase transition can be avoided. The liquid then becomes a super cooled liquid. We refer to the super cooled state as a metastable state, because the true equilibrium state is the crystal.

The characteristic time it takes for the molecules to rearrange to the new volume as the temperature is changed is called the structural relaxation time τ_α, which is closely related to the viscosity. As the temperature of the super cooled liquid is lowered, the viscosity and the structural relaxation time increases dramatically. As a result, the time

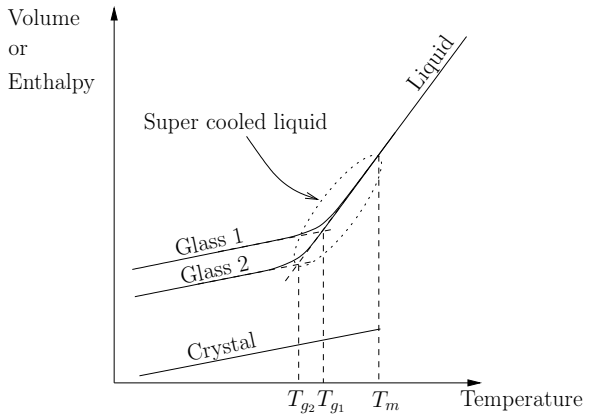

Figure 2.1 Schematic of volume or enthalpy as a function of temperature for a typical liquid. At the melting temperature T_m the liquid may go through a phase transition and crystallize, or if cooled sufficiently fast become super cooled. At some temperature T_g, depending on cooling rate, the liquid will fall out of equilibrium and become a glass. Glass 1 is the result of a larger cooling rate than Glass 2.

it takes for the volume to adjust to the new temperature will be increasingly longer until eventually the volume will not have time to equilibrate at the given cooling rate and the liquid falls out of equilibrium and becomes a glass. The temperature at which the liquid falls out of equilibrium is called the glass transition temperature, T_g. Since the structure of the glass does not change (on the timescale of typical observations), the glass is a disordered solid with the same structure as the liquid at T_g.

The volume of the glass still decreases slightly with temperature due to a decrease in the distance between the molecules. The slope of the curve in the glass is similar to the slope of the solid reflecting that the expansion coefficient in the glass is similar to the crystal. As illustrated in figure 2.1 the glass transition temperature depends on the cooling rate, a slower cooling rate results in a lower T_g. Traditionally, T_g refers to the temperature where the liquid falls out of equilibrium when cooled under standard experimental cooling rates. This corresponds to a viscosity around $10^{12} - 10^{13}$ Pas, or a relaxation time around 100-1000 s. T_g is then sometimes defined as the temperature at which $\tau_\alpha = 100$ s.

The fact that the glass is out of equilibrium means that its properties (like for instance volume) changes with time, it ages. Consider for instance one of the glasses in figure 2.1. If we wait long enough the volume (or enthalpy) of the glass will approach the equilibrium liquid line. This also means that the properties of the glass depends on its thermal history.

A glass can also be produced by compression at constant temperature, and we would then talk about a glass transition pressure equivalent to the glass transition temperature. The slope of the curve in a Volume versus Pressure plot would then reflect the compressibility. We could also decrease the temperature of a liquid at a constant pressure different from atmospheric pressure. In that case the glass transition temperature would be different from that obtained at atmospheric pressure. The different routes to

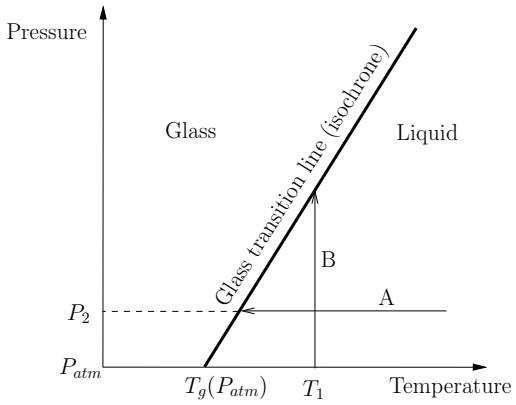

Figure 2.2 Illustration of the temperature and pressure dependence of the glass transition, defined as $\tau_\alpha = 100$ s. The glass transition then constitude a line of constant relaxation time, an isochrone. Route A illustrates a situation where the liquid is cooled isobarically at pressure P_2, and route B illustrates a situation where the liquid is compressed isothermally at temperature T_1.

the glass transition is illustrated in figure 2.2. The glass transition is here defined as the state point at which the relaxation time reaches e.g. 100 s. The glass transition line is then a line of constant relaxation time, an isochrone.

The fact that the viscosity and relaxation time increases so dramatically in the super cooled liquid, means that the properties of the liquid becomes time or frequency dependent. The relaxation time can be measured in a linear response experiment, where the response to an external perturbation is measured. Linear response can be measured in the time domain where the time dependence of the output is measured after for instance a step input, or in the frequency domain, where an oscillating input results in an oscillating output. A linear response measurement will then show a characteristic transition from a short time or high frequency response to a long time or low frequency response (see figures 2.3 and 2.5). The short time or high frequency response is the elastic solid-like response resulting from an almost instantaneous isostructural change in the distance between the molecules in the liquid. The long time or low frequency response is the viscous liquid-like response of the structural relaxation of the molecules. The relaxation time is then the time characterizing the transition from solid-like to liquid-like behavior, in the frequency domain often defined as the inverse angular loss peak frequency.

Understanding the origin of the viscous slowing down with decreasing temperature and increasing pressure is one of the main challenges in the research field. Another important question governs the characteristic of the relaxation in linear experiments. Simple exponential relaxation is almost never seen [Mazurin 1977, Böhmer, Ngai, Angell & Plazek 1993, Chamberlin 1998]. In stead, the relaxation is found to be broader than exponential relaxation. This is referred to as stretching of the relaxation. In the frequency domain, the stretching shows up as an asymmetric loss peak, with a high frequency slope in a log-log representation usually approaching 1 (exponential), and a low frequency slope numerically smaller than 1.

2.2 Formalism

2.2.1 Linear response

In a linear response experiment, the external perturbation is so small that the output is assumed to be linearly dependent on the input. The change in input $dI(t')$ at time t' leads to a contribution in output $dO(t)$ at time t:

$$dO(t) = R(t-t')dI(t'). \tag{2.1}$$

It is here assumed that the change in output only depends on the time difference $(t-t')$. Causality implies that

$$R(t) = 0 \text{ for } t < 0. \tag{2.2}$$

Integrating on both sides of Eq. (2.1):

$$O(t) = \int_{-\infty}^{t} R(t-t')dI(t'), \tag{2.3}$$

and substituting $t'' = t - t'$ and writing $\dot{I}(t) = \dfrac{dI(t)}{dt}$

$$O(t) \quad = \quad -\int_{\infty}^{0} R(t'')\dot{I}(t-t'')dt''. \tag{2.4}$$

Changing t'' to t':

$$O(t) = \int_{0}^{\infty} R(t')\dot{I}(t-t')dt'. \tag{2.5}$$

If the input is a Heaviside function:

$$I(t) = I_0 H(t) = I_0 \begin{cases} 0 & \text{for } t \leq 0 \\ 1 & \text{for } t > 0 \end{cases}$$

then

$$O(t) = I_0 \int_{0}^{\infty} R(t')\delta(t-t')dt' = I_0 R(t), \tag{2.6}$$

and it is seen that $R(t)$ is the output from a Heaviside step input. Figure 2.3 shows a sketch of input and output for a time domain step input.

Linear response can also be studied in the frequency domain. In the case of a harmonic oscillating input $I(t) = I_0 e^{i(\omega t + \phi_I)}$, the output $O(t) = O_0 e^{i(\omega t + \phi_O)}$ will be a periodic signal with the same frequency ω, but there can be a phase shift of the output relative to the input (see figure 2.4). From Eq. (2.5) the output is

$$\begin{aligned} O(t) &= \int_{0}^{\infty} R(t')i\omega I_0 e^{i\phi_I} e^{i\omega(t-t')}dt' \\ &= I_0 e^{i\omega t} e^{i\phi_I} i\omega \int_{0}^{\infty} R(t')e^{-i\omega t'}dt' \\ &= I(t)R(\omega), \end{aligned} \tag{2.7}$$

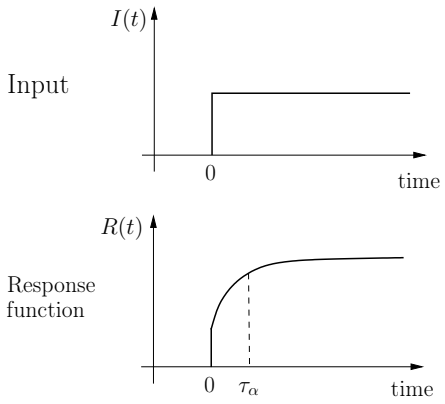

Figure 2.3 Illustration of a linear response measurement in the time domain. The input $I(t)$ (top) is a step input at time $t = 0$. The response function $R(t)$ has an instantaneous response that is due to fast relaxations shorter than the experimental time window.

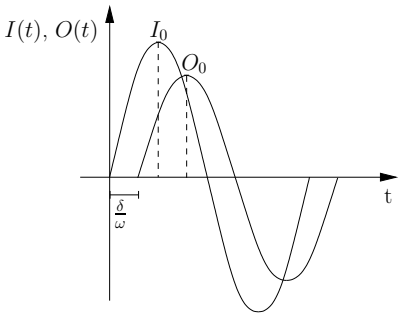

Figure 2.4 Illustration of frequency dependent input and output. I_0 and O_0 are the amplitudes of the input and output respectively, and $\delta = \phi_O - \phi_I$ is the phase difference between input and output.

where $R(\omega)$ is the frequency domain response function, which is given by the Laplace transform of $R(t)$ times $i\omega$:

$$R(\omega) = i\omega \int_0^\infty R(t')e^{-i\omega t'}\,dt'. \tag{2.8}$$

From equation 2.7:

$$O_0 e^{i(\omega t \phi_O)} = R(\omega) I_0 e^{i(\omega t + \phi_I)} \tag{2.9}$$

$$O_0 e^{i\phi_O} e^{i\omega t} = R(\omega) I_0 e^{i\phi_I} e^{i\omega t}, \tag{2.10}$$

and it is seen that the frequency domain response function is given by the ratio of the

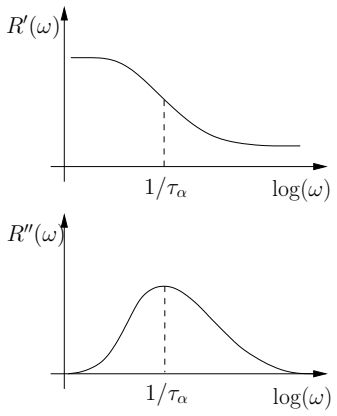

Figure 2.5 Example of the real (top) and imaginary (bottom) part of a frequency domain linear response function. The relaxation time τ_α is defined as the inverse angular loss peak frequency.

amplitudes and the phase difference δ between input and output:

$$R(\omega) = \frac{O_0}{I_0} e^{i(\phi_O - \phi_I)} \tag{2.11}$$

$$= \frac{O_0}{I_0}(\cos\delta + i\sin\delta). \tag{2.12}$$

Figure 2.5 shows a sketch of a frequency domain response function.

The linear response relation is often expressed in an alternative formulation where the linearity assumption is expressed by

$$O(t) = \int_{-\infty}^{t} \mu(t-t')I(t')dt', \tag{2.13}$$

where μ is sometimes called the memory function, or sometimes also the response function. The use of the word response function for $\mu(t)$ is somewhat inconvenient though because it has a different dimension compared to the frequency-domain response function $R(\omega)$.

Substituting again ($t'' = t - t'$) in equation 2.13 and changing t'' to t'

$$O(t) = \int_{0}^{\infty} \mu(t')I(t-t')dt'. \tag{2.14}$$

Applying a Heaviside input again

$$O(t) = \int_{0}^{\infty} \mu(t')I_o H(t-t')dt'$$

$$= I_0 \int_{0}^{t} \mu(t')dt'. \tag{2.15}$$

From Eq. (2.6) and (2.15) we have

$$R(t) = \int_0^t \mu(t')dt',$$

and therefore

$$\frac{dR(t)}{dt} = \mu(t). \tag{2.16}$$

In the memory function formalism the frequency domain response is again found by inserting a harmonic oscillating input. In this case the result becomes

$$R(\omega) = \int_0^\infty \mu(t')e^{-i\omega t'}dt' = \int_0^\infty \frac{dR(t)}{dt}e^{-i\omega t'}dt', \tag{2.17}$$

where the last equality comes from inserting Eq. (2.16). This expression is formally equivalent to Eq. (2.8) which can be shown by integration by parts and by invoking $R(t = 0) = 0$. When differentiating the time domain response function, any information of an (almost) instantaneous response ($R(t \to 0) \neq 0$) will be lost. Moreover, from a practical point of view, differentiation of numerical data is never desired, since it introduces increased noise. For these reasons equation 2.8 is here preferred over equation 2.17.

2.2.2 Fluctuation versus response

The measured response of a system to an external field, whether in the time domain or in the frequency domain, is directly related to the equilibrium thermal fluctuations of the system. This is expressed formally through the fluctuation dissipation theorem (FDT), which expressed in the time domain is [Doi & Edwards 1986]:

$$\frac{dR(t)}{dt} = -\frac{1}{k_B T}\frac{d}{dt}\langle \Delta A(t)\Delta B(0)\rangle. \tag{2.18}$$

Sharp brackets refers to ensemble averages. A is the measured physical quantity (the output) and B has to be conjugated to the applied input/field. The function $\langle \Delta A(t)\Delta B(0)\rangle$ is the correlation function, which in the simple case where $A = B$ reduces to the auto correlation function.

Integrating on both sides of equation 2.18 and inserting $R(t = 0) = 0$ gives the time domain response function:

$$\begin{aligned} \int_0^t \frac{dR(t')}{dt'}dt' &= -\int_0^t \frac{1}{k_B T}\frac{d}{dt'}\langle \Delta A(t')\Delta B(0)\rangle dt' \\ R(t) &= \frac{1}{k_B T}(\langle \Delta A(0)\Delta B(0)\rangle - \langle \Delta A(t)\Delta B(0)\rangle). \end{aligned} \tag{2.19}$$

Combining this with equation 2.8 gives the FDT in the frequency domain:

$$\begin{aligned} R(\omega) &= -\frac{i\omega}{k_B T}\int_0^\infty \langle \Delta A(t)\Delta B(0)\rangle - \langle \Delta A(0)\Delta B(0)\rangle e^{-i\omega t}dt \\ &= \frac{1}{k_B T}\langle \Delta A(0)\Delta B(0)\rangle - \frac{i\omega}{k_B T}\int_0^\infty \langle \Delta A(t)\Delta B(0)\rangle e^{-i\omega t}dt \end{aligned} \tag{2.20}$$

An example: The isobaric expansion coefficient

Consider a linear experiment where a small temperature step δT is applied to a system at constant pressure at time $t = 0$, and its volume response is measured as a function of time:

$$\delta V(t) = R(t - t')\delta T(t'), \tag{2.21}$$

then the response function $R(t)$ is given by $R(t) = \frac{\delta V(t)}{\delta T}$. The time-dependent isobaric expansion coefficient is defined by

$$\begin{aligned} \alpha_p(t) &= \frac{1}{V}\frac{\delta V(t)}{\delta T} \\ &= \frac{R(t)}{V} \end{aligned} \tag{2.22}$$

In terms of the time domain FDT (equation 2.19), the relevant fluctuations for $\alpha_p(t)$ are volume and entropy:

$$\alpha_p(t) = \frac{1}{Vk_bT}\left(\langle \Delta V(0)\Delta S(0)\rangle - \langle \Delta V(t)\Delta S(0)\rangle\right), \tag{2.23}$$

which is an increasing function of time. The frequency domain FDT for $\alpha_p(\omega)$ is then (equation 2.20)

$$\alpha_P(\omega) = \frac{1}{Vk_BT}\langle \Delta V(0)\Delta S(0)\rangle - \frac{i\omega}{Vk_BT}\int_0^\infty \langle \Delta V(t)\Delta S(0)\rangle e^{-i\omega t}dt. \tag{2.24}$$

3 Frequency dependent bulk modulus

Understanding the relation between the different response functions is an important step towards understanding the nature of viscous liquids. Data on the frequency dependent bulk modulus are scarce in literature compared to especially dielectric data. The "Glass and Time" group has developed several experimental techniques for measuring different frequency dependent response functions, including the Piezo electric bulk modulus gauge for measuring the adiabatic bulk modulus $K_S(\omega)$. The technique was first described by Christensen and Olsen [Christensen & Olsen 1994], and an extended account of the technique and data analysis is given by Hecksher [Hecksher 2011]. In this chapter two data sets on $K_S(\omega)$ is presented.

The bulk modulus is the response to a shape preserving volume deformation, defined as

$$K = V\frac{\delta p}{\delta V}. \tag{3.1}$$

Such a response can be measured under two different conditions, namely adiabatic (K_S) or isothermal (K_T). The present setup meassures the adiabatic bulk modulus K_S.

3.1 Experimental

3.1.1 Liquids

Experiments were performed on two molecular liquids: DC705 (trimethyl-pentaphenyl-trisiloxane) and DBP (dibuthyl phtalate). Both liquids are stable, and easy to handle at room temperature. The liquids were used as acquired without any further treatment. The transducer was loaded at room temperature and at atmospheric conditions with a syringe through the pipe. Loading is done slowly in order to minimize the risk of bubbles in the transducer.

The thermodynamic glass transition temperature of both liquids was found from a calorimetric measurement. The results are shown in table 3.1. The chemical structure of the liquids are shown in figure 3.1.

3.1.2 The transducer

The bulk transducer is a spherical shell of piezo electric ceramic material polarized in the radial direction. The inner and outer surfaces of the transducer is coated with silver electrodes and connected to an oscillating voltage generator. The potential difference between the inner and outer surface of the transducer will cause the polarized shell to

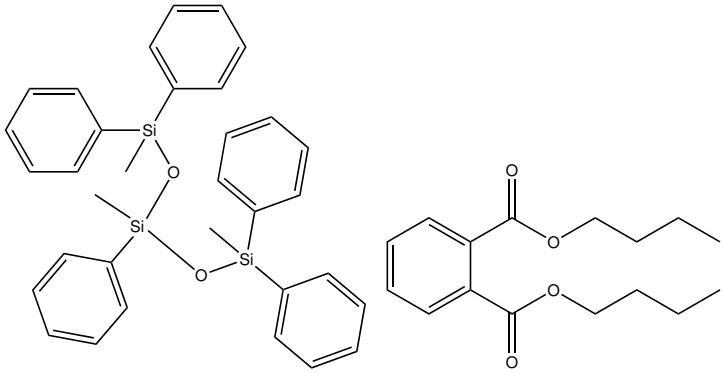

1,3,5-trimethyl-1,1,3,5,5-pentaphenyltrisiloxane
Chemical Formula: $C_{33}H_{34}O_2Si_3$
Molecular Weight: 546,88

dibutyl phthalate
Chemical Formula: $C_{16}H_{22}O_4$
Molecular Weight: 278,34

Figure 3.1 Chemical structure of DC705 and DBP.

deform and give rise to a bulk deformation of a liquid contained within the sphere. The motion of the shell will be affected by the stiffness of the liquid, and the capacitance of the sphere will depend on whether the transducer is empty and freely moving or filled and partially clamped. By measuring the capacitance of the shell both with and without liquid, the stiffness of the liquid can be calculated and in turn the bulk modulus.

The transducer is provided with a hole at the top, which is equipped with a tube. Figure 3.2 shows a sketch of the transducer with tube. When the transducer is loaded at room temperature, the transducer is filled with liquid to the top of the tube. This is to assure that the sphere is always filled with liquid at lower temperatures where the liquid volume decreases.

3.1.3 Measurements

Measurement protocols for the bulk modulus measurements was chosen from a few degrees above the measured T_g and up. Temperatures very close to T_g are avoided to reduce the risk of breaking the brittle ceramics when the liquid becomes too viscous. Both heating and cooling are done in controlled steps with adequate equilibration time, even when no measurements are done, in order to minimize the risk of breaking the ceramics due to thermal expansion and contraction of the liquid.

At each temperature the measurement was preceded by a two hour equilibration time. Two measurements were performed at the lowest temperatures to ensure that equilibrium was reached, the second measurement was taken immediately after the first without any further waiting time. Table 3.1 shows the measured temperatures for both liquids.

Capacitances are measured from 1 mHz to 1 MHz, but due to a resonance peak between 10 kHz and 100 kHz resulting from the mechanical properties of the transducer, the frequency window for the bulk modulus relaxation is limited above 10 kHz. Two types

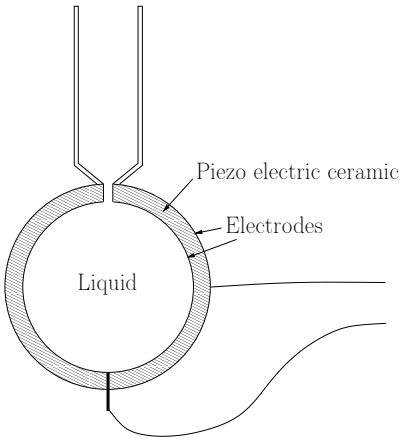

Figure 3.2 Diagram of the bulk transducer. The inner diameter of the sphere is $18.05 \cdot 10^{-3}$ mm and the thickness of the ceramics is $0.5 \cdot 10^{-3}$ mm. The diameter of the hole is small in order to minimize the change in the geometry of the transducer.

Liquid	T_g (K)	Measured temperatures (K)
DC705	228	310, 295, 280, 265, **249**, **246**, **243**, **240**, **237**, **235.5**, **234**, (235.5, 237)
DBP	183	310, 295, 280, 265, 250, 235, 220, 205, 198, 196, 194, 192, 190, **188**, **186**, **184**

Table 3.1 The measured temperatures of the two liquids. The temperatures in bold are measured twice. The temperatures in paranthesis is not used in the data analysis. The glass transition temperatures are found from calorimetric measurements.

of measurements are done: a logarithmic scan from 10^{-3} Hz to 10^6 Hz, and a scan that is linear in frequency from 10^3 Hz to 10^6 Hz. The two scans are used for different parts of the data analysis. For technical reasons, no linear scan was obtained for DC705, which limits the data analysis for this liquid.

It is necessary to do a reference measurement following the same measurement protocol as the liquid measurement. This is important since the properties of the ceramics is highly temperature dependent and thermal history dependent. As will be clear later on, it is essential for the data analysis that the reference and liquid measurement match each other, i.e. that they coincide at low frequencies where the liquid is able to flow out of the transducer and into the pipe. Consequently, the measured capacitances of the filled transducer should be identical to the capacitance of the empty transducer at low frequenciessince the motion of the transducer is not affected by the liquid. However, often there is a slight difference between the liquid and reference spectrum. To compensate for this, a scaling of the reference can be done (see section 3.2.2).

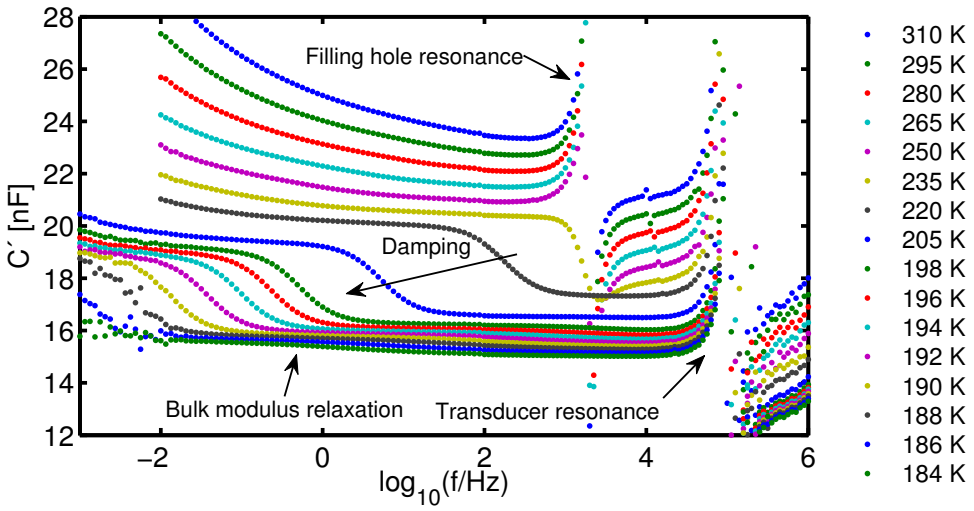

Figure 3.3 Example of measured real part of the capacitance for DBP. The mechanical resonance of the transducer and the "filling hole resonance" are clearly visible, while the bulk modulus relaxation can hardly be seen. As the temperature is lowered, the resonance of the flow through the hole gets damped and eventually moves down in frequency.

3.2 Data

3.2.1 Capacitance data

Figure 3.3 shows an example of the real part of the capacitance data for DBP at the measured temperatures. The raw data is characterized by two clearly identifiable transitions or dispersion regions. The resonance near 10^5 Hz is the mechanical resonance of the transducer with liquid. At higher frequencies than this, a number of smaller resonances are found resulting from standing waves in the liquid, but these can only be seen clearly in a linear frequency scan. The slowest transition is the resonance of the liquid flowing in and out of the transducer. At frequencies lower than this resonance frequency, the liquid is able to flow in and out of the transducer to and from the reservoir, while at higher frequencies, the liquid will not have time to flow through the hole and will be effectively trapped in the sphere. As the liquid becomes increasingly viscous with decreasing temperature, the resonance becomes damped and moves down in frequency. The bulk relaxation then shows up at lower temperatures as a small bump between the hole resonance and the resonance of the transducer. This can just barely be seen for the lowest temperatures in figure 3.3.

A noticeable frequency dependence of the capacitance is noted at low frequencies. This effect is taken into account in the data analysis (see section 3.3.3).

For the lowest temperatures the low frequency end of the spectrum shows some noise. The origin of the noise is presently not understood.

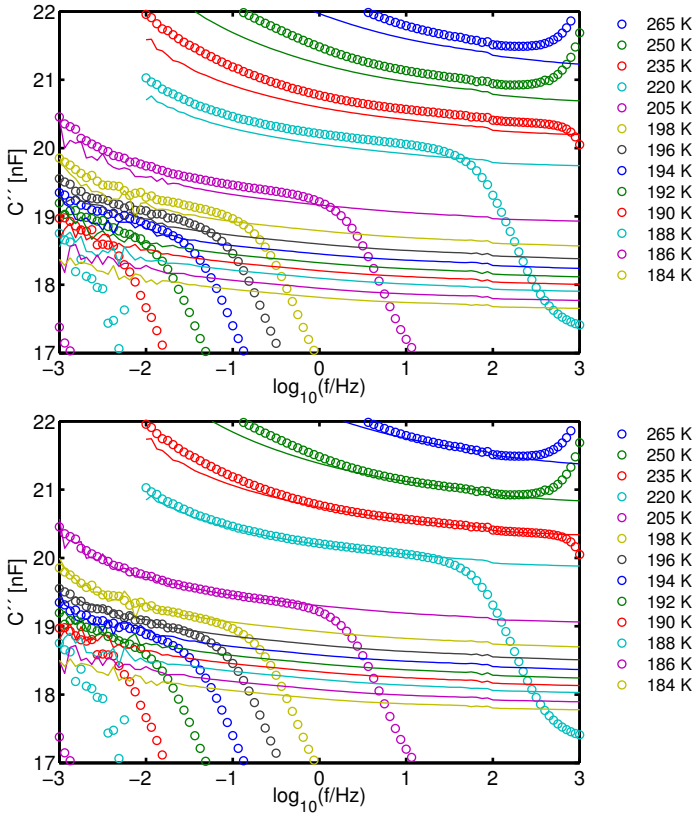

Figure 3.4 Example of scaling of the reference for DBP. Top: Real part of measured liquid (circles) and reference (lines) capacitance spectra. Bottom: The reference spectrum has been scaled (lines) to better match the measured liquid spectrum (circles).

3.2.2 Liquid and reference measurement

Figure 3.4 top shows an example of liquid and reference spectra for DBP. As mentioned earlier, the data should collapse at low frequencies where the movement of the transducer is not affected by the liquid since it is able to flow out of the transducer to the reservoir. For this measurement, the level of the reference is lower for all comparable temperatures. In order to determine the liquid properties, the reference spectrum is scaled to better match the liquid spectrum. The reference spectrum of DBP scaled by a factor of 1.007 is plotted in the bottom of figure 3.4 along with the liquid spectrum. A similar scaling is necessary for DC705, but in this case, a slightly temperature dependent scaling factor ranging from 1.002 to 1.006 is chosen. As seen from the figure, even after scaling the reference, the liquid and reference spectra for DBP do not overlap entirely at the highest temperatures, but this should not be a problem for the resulting bulk modulus' since these are obtained at the lower temperatures.

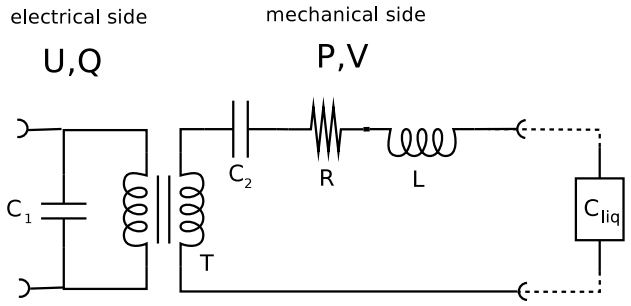

Figure 3.5 Electrical network model of the bulk transducer with liquid. The transducer element T represents the transformation of energy from electrical to mechanical. C_1 represents the electrical capacitance of the transducer, and on the mechanical side, the elastic properties of the transducer is represented by C_2 while L represents the inertial properties and R the dissipative properties of the transducer. The dashed line with the element C_{liq} represents the elastic properties of the liquid. From [Hecksher 2011] with permission.

3.3 Modelling and fitting

3.3.1 The circuit model

The system consisting of the transducer with liquid can be modeled with an electrical network model as seen in figure 3.5. The electrical and mechanical properties of the transducer and liquid are all represented as electrical components in either series or parallel connection. The transducer element T represents the transformation of energy from electrical to mechanical. C_1 represents the electrical capacitance of the transducer, and on the mechanical side, the elastic properties of the transducer is represented by C_2 while L represents the inertial properties and R the dissipative properties of the transducer. The dashed line with the element C_{liq} represents the elastic properties of the liquid.

3.3.2 The empty transducer

From the network model, an expression for the total capacitance of the empty transducer can be written:

$$C_{tot,empty} = C_1 + T^2 \frac{1}{\frac{1}{C_2} - \omega^2 L + i\omega R}. \tag{3.2}$$

At high frequencies, the fraction in this expression goes to zero, so the total capacitance approaches C_1. We then define

$$C_{tot,empty}(\omega \to \infty) = C_{cl} = C_1, \tag{3.3}$$

where C_{cl} refers to the situation where the transducer is clamped by the liquid. At low frequencies, the movement of the transducer is not affected by the liquid inside, and the expression reduces to

$$C_{tot,empty}(\omega \to 0) = C_{free} = C_1 + T^2 C_2, \tag{3.4}$$

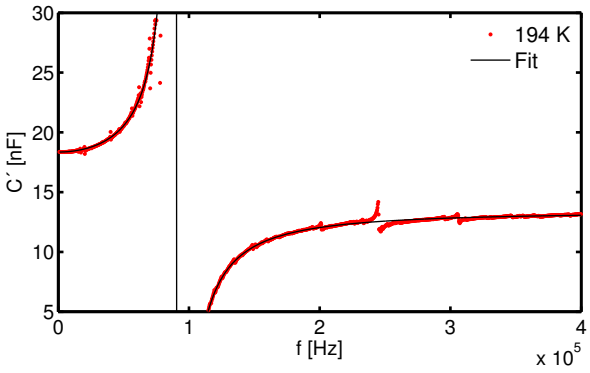

Figure 3.6 Example of a fit to the empty spectrum (linear scan). Red dots are the measured data points, and the black line is the fit to data.

where C_{free} represents the elastic properties of the transducer when it moves freely without resistance. By introducing the resonance frequency $\omega_0 = \frac{1}{\sqrt{LC_2}}$ and the quality $Q = \frac{1}{R}\sqrt{\frac{L}{C_2}}$, the expression for the total capacitance is then rewritten with the above definitions:

$$C_{tot,empty} = C_{cl} + \frac{C_{free} - C_{cl}}{1 - \frac{\omega^2}{\omega_0^2} + i\frac{\omega}{Q\omega_0}}. \tag{3.5}$$

By fitting this expression to the spectrum of the empty transducer, the four parameters Q, ω_0, C_{free} and C_{cl} can be determined. An example of the fit is shown in figure 3.6.

3.3.3 The filled transducer

The model expression for the filled transducer using the above definitions is:

$$C_{tot,filled} = C_{cl} + \frac{C_{free} - C_{cl}}{1 - \frac{\omega^2}{\omega_0^2} + i\frac{\omega}{Q\omega_0} + \frac{C_2}{C_{liq}}}. \tag{3.6}$$

In order to find the stiffness of the liquid $S = 1/C_{liq}$ we need to find C_2, which is given by the inductance L and the resonance frequency ω_0 as described above. L is the mechanical equivalence of the electrical inductance L_e, which is the constant of proportionality between voltage U and current change $\frac{dI}{dt}$:

$$U = L_e\frac{dI}{dt} = L_e\frac{d^2Q}{dt^2}, \tag{3.7}$$

where Q is electrical charge. In the mechanical analog this corresponds to

$$\delta p \quad = \quad L\delta\ddot{V}, \tag{3.8}$$

where δV is volume change, δp is pressure difference and $\delta\ddot{V}$ is volume acceleration. Pressure is force $F = m \cdot a$ per area A, and hence

$$L\delta\ddot{V} = \frac{ma}{A}, \tag{3.9}$$

where a is the radial acceleration. Since the volume changes of the transducer is small we can write $\delta\ddot{V} = Aa$, and hence

$$L = \frac{m}{A^2}. \tag{3.10}$$

An estimate of the mass can be made by weighing the transducer and subtracting the weight of the reservoir pipe. An estimate of L can also be found from the high temperature data as described in section 3.3.5.

The stiffness of the liquid is now found by isolating $S = 1/C_{liq}$ in equation 3.6 and inserting $C_2 = \frac{1}{L\omega_0^2}$:

$$S(\omega) = L\omega_0^2 \left(\frac{C_{free} - C_{cl}}{C_{tot,filled} - C_{cl}} - 1 - \frac{i\omega}{\omega_0 Q} + \left(\frac{\omega}{\omega_0}\right)^2 \right). \tag{3.11}$$

As seen from figure 3.3 the value of C_{free} is not constant as one would expect from the model, but rather it shows a frequency dependence that is due to dispersion in the dielectric constant of the ceramics. A similar tendency is seen for C_{cl}. We can compensate for this in the modeling by assuming first that the frequency dependence of C_{free} and C_{cl} is the same. In this case the ratio of the two will be a constant. We will write the first term in the parenthesis

$$\frac{C_{free} - C_{cl}}{C_{tot,filled} - C_{cl}} = \frac{1 - \frac{C_{cl}}{C_{free}}}{\frac{C_{tot,filled}}{C_{free}} - \frac{C_{cl}}{C_{free}}}. \tag{3.12}$$

By the above assumption all terms in this expression except the $\frac{C_{tot,filled}}{C_{free}}$-term are constant. The justification of the assumption lies in the fact that it results in flat plateaus of the bulk modulus. From figure 3.4 it is also seen that the liquid and reference spectrum as we would expect show the same frequency dependence at low frequencies (for the lowest temperatures with the scaled reference). This means that we can write the expression for the stiffness as

$$S(\omega) = L\omega_0^2 \left(\frac{1 - \frac{C_{cl}}{C_{free}}}{\frac{C_{tot,filled}}{C_{ref}} - \frac{C_{cl}}{Cfree}} - 1 - \frac{i\omega}{\omega_0 Q} + \left(\frac{\omega}{\omega_0}\right)^2 \right), \tag{3.13}$$

where C_{free} has been replaced by C_{ref} in the denominator.

From the equations of motion, the stiffness of a spherical isotropic viscoelastic solid can be derived [Landau & Lifshitz 1986]:

$$S(\omega) = \frac{1}{V}\left(K_S - M_S \left(1 + \frac{1}{3} \frac{(k_l r)^2 \sin(k_l r)}{(k_l r)\cos(k_l r) - \sin(k_l r)} \right) \right), \tag{3.14}$$

where K_S is the adiabatic bulk modulus, $M_S = K_S + 4/3G$ is the longitudinal modulus, G is the shear modulus, $k_l = \sqrt{\frac{\rho_l}{M_S}}\omega$ the longitudinal wave vector, r is the radius of the sphere and ρ_l is the density of the liquid. For small $x = k_l r$ a Taylor expansion of the fraction in equation 3.14 gives

$$\frac{x^2 \sin x}{x\cos x - \sin x} \approx \frac{x^2(x - \frac{1}{6}x^3)}{x(1 - \frac{1}{2}x^2) - (x - \frac{1}{6}x^3)} = -3 + \frac{x^2}{2}, \tag{3.15}$$

which for small x reduces to -3. Hence, when $\omega \to 0$ the stiffness can be approximated by

$$S(\omega) = K_S/V \text{ for } \omega \to 0 \tag{3.16}$$

and from this then the bulk modulus is found. The frequency region where this applies (approximately up to 10^4 Hz) is called the quasi-static region.

3.3.4 Flow through the hole

At high frequencies (what this means depends on temperature), the liquid will not have time to flow through the small hole of the transducer and into the pipe, but at low frequencies the flow to and from the pipe will constitute a resonance in the filled spectrum, which will become damped and move down in frequency with decreasing temperature. Figure 3.7 shows bulk modulus' of DBP and DC705 at different temperatures. The hole resonance can be seen as the large resonance at the low frequency side of the bulk relaxation. The imaginary part of the modulus should go to zero on the low frequency side of the bulk loss peak. This is not the case for any of the data sets, which indicates that the liquid is not completely clamped inside the sphere at low frequencies. For DC705 this effect seems to increase with decreasing temperature.

The effect of the liquid flowing through the hole can be compensated for by including the flow through the hole in the electrical network model. The flow is modeled by a resistor in parallel to the liquid as seen in figure 3.8 (inertial effects are omitted because the flow is slow). The impedance of the two liquid elements is then

$$Z = \frac{1}{\frac{1}{R_h} + i\omega C_{liq}} = \frac{R_h}{1 + i\omega\tau}, \tag{3.17}$$

where $\tau = R_h C_{liq}$. When plotted in a Nyquist plot (real part versus imaginary part), the impedance will trace out a semi circle, where the resistance R_h can be found from the high frequency foot point of the semi circle. For some temperatures, the relaxation lies partly outside the measured frequency range, which means that the foot points can not be found directly from the Nyquist plot. In that case, an extrapolation have been made from the data where a determination of R_h was possible.

The expression for the stiffness after adding the resistor element R_h in the model is (compare to equation 3.13):

$$S(\omega) = \left(\left[L\omega_0^2 \left(\frac{1 - \frac{C_{cl}}{C_{free}}}{\frac{C_{tot,filled}}{C_{ref}} - \frac{C_{cl}}{Cfree}} - 1 - \frac{i\omega}{\omega_0 Q} + \left(\frac{\omega}{\omega_0}\right)^2 \right) \right]^{-1} + \frac{1}{i\omega R_h} \right)^{-1}. \tag{3.18}$$

The resulting bulk modulus are shown in figure 3.7 as dashed lines. The low frequency behavior is clearly improved for both data sets, although for DC705 the low frequency loss is not completely reduced. The problem is clearly temperature dependent. The reason is most likely that the frequency dependence of the liquid and reference measurement were sllightly different.

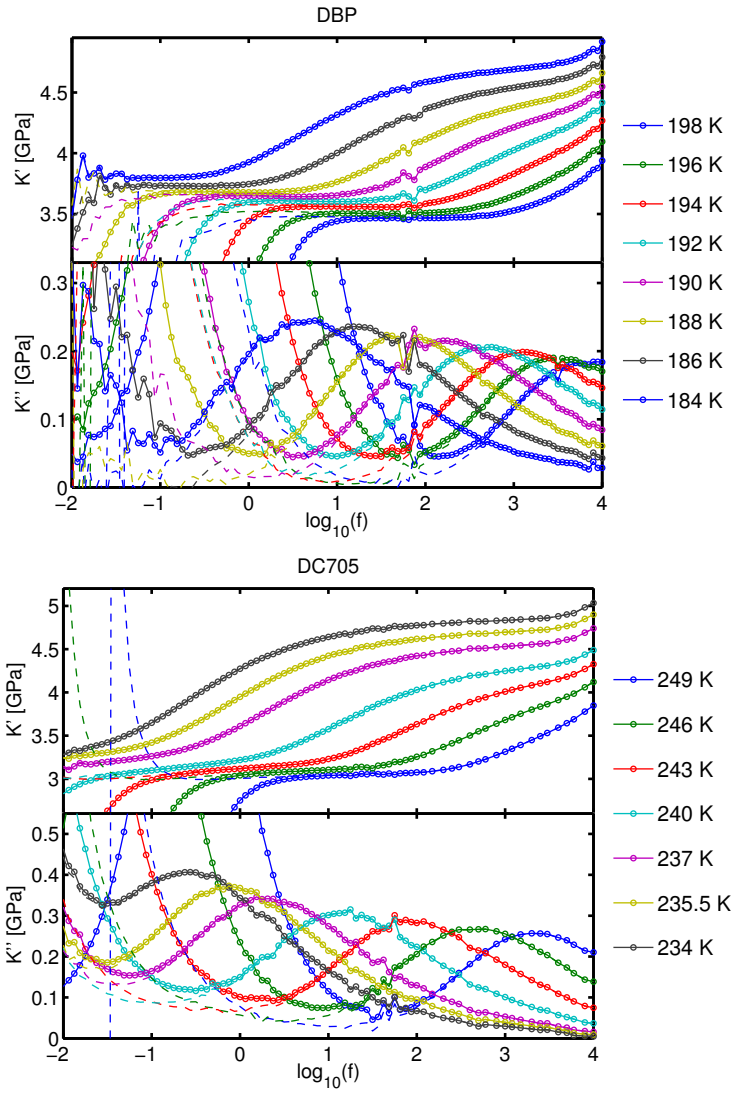

Figure 3.7 Real and imaginary part of bulk modulus for DBP and DC705 at the measured temperatures (lines with circles). The large resonance to the left of the bulk relaxation is the flow through the hole of the transducer. The flow though the hole interfers with the bulk relaxation so that the imaginary part is nonzero at the low frequency side of the bulk loss peak. The dashed lines are the calculated bulk modulus after including the flow through the hole in the model.

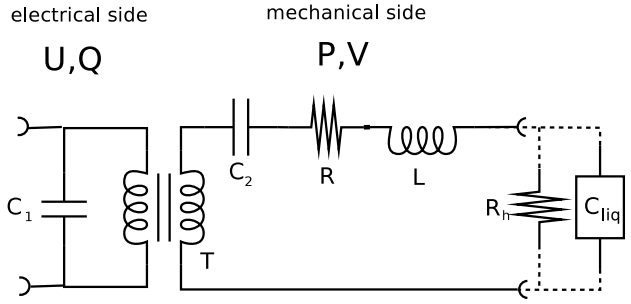

Figure 3.8 Electrical network model of the bulktransducer with liquid. The extra resistance R_h is added to include the flow through the hole of the transducer. From [Hecksher 2011] with permission.

3.3.5 The resonance method

At low temperatures where the liquid is viscous, the stiffness of the liquid is influenced by both a bulk modulus and a shear modulus (see equation 3.14). At high temperatures however, the shear contribution vanishes (and $M_S = K_S$ is virtually frequency independent) and the expression for the stiffness is (after introducing the resonance frequency $\omega_0' = \sqrt{\frac{K_S}{\rho_l}}\frac{1}{r}$):

$$S = \frac{1}{V}\left(K_S \frac{1}{3} \frac{\left(\frac{\omega}{\omega_0'}\right)^2 sin\left(\frac{\omega}{\omega_0'}\right)}{\left(\frac{\omega}{\omega_0'}\right) cos\left(\frac{\omega}{\omega_0'}\right) - sin\left(\frac{\omega}{\omega_0'}\right)}\right) \tag{3.19}$$

Under these circumstances the model expression for the measured capacitance is

$$C = C_{cl} + \frac{C_{free} - C_{cl}}{1 - \left(\frac{\omega}{\omega_0}\right)^2 + \frac{i\omega}{Q\omega_0} - \frac{K_s}{L\omega_0^2 3V}\frac{\left(\frac{\omega}{\omega_0'}\right)^2 sin\left(\frac{\omega}{\omega_0'}\right)}{\left(\frac{\omega}{\omega_0'}\right) cos\left(\frac{\omega}{\omega_0'}\right) - sin\left(\frac{\omega}{\omega_0'}\right)}}, \tag{3.20}$$

This expression can be fitted to the high temperature high frequency data, from which the static value of the bulk modulus K_0, corresponding to $K(\omega \to 0)$, can be found from the resonances. This method is called the **resonance method**. Comparing the K_0's found from the quasi static method to the K_0's found from the resonance method provides a check of the validity of the quasi static procedure.

When fitting equation 3.20 by the resonance method, L can also be found as a fitting parameter. This gives a better estimate of L (which is used for the data in figure 3.7). Figure 3.9 shows an example of a fit of equation 3.20 to the (linear scan) data of DBP, where both L and K_0 are fitted. Since no linear scan was obtained for DC705 this check can not be made. Luckily, L is a transducer specific parameter, and since the same transducer was used for the two measurements, the L value found for DBP should also apply for DC705.

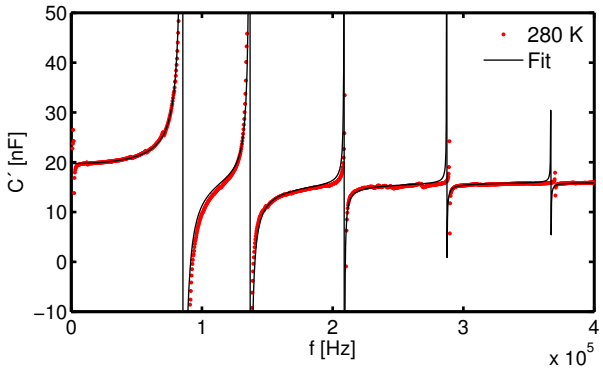

Figure 3.9 Example of a fit of equation 3.20 to data for DBP. L determines the low frequency plateau, while K_0 determines the resonanse frequencies.

3.4 Uncertainties

Experimental work is always affected by some amount of uncertainty due to the accuracy and capability of the setup. The setups used for measuring bulk modulus are described in detail by Igarashi *et al.* [Igarashi, Christensen, Larsen, Olsen, Pedersen, Rasmussen & Dyre 2008a, Igarashi, Christensen, Larsen, Olsen, Pedersen, Rasmussen & Dyre 2008b]. In addition, many different aspects of the rather involved data analysis can give rise to uncertainties in the determined bulk modulus. A more thorough and quantitative account of the possible sources and magnitudes of errors are given in [Hecksher 2011]. Here only a discussion of selected sources of uncertainty will be given.

The two most significant sources of uncertainties in the determined bulk modulus is probably the degree of match of the reference and liquid measurement, and the estimate of the inductance L. As shown in section 3.2.2, the liquid and reference measurement did not match ideally in any of the two measurements, and a scaling of the reference was necessary. As seen from figure 3.4, even after scaling the reference the frequency dependence of the liquid and reference spectra does not match perfectly, and this may well have an effect on the bulk modulus. An estimate of the effect of different scaling factors on the value of $K(\omega)$ for DC705 was tried giving a variation in $K(\omega)$ of around 5%, but only very little variation in the relaxation strength and spectral shape.

The difference in the estimated value of L from the mass and dimensions of the transducer and the fitted values is large: The calculated value is $L = 4150$ kg/m^4 while the fitted value is $L = 3600$ kg/m^4. Such a difference changes the quasi static $K(\omega)$ by up to 14%. Luckily, it is fairly easy to judge from the fit whether the estimate on L is reasonable, since L determines the level of the low frequency plateau of the fit. Hence, the L-value found from the fit is more reliable than the L-value calculated from the mass of the transducer. Figure 3.11 shows a comparison of the values obtained by the two methods for DBP. The agreement is excellent for this liquid.

Other fitting choices affect $K(\omega)$ calculated from the quasi static method in varying degree, among the most significant are the values of C_{free} and C_{cl} as described by Hecksher [Hecksher 2011].

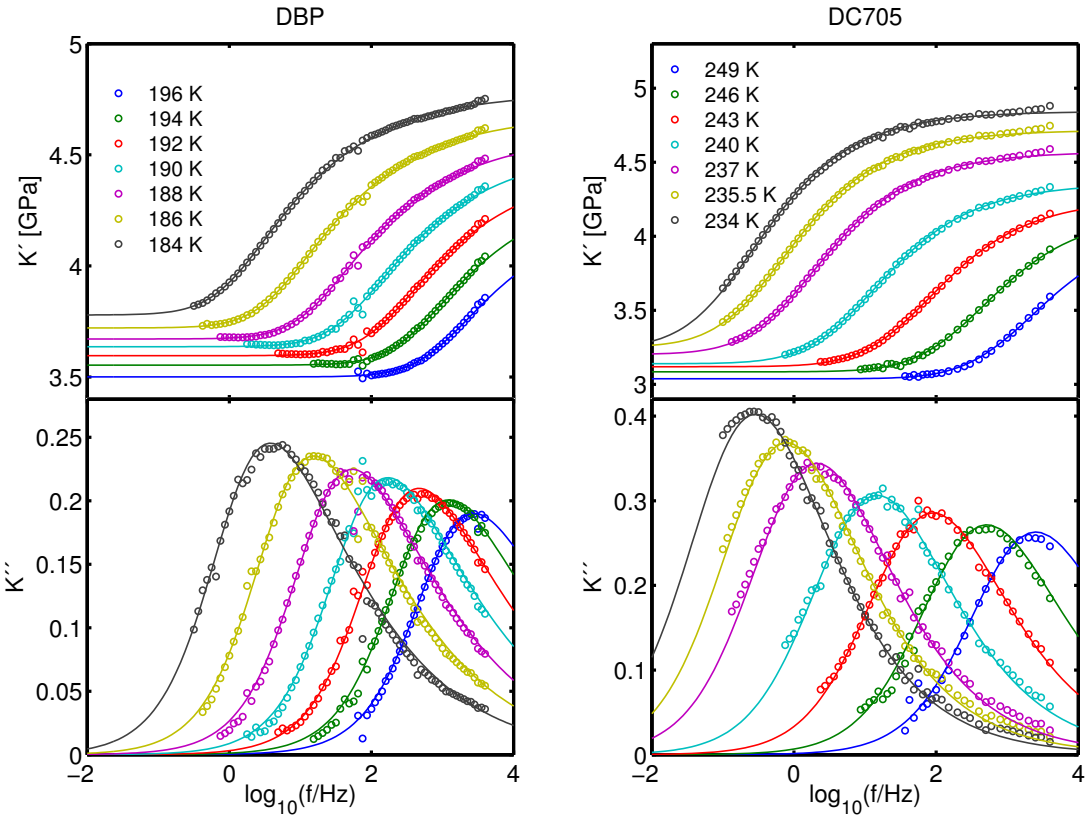

Figure 3.10 Real and imaginary parts of bulk modulus for DBP and DC705. Data has been fitted with an extended Maxwell expression.

3.5 Results

3.5.1 Bulk modulus

Figure 3.10 shows finalized real and imaginary parts of bulk modulus' for DBP and DC705. Both data sets show the characteristic transition in the real part from a (low) low frequency level corresponding to the liquid-like response, to a (higher) high frequency level corresponding to the solid-like response. The imaginary part shows the characteristic loss peak moving down in frequency with decreasing temperature. The rather dramatic increase in the loss peak maximum value at the lowest temperatures for DC705 is unusual and could be due to a mismatch of the liquid and reference measurement as discussed in sections 3.2.2 and 3.3.4. The values of bulk modulus' are typical for this type of liquids.

The real part of the bulk modulus for DBP as a function of temperature for different fixed frequencies are shown in figure 3.11. The figure also shows the K_0 values found from the resonance method. The K_0 level of the quasi static data matches the K_0 from the resonance method quite well. The K_∞ level can only barely be seen for the highest

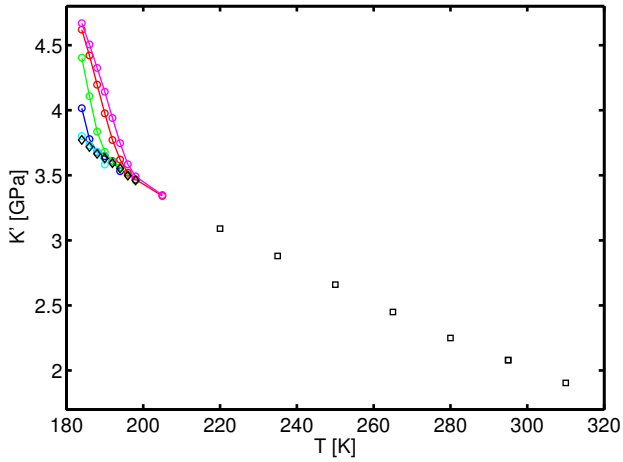

Figure 3.11 K_0 calculated from the resonance method (squares) and K measured by the quasistatic method (lines with circles) at different fixed frequencies of 1 Hz, 10 Hz, 100 Hz, 1000 Hz, $10^{3.5}$ Hz. Each color represents a frequency. Also shown are K_0 values (diamonds) from the extended Maxwell fit (section 3.5.4)

frequencies.

Shear modulus measurements [Maggi, Jakobsen, Christensen, Olsen & Dyre 2008] have shown traces of a beta process for DBP (although the peak of this relaxation was outside the frequency interval of the measurements), confirming results from dielectric measurements on DBP [Dixon, Wu, Nagel, Williams & Carini 1990] of the presence of a beta process around 10^6 Hz. The high frequency tail in the bulk loss of DBP for the lowest temperatures could be due to this beta process, but the quality and frequency range of the data does not allow a clear identification of secondary processes. DC705 does not show any sign of secondary processes, which also match the results from Shear modulus measurements [Maggi et al. 2008].

3.5.2 Times

Loss peaks were fitted with a second order polynomial to the maximum 9 points of $\log(f)$ vs $\log(K'')$. Figure 3.12 shows a plot of the loss peak frequency as a function of scaled temperature $(T - T_g)$, where T_g is here defined as the thermodynamical glass transition temperatures of table 3.1 found from calorimetric measurements.

3.5.3 TTS

TTS stands for time temperature superposition and refers to the fact that, for some liquids, the shape of the alpha relaxation loss peak of some measured response function is temperature independent. TTS was assumed to hold for most liquids for many years (at least if no secondary relaxation was present to interfere with the alpha relaxation), but as an increasing number of exceptions to TTS was reported the interest deteriorated [Olsen, Christensen & Dyre 2001]. More recently it has been suggested that TTS

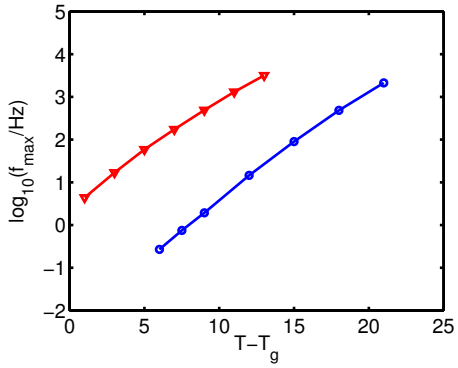

Figure 3.12 Loss peak frequency as a function of scaled temperature. Blue circles: DC705 ($T_g = 183$ K), red triangles: DBP ($T_g = 228$ K)

maybe after all is a more general feature, and that there is a correlation between TTS behavior and the high frequency slope of the alpha relaxation [Olsen et al. 2001, Nielsen, Christensen, Jakobsen, Niss, Olsen, Richert & Dyre 2009].

TTS is obeyed whenever a collapse of data is obtained by scaling the loss by the loss peak height and the frequency by the loss peak frequency. This type of TTS check, which is the most common, is shown in figure 3.13 for both DBP and DC705. The figure also shows an alternative TTS representation, namely the normalized Cole-Cole plot, which is a plot of the real part subtracted by the low frequency value, and normalized to the relaxation strength, versus the imaginary part normalized to the relaxation strength. The first thing to notice is the low frequency variation in slope for DC705. TTS is almost always seen on the low frequency side of the loss peak, and considering the already discussed problems with the low frequency behavior for this liquid, it is most likely that the lack of low frequency TTS is a result of these problems. On the high frequency side, however, DC705 shows clear TTS behavior, in agreement with reported shear measurements [Maggi et al. 2008]. For DBP the low frequency side shows TTS as expected, while there seem to be a small deviation from TTS on the high frequency side. This could be due to a beta process at higher frequencies and is consistent with results from shear measurements [Maggi et al. 2008].

3.5.4 Slope of the alpha relaxation

As mentioned in section 3.5.3, a correlation between the degree of TTS behavior and the high frequency slope of the relaxation has been found in dielectric data for a number of liquids [Nielsen et al. 2009]. According to these findings, liquids that obey TTS have an approximate slope of $-1/2$ of the high frequency loss. In the reported studies, the slopes (α) were found from dielectric data by taking the logarithmic derivative of the high frequency flank of the imaginary part of the spectrum:

$$\alpha = \frac{d \log \epsilon''}{d \log f}. \tag{3.21}$$

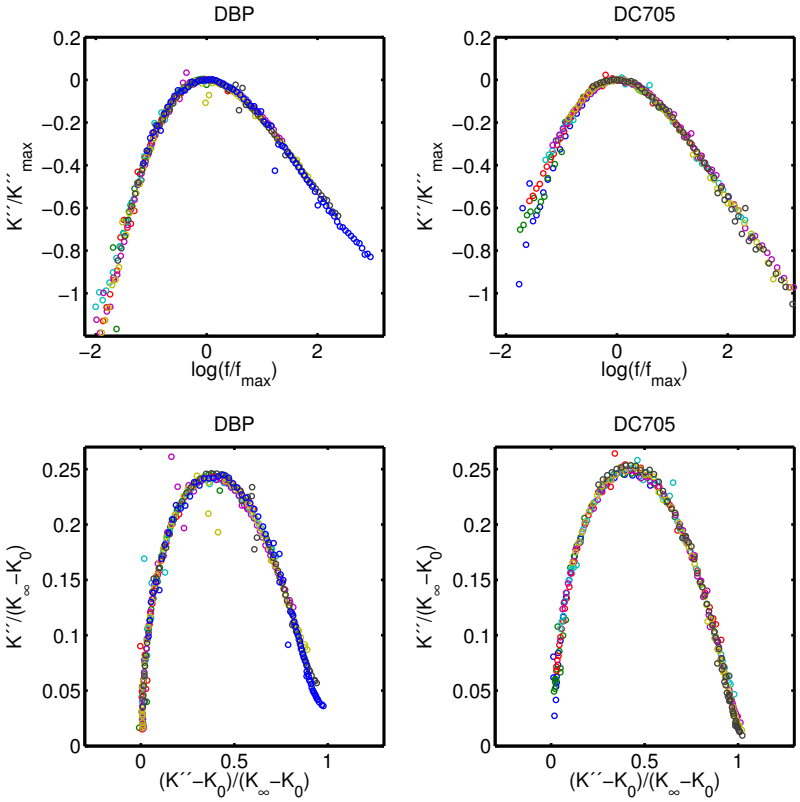

Figure 3.13 TTS plots of DBP (left) and DC705 (right).

The minimum slopes α_{min} are then found by minimizing this expression (α is a negative number). This procedure works well for dielectric data due to the low noise level, and have also been used on shear data [Maggi et al. 2008]. The bulk mechanical data have a considerable amount of noise compared to the dielectric data, which affects the determination of slopes found from this procedure. Figure 3.14 shows minimum slopes for both liquids found by a running fit of a straight line through 5 consecutive points. Although this should give less noise in the slopes, these are still very noisy making it very difficult to draw any conclusion on the minimum slope. From a visual inspection of figure 3.14 it seems that the slopes approach a value between -0.4 and -0.5 for both liquids. In order to get a better estimate of the slopes, a model expression is fitted to data.

The chosen fitting function is an extended Maxwell model ([Christensen & Olsen 1994]) and is shown in figure 3.15. The capacitor C_2 has been inserted to account for the low frequency value of the bulk modulus. The insertion of the constant phase element CPE in parallel with the resistor corresponds to replacing the static viscosity in the Maxwell model by a dynamical frequency dependent viscosity. The capacitance of the CPE is

$$C_{CPE}(\omega) = k(i\omega)^{-\alpha}, 0 < \alpha < 1, \tag{3.22}$$

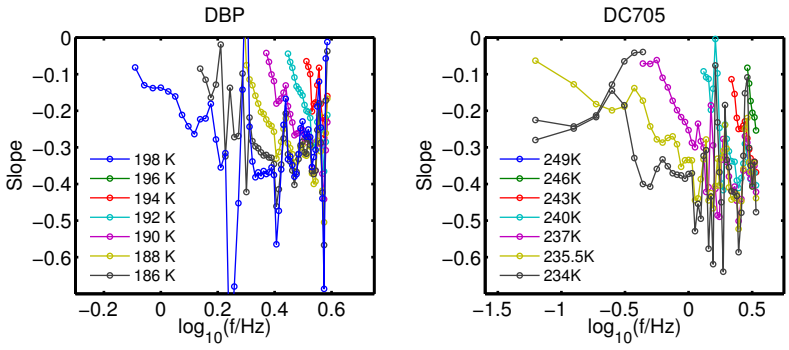

Figure 3.14 Minimum slopes of DBP (left) and DC705 (right). The curves are two noisy to extract a reliable value for the minimum slope, but there seem to be a tendency of an approach of α_{min} towards a value between -0.4 and -0.5.

where k has dimension of capacitance×time$^{-\alpha}$. The limits of α corresponds to a capacitor ($\alpha = 0$) and a resistor ($\alpha = 1$). The total capacitance of the circuit is then

$$C_{tot} = \frac{1}{\frac{1}{C_2} + \frac{1}{C_1 + \frac{1}{i\omega R} + k(i\omega)^{-\alpha}}}, \tag{3.23}$$

or in terms of the stiffness

$$S(\omega) = \frac{1}{C_{tot}(\omega)} = \frac{1}{C_2} + \frac{1}{C_1 + \frac{1}{i\omega R} + k(i\omega)^{-\alpha}}. \tag{3.24}$$

For low frequencies expression 3.24 reduces to $S(\omega \to 0) = S_0 = 1/C_2$, and for large frequencies $S(\omega \to \infty) = S_\infty = 1/C_2 + 1/C_1$, which means that $1/C_1 = S_\infty - S_0$. Hence the expression for the bulk modulus is (since $K(\omega) \propto S(\omega)$):

$$K = K_0 + \frac{K_\infty - K_0}{1 + \frac{1}{i\omega\tau_M} + q(\frac{1}{i\omega\tau_M})^\alpha}, \tag{3.25}$$

where $\tau_M = RC_1$ is the Maxwell relaxation time, and $q = k\frac{\tau_M^\alpha}{C_1}$ and α are fitting parameters expressing the width and the high frequency slope of the loss peak respectively.

Figure 3.13 shows that the shape of the alpha relaxation is to a good approximation constant in the measured temperature range, i.e. that TTS is obeyed, except maybe for the highest frequencies for DBP. This means that it is fair to use the same q and α for all temperatures when fitting the above expression to data. The following fitting procedure was followed: A peak was chosen in the middle of the temperature range with maximum number of data points on both flanks of the peak. The expression was fitted to this peak to give q and α. The remaining peaks was then fitted with the found q and α. The data and fits are shown in figure 3.10. For DBP the fitting returned $q = 1.4$ and $\alpha = -0.42$ and for DC705 $q = 96$ and $\alpha = -0.5$. The results are consistent with the findings of [Nielsen et al. 2009] that the high frequency side of

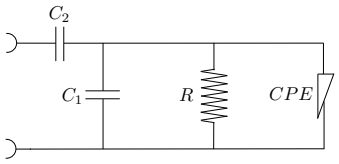

Figure 3.15 Electrical network model of the extended Maxwell model. The capacitor C_1 represents the strength of the bulk relaxation $\Delta K = K_\infty - K_0$ and the capacitor C_2 the low frequency limit of the bulk modulus K_0. The constant phase element CPE in parallel with the resistor R represents the dynamical bulk viscosity of the liquid.

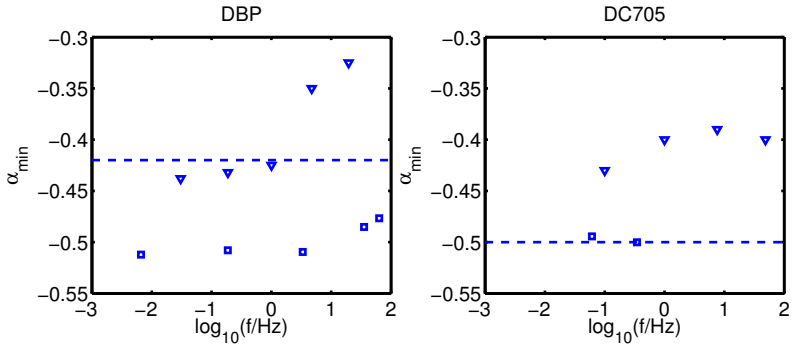

Figure 3.16 Minimum slopes of dielectric (squares) [Nielsen et al. 2009] and shear modulus (triangles) [Maggi et al. 2008] plottet together with the minimum slopes found from the fitting of the bulk modulus data.

the alpha relaxation approaches -1/2 at low temperatures if no secondary relaxation is present. The fact that the DBP data results in a numerically smaller slope could be due to the secondary relaxation seen in shear and dielectric data as mentioned earlier.

Figure 3.16 shows the minimum slopes for the two liquids found from shear modulus [Maggi et al. 2008] and dielectric measurements [Nielsen et al. 2009] together with the values from the bulk modulus data.

4 High pressure dielectric spectroscopy setup

As mentioned in the last chapter, more knowledge of the nature of viscous liquids can be obtained by measuring different response functions, and through the years the "Glass and Time"-group has developed a number of techniques for measuring different frequency (or time) dependent response functions as a function of temperature. It is however clear, that in order to fully understand the origin of the viscous slowing down, the influence of volume on the relaxation time, and the relative effect of volume and temperature is of key importance. High pressure measurements is a mean to study these effects, and during the last decade they have become increasingly employed in the field. Dielectric measurements are easy to perform and covers a large frequency range (typically at least $10^{-3} - 10^{6}$ Hz). Moreover the simplicity and robusteness of the dielectric cell makes it suited for high pressure measurements. The density scaling relation is an important result that to a large extent comes from high pressure dielectric spectroscopy. It has therefore been an ambition of the group to expand the experimental possibilities with a setup for high pressure dielectric spectroscopy, and a main objective of this PhD has been to acquire and implement such a setup. This chapter describes the acquired setup and some challenges involved with the implementation.

4.1 Dielectric spectroscopy

The dielectric constant ϵ is a measure of how polarized a material gets when subjected to an electric field $\mathbf{E}$. The displacement field $\mathbf{D}$ is given by

$$\mathbf{D} = \mathbf{P} + \epsilon_0 \mathbf{E}, \tag{4.1}$$

where the polarization $\mathbf{P} = \epsilon_0 \chi \mathbf{E}$, χ is the electric susceptibility and ϵ_0 is the vacuum permittivity. $\mathbf{D}$ can then also be expressed as

$$\mathbf{D} = \epsilon_0 \chi \mathbf{E} + \epsilon_0 \mathbf{E} \tag{4.2}$$

$$= \epsilon_0 \epsilon_r \mathbf{E}, \tag{4.3}$$

where $\epsilon_r = \chi + 1$ is the relative permittivity. The dielectric constant is then the the response function when the applied electric field is the input and the displacement field is the output. It has units of Farads per meter.

Unless the material is non-polar, the polarization of the material has two contributions: the induced polarization due to an almost instantaneous redistribution of the charges in a single molecule, and the rotational polarization that is due to a reorientation of the permanent dipoles.

In a measurement of the frequency dependent dielectric constant, the magnitude of the polarization and the phase difference between the field and the polarization is described by the complex permittivity $\epsilon(\omega)$. While the induced polarization only contributes to the level of the polarization, since this contribution is almost instantaneous, the frequency dependence of the dielectric constant is caused by the rotational polarization. At low frequencies, the dielectric constant will approach its equilibrium value, but at higher frequencies, the dipoles will not have time to adjust to the field, and the real part of the dielectric constant will reach a plateau that is lower than the equilibrium value.

$\epsilon(\omega)$ is measured by placing the liquid between two capacitor plates and measuring the complex frequency dependent capacitance:

$$C(\omega) = \epsilon_0 \epsilon_r(\omega) \frac{A}{d} \tag{4.4}$$

$$= \epsilon(\omega) C_{empty}, \tag{4.5}$$

where A is the area of the capacitor, d is the distance between the plates. C_{empty} is the capacitance of the empty capacitor.

4.2 The high pressure setup

The setup consists of a pressure vessel connected to a pump and a thermal bath, and a PVT probe that can be inserted in the pressure vessel. The pressure vessel (MV1), PVT probe and pump (type U111) was acquired from Unipress Equipment in Warsaw Poland, while the thermal bath is a Julabo F81-ME. The dielectric sample cell is homemade.

4.2.1 Sample cell and pressure vessel

The sample is placed between two stainless steel capacitor plates separated by a circular teflon spacer. The diameter of the plates is 19.5 mm and the distance between the plates depends on the spacer thickness, but typically spacers are 0.05 mm, thick resulting in an empty capacitance of 42.6 pF (disregarding the dielectric constant of the spacers). The capacitor is placed in a pressure vessel, where it is surrounded by a pressure transmitting fluid. When placed in the pressure vessel, the capacitor is wrapped in teflon and rubber to prevent the pressure medium from mixing with the sample while still allowing pressure to be transmitted to the sample. Electrical wires connect the capacitor to electrodes in the top plug of the pressure vessel, which are connected to the electronic equipment via 4 electrical feedthroughs. The plug is sealed with a combination of metal and rubber o-rings.

The pressure vessel is connected to a pump via a capillary in the bottom of the vessel. A thermostating jacket surrounds the pressure vessel, and a heat bath controls the temperature through a circulating cooling liquid. Finally the pressure cell and jacket is wrapped in an insulating material to minimize heat flow and to prevent ice formation on the vessel. Figure 4.1 shows a sketch of the pressure vessel without insulation, and table 4.1 shows the specifications of the vessel.

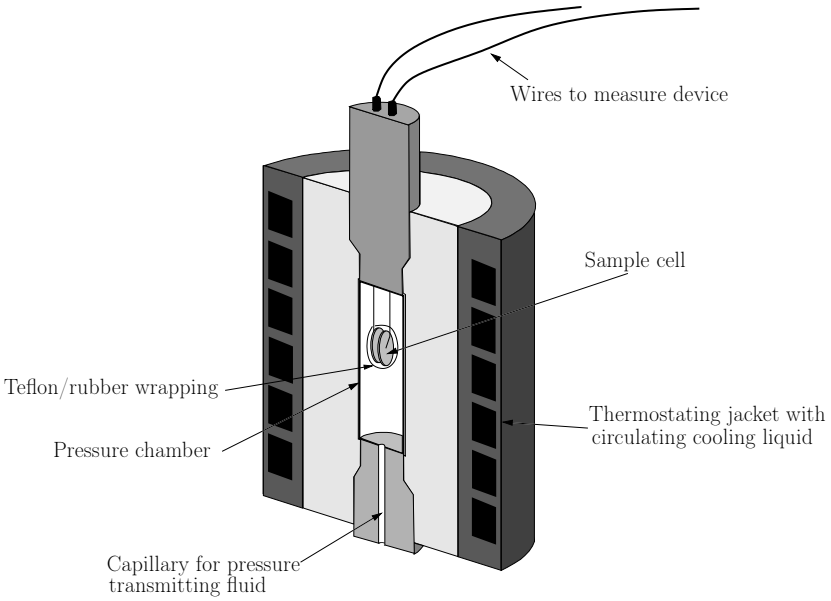

Figure 4.1 A sketch of the high pressure vessel.

Specifications of the pressure vessel	
P_{max}	600 MPa
T	173 K-393 K
Volume	50 ml
Inner diameter	30 mm
Inner height	70 mm
Material	CuBe25
Plug sealing	metal and rubber
Pressure medium	silicon oil
Cooling liquid	water + ethylene glycol

Table 4.1 Specifications of the pressure vessel.

Specifications of the PVT probe	
P_{max}	600 MPa
T-range	253 K-353 K
Volume	13 ml
Inner diameter	20 mm
Inner height	40 mm
Maximum displacement	20 mm
Material	Stainless steel
Sealing	Viton

Table 4.2 Specifications of the PVT probe.

4.2.2 PVT probe

The notion PVT refers to pressure-volume-temperature. In most experiments, the control variables are pressure and temperature. In order to determine the density or the volume as a function of pressure and temperature, PVT measurements are needed.

There are two main techniques for PVT measurements [Roland, Hensel-Bielowka, Paluch & Casalini 2005], the "piston-die"-technique, and the "confining fluid" -technique. The present type is a "piston-die" type and the prinsciple is the following: The PVT probe consists of a cylindrical sample container with a piston at the top. When the volume of the sample changes due to changes in temperature or pressure, the displacement of the piston is read by an $LVDT$ transducer which is connected to a measuring bridge. The volume change can then be calculated from the displacement of the piston. The PVT probe is placed in the pressure vessel, where pressure is transmitted through the pressure medium surrounding the probe. A sketch of the PVT probe inserted in the pressure vessel is shown in figure 4.2. The specifications of the probe is shown in table 4.2.

4.3 Temperature control

Temperature is controlled through a commercial heat bath (Julabo F81-ME) with a temperature range from 192 K to 373 K and a temperature stability of ± 0.02 K. The cooling capacity of the bath is the following (for ethanol as the cooling medium) [Julabo 2009]:

Temperature [°C]	20	0	−20	−40	−60	−80
Power [kW]	0.45	0.38	0.36	0.32	0.27	0.070
Cooling rate [C/min]	2.4	2.0	1.9	1.7	1.4	0.4

The cooling rates are calculated from the heat capacity of ethanol.

Initially a silicon oil was used as cooling medium, but due to problems with electrostatic discharges caused by ice crystals in the oil, an alternative was needed. A mixture of water and glycol is now used in stead. There has been no electrical interference from the cooler with this mixture, and although the temperature range of the water-glycol

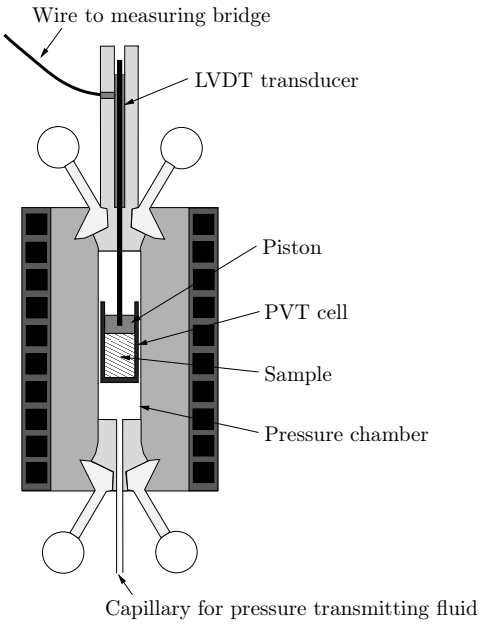

Figure 4.2 A sketch of the PVT probe when inserted in the high pressure vessel.

mixture (253 K to 353 K) is narrower than the silicon oil, the former is adequate for many measurements. The temperature of the bath can be controlled both manually at the display of the cooler and from a computer. The bath fluid is circulated around the pressure cell through insulated rubber tubes. A thermocouple measures the temperature in a small hole in the cell close to the sample chamber.

4.4 Temperature callibration

The temperature of the thermocouple is calibrated against a thermometer through the following procedure with the thermocouple and thermometer placed in the bath: the temperature of the bath is set, and temperature of thermometer and thermocouple voltage is measured after temperature equilibrium is established. Temperature of thermocouple is calculated by a shape preserving piecewise cubic interpolation of thermometer temperature as a function of thermocouple voltage for measured 17 points ranging from 233-313 K. The internal thermometer of the cooler is not calibrated against the thermometer, and shows at the moment approximately a 1 degree difference from the thermocouple. This means that the set temperature is off by approximately 1 degree.

4.5 Pressure control

Pressure is controlled from a commercial pump that can provide pressures up to 700 MPa. The pump has two settings for pressure application: auto and manual. In the

auto setting, the final pressure is set on a display and the pump gradually increases pressure until the preset value is reached. In case of subsequent pressure drops beyond 3 MPa, the pump will automatically reestablish the preset pressure level. In the manual setting, pressure is increased gradually by pushing down a button until the desired pressure is reached. No automatic adjustment of pressure exist for the manual setting. The rate with witch pressure is build up is adjusted by a turning knob. An electrical output from a high pressure transducer in the pump is available for data acquisition.

4.6 Limitations and uncertainties

The uncertainty on the measured pressure is not stated by the manufacturer, but provided that the build in pressure transducer measures relatively accurate, the uncertainty on the actual pressure in the vessel should be small. Pressure stability is limited by the preset allowed pressure drop of 3 MPa as mentioned above.

The temperature stability provided by the cooler is relatively accurate (± 0.02 degrees as stated by the manufacturer). The stability in the vessel on the other hand is not necessarily stable since room temperature variations could potentially affect the temperature in the vessel. The insulation and the thermal inertia of the vessel however should smooth out most of these temperature variations. This is supported by a study of the temperature stability where the relaxation time as a function of time was measured at constant temperature over a period of 57 hours, and this was not found to fluctuate significantly during the measuring period [Olsen & Videnkjær 2010].

Although the temperature in the vessel is measured close to the sample (see figure 4.1), we can not be sure that there is no temperature gradient throughout the vessel. Provided that the temperature at the sample as a function of the temperature in the bath is constant, the best way to determine the relation between measured temperature by the thermocouple and the actual temperature at the sample is to compare an ambient pressure dielectric measurement with a corresponding measurement in another setup, and determine the temperature from the position (frequency) of the loss peaks.

When performing PVT measurements by the "piston-die" technique, it is essential that the sample remains liquid so that a hydrostatic pressure is maintained. This means that measurements near the glass transition, where the shear modulus is comparable to the bulk modulus, yields unreliable results [Zoller & Walsh 1995]. Other possible sources of uncertainty is leakage around the piston, and friction between the piston and the sides of the cylinder.

In the "confining fluid" technique for PVT measurements, the sample is surrounded by a confining fluid, often mercury or silicone oil [Roland et al. 2005]. Volume changes of the sample and confining fluid is monitored and the volume of the sample is determined by subtraction of the volume of the confining fluid. This technique has the advantages compared to the "piston-die" -technique that the problems with friction and leakage and with maintaining hydrostatic pressure is avoided [Zoller & Walsh 1995]. Disadvantages is potential interaction between the sample and the confining fluid and that the PVT properties of the confining fluid must be known precisely and that the confining fluid must remain liquid during the measurement. An example of a commercial PVT apparatus is the GNOMIX apparatus, which has been used for the data presented in chapters 6 and 7). This apparatus has a temperature range from room temperature

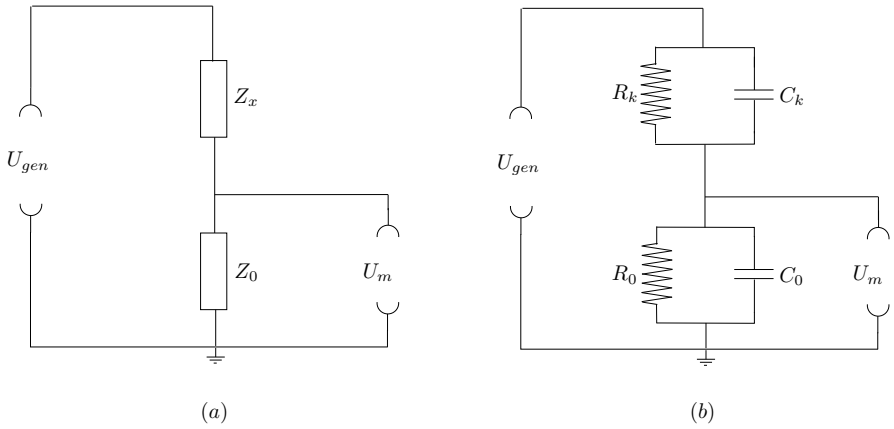

Figure 4.3 (a) Voltage divider technique for measuring impedance of sample capacitor Z_x. (b) Setup for determining internal impedance (C_0 and R_0) in terms of known values of R_k and C_k.

to above 400 ℃, and a pressure range up to 200 MPa. When studying liquids outside the experimental window of the PVT apparatus, one has to rely on extrapolations of the data. An advantage of the present "piston-die"-setup compared to the GNOMIX apparatus is that the temperature and pressure range of the former is more suited for measurements on the typical liquids (T_g below room temperature) studied by the "Glass and Time"-group, which minimizes the necessary extrapolation.

4.7 Data acquisition

The electronic equipment for measuring the dielectric constant in the high pressure setup is the standard equipment combination used for measuring capacitances in most of the setups in the Roskilde University lab. The setup is described in great detail in [Igarashi et al. 2008b], but some modifications have been made for the high pressure setup due to problems with conductivity. These modifications will be described in the following.

For measuring capacitances from 1 mHz to 100 Hz a custom-built frequency generator in combination with an Agilent 3458A multimeter is used, while a commercial Agilent E4980A LCR meter is used at frequencies from 100 Hz to 100 kHz .

4.7.1 Callibration of the multimeter

When measuring with the frequency generator and the multimeter, capacitance of the sample capacitor is not measured directly, but instead voltage is measured through a voltage divider as shown in figure 4.3 (a), which shows a diagram of the standard setup. The generator supplies voltage V_{gen} and the multimeter measures voltage V_m across a

known dummy load Z_0. The impedance of the sample capacitor is then

$$Z_x = \frac{V_x}{I_x} = \frac{V_{gen} - V_m}{V_m/Z_0} = Z_0(\frac{V_{gen}}{V_m} - 1). \tag{4.6}$$

In order to maximize the sensitivity of the measured voltage to changes in the sample impedance, the known load Z_0 should match Z_x. The sample cell can be modeled as a capacitor C in parallel with a resistor R, where the resistor represents any energy loss due to for instance leakage currents. Therefore Z_0 is chosen as a parallel connection of a resistor R_0 and a capacitor C_0, and the magnitudes of R_0 and C_0 are chosen to be similar to the magnitudes of R and C of the dielectric cells used. Typical values of dielectric cells and transducers used in the setups are from 100 pF to 25 nF. For the standard setup, C_0 is 10 nF and R_0 is around $10^9\Omega$.

In order to determine the precise values of R_0 and C_0, a calibration is needed. This is done by doing a multimeter measurement where the sample cell is replaced with a known capacitor C_k and the dummy load is treated as the unknown. The resistor R_k represents leakage currents in C_k. Through the calibration C_0 and R_0 are determined by adjusting R_k to obtain values of C_0 that are close to frequency independent. When Z_0 is determined, the frequency dependent impedance $Z(\omega)$ is calculated from equation 4.6 knowing V_{gen} and measuring V_m. Typical values of R_k are $10^{12} - 10^{14}\Omega$.

In the standard setups, special care is taken to minimize leakage currents in the different components and connections. The room temperature resistance between the plugs connecting the sample capacitor to the coaxial cables to the equipment is for instance of the order $T\Omega$. In the high pressure setup, the fact that the feedthroughs have to maintain pressures up to 600 MPa puts some constraints on the material that can be used for the feedthroughs. As a consequence, the pyrophyllite-sealed feedthroughs used have a room temperature resistance between the feedthroughs of the order $0.5 - 1G\Omega$. Drying of the plugs was tried, since pyrophyllite is hygroscopic, but this had no effect on the resistance. In addition, although a pressure medium (a silicon oil) is chosen with very low conductivity, it turns out that the conductivity of the oil does give some signal at low frequencies. Attempts to eliminate this effect was made in the form of electrical insulation of the electrodes and wires, but with little effect. As a result of these effects, a significant amount of the current will run through R_k at low frequencies, and this will give a contribution to the calculated capacitance.

Figure 4.4 shows the different potential leakage currents in the setup. R_1 is the leakage current through the oil, R_2 is the current running from the low voltage side of the sample capacitor to ground, and R_3 represents the leakage current from the high voltage side of the sample capacitor to ground. The leakage current between the feedthroughs due to conductivity of the electrode material are included in R_k.

In principle one could model ones way out of all these leakage currents and this was also tried, but the problem is that they are temperature dependent and not very reproducible, and it has not been possible to eliminate them.

To simplify the modeling, the different leakage contributions can be collected in a few contributions by moving the multimeter so that voltage is measured over the sample. This way all the leakage currents go to ground and they can hence be collected in a single resistor element. This new setup is shown in figure 4.5. The resistor R_1 represents all the mentioned leakage currents. Since this modification was done at a very late point, a successful calibration has not been obtained with this setup yet.

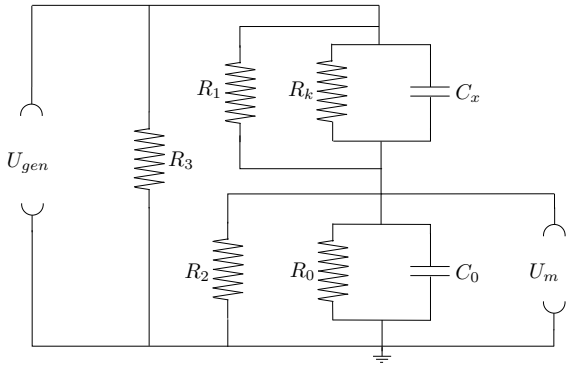

Figure 4.4 Diagram of the pathways of leakage currents in the standart setup. R_1 is the leakage current through the oil, R_2 is the current running from the low voltage side of the sample capacitor to ground, and R_3 represents the leakage current from the high voltage side of the sample capacitor to ground. The leakage current between the feedthroughs due to conductivity of the electrode material are included in R_k.

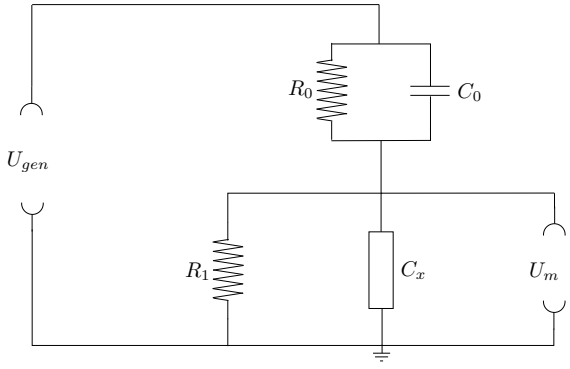

Figure 4.5 Diagram of the new setup with the pathway of leakage current. All leakage currents go to ground and can hence be collected in a single resistor element.

5 Strongly correlating liquids and isomorphs

This chapter gives an introduction to the relevant results and theory related to the concept of strongly correlating liquids and isomorphs, which is the basis of chapters 6 to 8. The development of the theoretical framework of strongly correlating liquids and isomorphs has been and are still developing fast. In order to give an understanding of the interplay between theory, computer simulations and experiments within this framework, the theoretical framework and the relevant results are here presented historically.

5.1 Background

5.1.1 Experimental findings

Density scaling

A simple model of molecules in a liquid is the soft sphere model, where the particles are modeled as spheres with only repulsive interactions, described by a pair potential $U \propto r^{-n}$. The notion soft refers to the fact that the particles do not have a characteristic size or radius. For soft spheres interacting through a repulsive pair potential, the relaxation time can be scaled by $\rho T^{-3/n}$. Inspired by this, Tölle [Tölle 2001] was among the first to show that the relaxation times (nanosecond time scale) of liquid oTP (orthoterphenyl) could be scaled by $\rho T^{-1/4}$. [Dreyfus, Aouadi, Gapinski, Matos-Lopes, Steffen, Patkowski & Pick 2003] was the first to show this scaling of the relaxation time measured over more than 10 orders of magnitude by light scattering for oTP with the same exponent.

A more general formulation without reference to interaction potentials was given by Alba-Simionesco *et al* [Alba-Simionesco, Kivelson & Tarjus 2002], who proposed the following expression:

$$\tau(\rho, T) = F\left(\frac{e(\rho)}{T}\right). \tag{5.1}$$

[Alba-Simionesco, Cailliaux, Alegria & Tarjus 2004] tested this expression with both a powerlaw and a linear dependence of $e(\rho)$ and found it to work for a number of glass-forming polymers, with no significant difference in the quality between the two functions. Casalini and Roland [Casalini & Roland 2004b] tested the power-law scaling on different glass formers and found it to work with different system specific exponents ranging from less than 1 to more than 8.

Density scaling has been confirmed for a number of liquids by several goups (see e.g. [Alba-Simionesco et al. 2002],[Tarjus, Kivelson, Mossa & Alba-Simionesco 2004],[Roland

et al. 2005],[Dreyfus, Grand, Gapinski, Steffen & Patkowski 2004]). More recently is has been shown that not all liquids obey density scaling, for example hydrogen bonded liquids, while it is quite established that van der Waals liquids do obey scaling in the power law form [Roland, Casalini, Bergman & Mattson 2008].

Isochronal superposition

For some liquids the shape of the dielectric loss peak is determined by the average relaxation time, i.e. state points with different temperature and pressure but same relaxation time, have the same relaxation spectra. This is called isochronal superposition. [Ngai, Casalini, Capaccioli, Paluch & Roland. 2005] showed that isochronal superposition was possible for a number of viscous liquids, but reported hydrogen bonded liquids as exceptions. This is supported by a study by [Nielsen et al. 2009] of a collection of different systems.

5.1.2 Computer simulations

Pressure-energy correlations

Independently of the experimental findings mentioned above, Pedersen *et al* [Pedersen, Bailey, Schrøder & Dyre 2008] found strong correlations between the instantaneous values of the configurational parts of pressure (the virial) and energy (potential energy) in a simulation of a Lennard-Jones liquid at constant volume. The Lennard-Jones potential ,$v_{LJ}(r)$, is a commonly used pair potential for simulating systems with van der Waals like interactions, which are weak attractive interactions resulting from induced dipole-induced dipole interactions. It is given by:

$$v_{LJ}(r) = 4\epsilon \left[\left(\frac{\sigma}{r}\right)^{12} - \left(\frac{\sigma}{r}\right)^{6} \right], \tag{5.2}$$

where r is the distance between two particles, σ is a characteristic length, and ϵ has dimensions of energy. The van der Waals interactions are represented in the r^{-6}-term, while the r^{-12}-term is chosen for convenience.

The virial, W, is the term that is added to the ideal gas term of pressure reflecting the interactions for systems with configurational interactions:

$$p = Nk_BT/V + W/V, \tag{5.3}$$

where p is pressure, N is the number of particles, k_B is the Boltzmann constant, T is temperature and V is volume. The virial is defined by

$$W = -\frac{1}{3}\Sigma \mathbf{r}_i \cdot \nabla_{\mathbf{r}_i} U, \tag{5.4}$$

where $U(\mathbf{r}_1, ..., \mathbf{r}_N)$ is the potential energy function.

The energy E for systems with configurational interactions is similarly the sum of kinetic (K) and potential (U) contributions:

$$E = K + U. \tag{5.5}$$

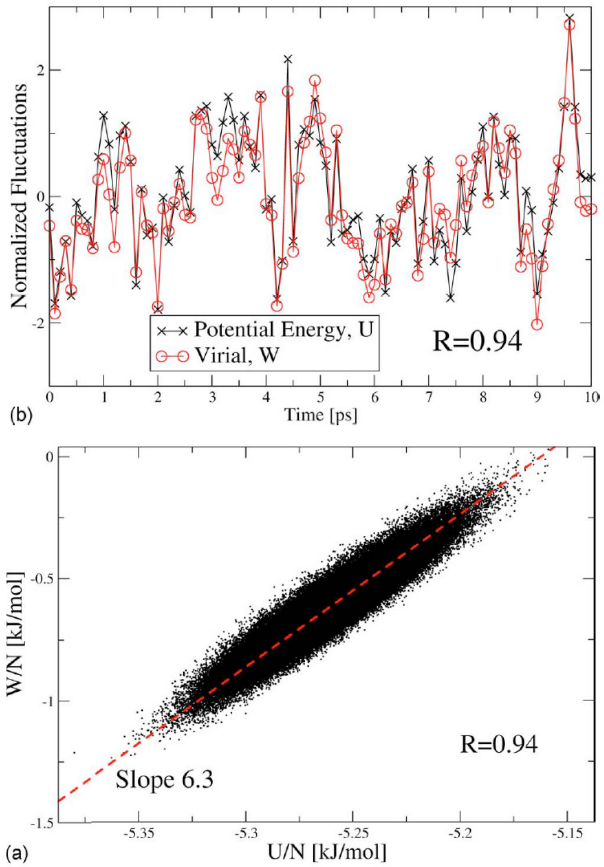

Figure 5.1 The top plot shows equilibrium fluctuations of potential energy U and virial W for a simulation in the NVT ensemble (at ρ=34.6 mol/l, T=80 (argon units), time averaged pressure 1.5 MPa) of a system of identical molecules interacting through the Lennard-Jones potential. The correlation between U and W is R=0.94. The bottom plot shows a scatter plot of the instantaneous values of U and W from the simulation of the top plot. The ellipse has a slope γ of 6.3. [Bailey et al. 2008b]

The kinetic energy and the ideal gas term are functions of particle momenta, while the potential energy and the virial are functions of particle positions.

For a system at constant volume in thermodynamic equilibrium at a given state point, the instantaneous total energy $E(t)$ and pressure $p(t)$ will fluctuate around their mean values $\langle E \rangle$ and $\langle p \rangle$.

Surprisingly, Pedersen *et al* [Pedersen et al. 2008] found that when looking at the fluctuations of the configurational parts of pressure and energy seperately, they followed each other closely as seen in the top plot of figure 5.1.

The degree of WU-correlations can be quantified in terms of the correlation coefficient:

$$R = \frac{\langle \Delta W \Delta U \rangle}{\sqrt{\langle (\Delta W)^2 \rangle \langle (\Delta U)^2 \rangle}}, R \leq 1, \tag{5.6}$$

where Δ refers to the deviation from the equilibrium value: $\Delta W(t) = W(t) - \langle W \rangle$. The correlation coefficient of the data of figure 5.1 is $R = 0.94$. Strong correlations were defined as $R > 90\%$ [Pedersen et al. 2008]. Figure 5.1 bottom shows a scatter plot of W and U for the same state point as the top plot. The strong correlations are evident from the elongation of the ellipse. The line through the points represents the slope γ of the ellipse, which gives the proportionality constant of the fluctuations: $\Delta W \simeq \gamma \Delta U$. For the data of figure 5.1 $\gamma = 6.3$.

Systems interacting through pair potentials of the form $v(r) = ar^{-n} + v_0$ exhibit perfect $W - U$ correlations (R=1), where $\Delta W(t) = n/3 \Delta U(t)$. The first assumption was therefore to search for an explanation for the strong $W-U$-correlations in the repulsive term of the Lennard-Jones potential. Although this would give $\gamma = 4$ for the Lennard-Jones system, the found $\gamma = 6.3$ was explained in terms of an "effective" exponent found by fitting an inverse power law to the Lennard-Jones potential [Pedersen et al. 2008].

Density scaling

Subsequently, Coslovich and Roland [Coslovich & Roland 2008] studied a number of Lennard-Jones systems and found that these liquids obeyed density scaling with the density scaling exponent to a good approximation given by the "effective" exponent of the repulsive part of the LJ-potential.

The found connection between the slope of the WU-correlations in a scatter plot and the "effective" exponent of the repulsive part of the potential on one hand [Pedersen et al. 2008], and between the "effective" exponent (although defined slightly different than in [Pedersen et al. 2008]) of the repulsive part of the potential and the density scaling exponent on the other hand [Coslovich & Roland 2008], inspired the theory that the density scaling exponent is given by the WU correlations. This was demonstrated by both Schrøder et al [Schrøder, Pedersen, Bailey, Toxværd & Dyre 2009] and Coslovich and Roland [Coslovich & Roland 2009].

5.2 Scale invariance

As mentioned above, inverse power law (IPL) systems has perfect correlations between virial and potential energy $W = \gamma U$, where $\gamma = n/3$. This follows from the definition of the virial (equation 5.4).

Inverse power law liquids are simple in the sense that they are scale invariant, meaning that they have no characteristic length and time. This means that, when expressed in reduced units, a number of properties are given by a single scaling variable ρ^γ/T, where ρ is density and T is temperature. For instance, the reduced unit relaxation time, $\tilde{\tau} = \frac{\rho^{1/3}}{\sqrt{m/k_B T}} \tau$ is a function of ρ^γ/T, which means that density scaling applies perfectly.

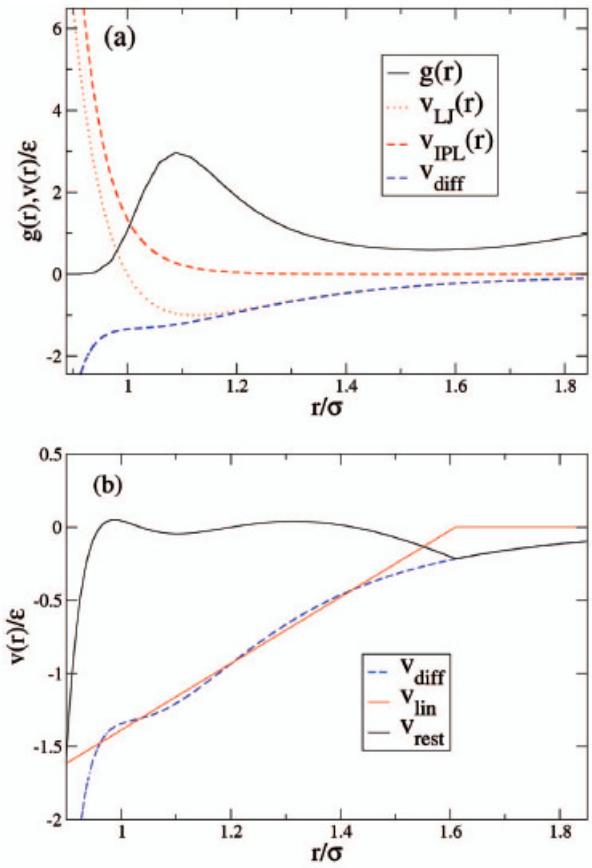

Figure 5.2 Top: Illustration of the difference between the LJ potential $v_{LJ}(r)$, an inverse power law potential $v_{IPL}(r)$ (n = 18.9) and their difference v_{diff}. Bottom: The difference v_{diff} plotted with a linear fit v_{lin} and the rest v_{rest}. [Schrøder et al. 2009]

Strong WU-correlations in Lennard-Jones liquids can be understood in terms of a so called extended effective inverse power law potential [Bailey et al. 2008b, Schrøder et al. 2009]. Figure 5.2 shows the Lennard-Jones potential plotted together with an inverse power law potential with exponent 18.9 and the difference between the two potentials. The bottom of the figure shows the difference plotted with a linear fit. As seen the linear fit fits the difference term relatively well over the region of the first peak of the radial distribution function. This means that the LJ-potential can be approximated by an inverse power law term, a linear term and a constant [Bailey et al. 2008b, Schrøder et al. 2009]:

$$v_{LJ} \simeq Ar^{-n} + B + Cr, \tag{5.7}$$

where A, B and C are constants. The contribution from the linear term to W and U fluctuates little at constant volume (the decrease in one nearest-neighbor interatomic distance is (almost) balanced by the increase of another so that the sum remains

almost constant), which explains the resemblance of the LJ-potential to IPL-potentials as regards WU-correlations [Gnan, Schrøder, Pedersen, Bailey & Dyre 2009]. As a consequence, LJ potentials inherits a number (but not all) of the IPL-properties.

In [Bailey, Pedersen, Gnan, Schrøder & Dyre 2008a] 13 different systems were studied regarding W-U correlations. The results showed that liquids with van der Waals type interactions and metallic liquids are strongly correlating, while systems with competing interactions and network forming liquids are not. Hence hydrogen bonded, covalently bonded and strongly ionic liquids are not strongly correlating.

5.3 Isomorphs

The properties of strongly correlating liquids are summarized in the concept of isomorphs, which are curves in the phase diagram along which a number of properties are invariant. For any liquid it is possible to create curves in its phase diagram with some constant property, like constant reduced unit relaxation time, constant excess entropy and constant isochoric specific heat. Only IPL liquids have exact isomorphs, which means that these properties fall on the same line. Strongly correlating liquids have isomorphs to a good approximation [Gnan et al. 2009].

5.3.1 Definition of isomorphs

Two state points (1) and (2) with temperatures T_1 and T_2 and densities ρ_1 and ρ_2, respectively, are isomorphic if any two physically relevant configurations of state points (1) and (2), $(\mathbf{r}_1^{(1)}, ..., \mathbf{r}_N^1)$ and $(\mathbf{r}_1^{(2)}, ..., \mathbf{r}_N^2)$, which trivially scale into one another,

$$\rho_1^{1/3}\mathbf{r}_i^{(1)} = \rho_2^{1/3}\mathbf{r}_i^(2), \tag{5.8}$$

where $i = 1, ..., N$, have proportional configurational Boltzmann statistical weights:

$$e^{-U(\mathbf{r}_1^1,...,\mathbf{r}_N^{(1)})/k_BT_1} = C_{12}e^{-U(\mathbf{r}_1^2,...,\mathbf{r}_N^{(2)})/k_BT_2}. \tag{5.9}$$

[Schrøder, Gnan, Pedersen, Bailey & Dyre 2011, Gnan et al. 2009] The constant C_{12} depends only on the state points (1) and (2). For IPL liquids C_{12} is 1.

Not all IPL invariants give rise to general isomorph invariants. IPL properties involving volume derivatives do not give rise to isomorph invariants [Gnan et al. 2009]. One important isomorph invariant is the scaling variable

$$\frac{\rho^\gamma}{T} = constant, \tag{5.10}$$

where γ is the slope of the WU-correlations.

There are 3 ways of determining γ in terms of the equilibrium fluctuation averages of W and U:

$$\gamma_1 = \frac{\langle \Delta W \Delta U \rangle}{\langle (\Delta W)^2 \rangle}, \gamma_2 = \sqrt{\frac{\langle (\Delta W)^2 \rangle}{\langle (\Delta U)^2 \rangle}}, \gamma_3 = \frac{\langle (\Delta W)^2 \rangle}{\langle \Delta W \Delta U \rangle}. \tag{5.11}$$

These are identical for perfectly correlated WU-fluctuations, i.e. for inverse power law systems, but will vary slightly for strong correlations. γ_1 is the exponent one gets for a configurational adiabat, i.e. a line with constant excess entropy [Gnan et al. 2009]. γ_1 will from now on be refered to as γ_{isom}.

5.3.2 Density dependence of γ

It has recently been shown [Ingebrigtsen, Bøhling, Schrøder & J. C. Dyre 2011] that for a strongly correlating liquid in the NVT ensemble, temperature and is a product of a function of the excess entropy S_ex and a function of the density $g(\rho)$:

$$T = f(S)g(\rho). \tag{5.12}$$

γ_1 of equation 5.11 is also given by [Gnan et al. 2009]:

$$\gamma_{isom} = \left(\frac{\partial \ln T}{\partial \ln \rho}\right)_{S_{ex}} = \left(\frac{\partial \ln T}{\partial \ln \rho}\right)_{\tilde{\tau}}. \tag{5.13}$$

It follows from equation 5.12 that

$$d\ln T = d\ln f(S) + d\ln g(\rho), \tag{5.14}$$

which along an isomorph means

$$d\ln T = d\ln g(\rho). \tag{5.15}$$

From equation 5.13 it then follows that

$$\gamma_{isom} = \frac{d\ln g(\rho)}{d\ln \rho}, \tag{5.16}$$

which means that γ_{isom} depends on density only. This is tested experimentally in chapter 7.

5.3.3 Aging behaviour

It follows from the definition of isomorphs in section 5.3.1, that jumps between state points on an isomorph takes the system to equilibrium instantaneously if the system was at equilibrium initially. Furthermore, two jumps from two mutually isomorphic state points to a third state point which is not isomorphic to the two initial state points follow the same relaxation pattern for all physical quantities. In summary, isomorphic state points are equivalent during any aging process [Gnan et al. 2009].

These theoretical predictions have been confirmed in computer simulations [Gnan et al. 2009], the results of which are shown in figure 5.3. The top figure shows potential energy relaxation after three different jumps: a jump between two isomorphic state points (1 to 2), a jump between two different isochoric state points to a third state point (3 to 2 and 4 to 2). Jumps 3 to 2 and 4 to 2 both show slow relaxation, while the isomorphic jump (1 to 2) does not show any relaxation. This shows that the two non-isomorphic jumps are out of equilibrium, while the isomorphic jump takes the liquid to equilibrium instantaneously. The bottom of figure 5.3 shows the potential energy as a function of time for two jumps from state points on the same isomorph to a third state point which is isochoric to one of the two initial state points. The potential energy relaxes in both cases, and the relaxation behavior is identical for the two jumps.

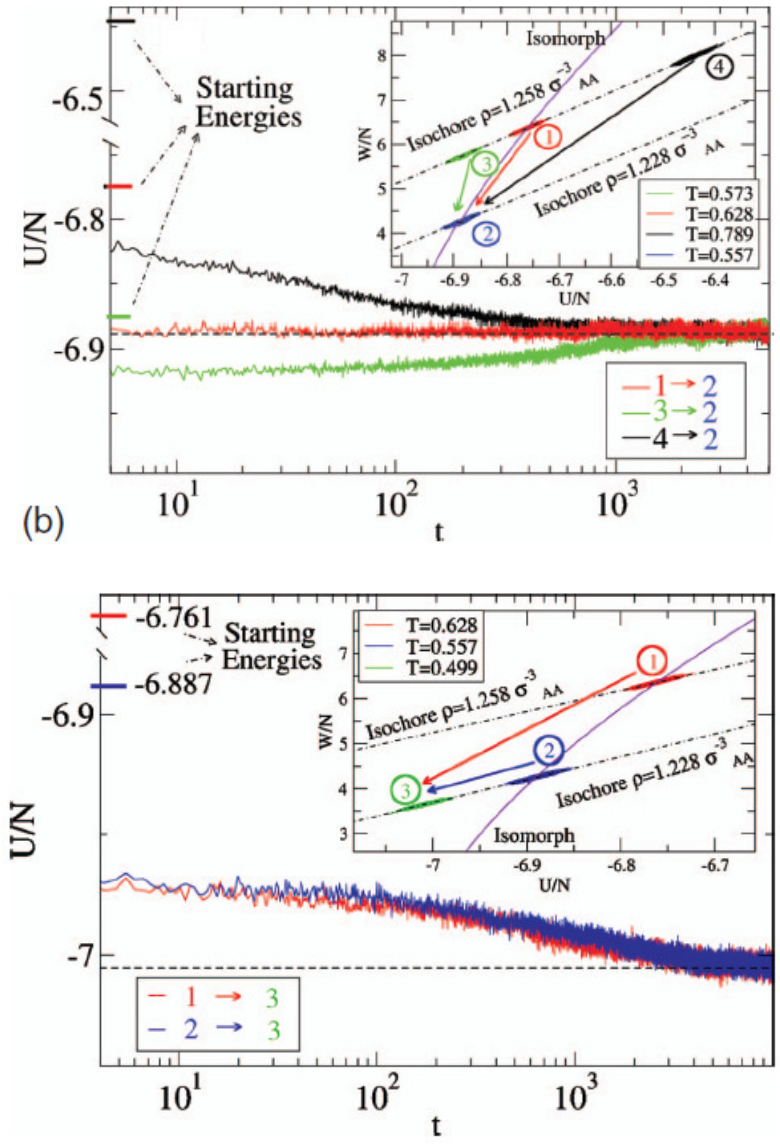

Figure 5.3 Simulation results for different jumps between state points. The plots shows potential energy per particle as a funciton of time. Top: potential energy relaxation after three different jumps from state points on an isochore. The two jumps from state points (3 and 4) that are not isomorphic to the final state point (2) shows two different relaxation patterns. The jump between two isomorphic state points (1 and 2) shows no relaxation. Bottom: potential energy relaxation after two jumps from mutually isomorphic state points (1 and 2) to a third state point (3) which is ischoric to state point 2. The relaxation pattern is identical for the two jumps. From [Gnan et al. 2009].

6 Prediction 1: $\gamma_{scale} = \gamma_{isom}$

As mentioned in the previous chapter, it follows from the isomorph theory that the density scaling exponent is identical to the fluctuation exponent. The predicted equality between γ_{scale} and γ_{isom} was shown to hold for a number of computer simulated liquids as mentioned in section 5.1.2 of the previous chapter. This chapter describes the first experimental test. In order to do so, the density scaling exponent, determined in the usual way through high pressure dielectric measurements, is compared to the fluctuation exponent, which, as will be shown in section 6.1, can be determined through linear response data.

6.1 From computer simulations to experiments

In computer simulations, instantaneous values of thermodynamic variables like pressure and energy can be calculated for a given ensemble of molecules at any given time. In experiments, obviously it is not possible to monitor the instantaneous values of the variables, but information on the fluctuations of these variables can be obtained from linear response measurements through the fluctuation dissipation theorem (FDT) as described in section 2.2.2.

γ_{isom} is given by the fluctuations of the configurational parts of pressure and energy as described in section 5.1.2. Unfortunately these are not directly experimentally accessible, as pressure and total energy fluctuations are, but this problem is solved by the nature of viscous liquids in the following way: When the liquid is cooled or compressed, the rearrangement of the molecules slows down, while vibrations of the molecules around their equilibrium positions stays fast (on a timescale of picoseconds). Recall the expressions for instantaneous pressure and energy, equations 5.3 and 5.5. The fluctuations of the kinetic terms results from the vibrations while the potential energy and virial has both fast fluctuations resulting from the vibrations and slower resulting from the configurational rearrangement. On the timescales that we measure linear response (we will call this timescale $\bar{t}$), which is a time scale much longer than picoseconds, but much shorter than the alpha relaxation time, the time average of the fast uncorrelated fluctuations will be constant, hence

$$p(\bar{t}) = Nk_B\langle T\rangle + W(\bar{t})/V \tag{6.1}$$

and

$$E(\bar{t}) = \langle K\rangle + U(\bar{t}), \tag{6.2}$$

From equations 6.1 and 6.2 it follows that $\Delta E(\bar{t}) = \Delta U(\bar{t})$ and $V\Delta p(\bar{t}) = \Delta W(\bar{t})$. This is illustrated in figure 6.1, which shows a sketch of the fluctuations of kinetic and configurational contributions to the energy and the total energy. On the timescale of $\bar{t}$

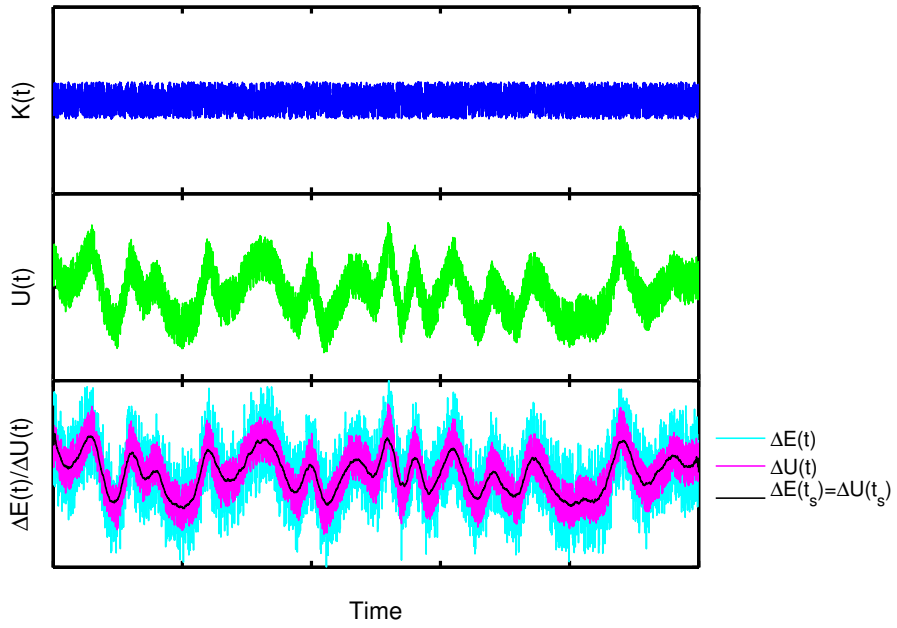

Figure 6.1 Illustration of instantantaneous fluctuations energy. The top shows the fast kinetic fluctuations resulting from the vibrations of the molecules, and the middle shows the potential energy fluctuations resulting from both vibrations and configurational rearrangements. The bottom plot shows the deviation from equilibrium of total energy and potential energy. When averaged over a timescale much longer than the vibrations but shorter than the configurational contributions, the fluctuations in total energy is equal to the fluctuations of the configurational parts.

the fluctuations in total energy is equal to the fluctuations of the configurational parts.

Since the instantaneous values of W and U are strongly correlated, their time averages ($W(\bar{t})$ and $U(\bar{t})$) will also be strongly correlated.

From the above considerations γ_{isom} can now be expressed in terms of experimentally accessible quantities:

$$\gamma_{isom} = \frac{\langle \Delta W \Delta U \rangle}{\langle (\Delta U)^2 \rangle} \simeq \frac{V \langle \Delta p \Delta E \rangle}{\langle (\Delta E)^2 \rangle}. \tag{6.3}$$

Energy and pressure are related to heat capacity and pressure coefficient through the FDT. In the frequency domain the FDT for the specific heat ($c_V = \frac{T}{V}(\frac{\partial S}{\partial T})_V$) is [Nielsen & Dyre 1996]:

$$k_B T^2 V c_V(\omega) = \langle (\Delta E)^2 \rangle - s \int_0^\infty \langle \Delta E(0) \Delta E(t) \rangle e^{-st} dt, \tag{6.4}$$

where $\langle \Delta E(0) \Delta E(t) \rangle$ is the autocorrelation function of the total energy fluctuations in equilibrium. $s = i\omega$ is the Laplace frequency. In the low frequency limit ($\omega \to 0$), this

reduces to:

$$c_V(0) = \frac{1}{k_B T^2 V}\langle(\Delta E)^2\rangle, \tag{6.5}$$

which is the ordinary dc specific heat. The high frequency limit corresponds to the glassy response where the structure is frozen in. In this limit ($\omega \to \infty$), only small values of $\bar{t}$ gives contributions to the integral of equation 6.4, and hence

$$-s\int_0^\infty \langle\Delta E(0)\Delta E(\bar{t})\rangle e^{-s\bar{t}}d\bar{t} = -\langle(\Delta E)^2\rangle^{structure}\cdot s\int_0^\infty e^{-s\bar{t}}d\bar{t} \tag{6.6}$$

$$= -\langle(\Delta E)^2\rangle^{structure} \tag{6.7}$$

$$\tag{6.8}$$

since we are still looking at the timescale of $\bar{t}$. The high frequency value of the specific heat is then

$$c_V(\infty) = \frac{1}{k_B T^2 V}\left(\langle(\Delta E)^2\rangle - \langle(\Delta E)^2\rangle^{structure}\right). \tag{6.9}$$

It follows then that the structural fluctuations of energy can be expressed in terms of the high- and low frequency limits of the frequency dependent specific heat:

$$\langle(\Delta E)^2\rangle^{structure}) = k_B T^2 V(c_V(0) - c_V(\infty)). \tag{6.10}$$

Similarly, the cross correlation of pressure and energy are related to the isochoric pressure coefficient $\beta_V = (\frac{\partial p}{\partial T})_V$, and through similar arguments,

$$\langle\Delta p\Delta E\rangle^{structure} = k_B T^2 V(\beta_V(0) - \beta_V(\infty)). \tag{6.11}$$

Accordingly

$$\gamma = \frac{\beta_V(\omega\to 0) - \beta_V(\omega\to\infty)}{c_V(\omega\to 0) - c_V(\omega\to\infty)}. \tag{6.12}$$

This provides a possibility to actually measure γ_{isom} for a real system.

6.1.1 Constant volume versus constant pressure

Computer simulations are often done for NVT ensembles, mainly for practical reasons. Experiments on the other hand are usually done at constant pressure, since this is the natural condition in the lab. Luckily it is possible to translate from NpT to NVT through thermodynamic identities. By measuring three independent thermoviscoelastic response functions, it is possible to calculate γ_{isom} from equation 6.12. From the identities

$$c_V = c_p - T\alpha_p^2 K_T \tag{6.13}$$

and

$$K_T = K_S\frac{c_V}{c_p}, \tag{6.14}$$

we get

$$c_V = c_p(T\alpha_p^2\frac{K_S}{c_p})^{-1} \tag{6.15}$$

and

$$K_T = K_S(T\alpha_p^2\frac{K_S}{c_p})^{-1}, \tag{6.16}$$

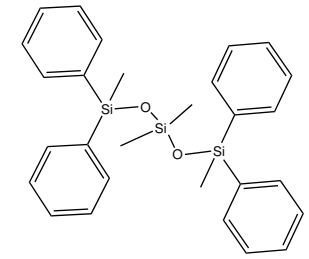

1,3,3,5-tetramethyl-1,1,5,5-tetraphenyltrisiloxane
Chemical Formula: $C_{28}H_{32}O_2Si_3$
Molecular Weight: 484,81

Figure 6.2 Chemical structure of DC704.

and further from equation 6.16 and

$$\beta_V = \alpha_p K_T \tag{6.17}$$

we get

$$\beta_V = \frac{c_p}{T\alpha_p}. \tag{6.18}$$

Hence, γ can be calculated from measurements of the following frequency dependent response functions: the isobaric specific heat c_p, the isobaric expansion coefficient α_p and the adiabatic bulk modulus K_S.

6.2 Test substance

As a test substance is chosen the van der Waals bonded silicone oil tetramethyl-tetraphenyl-trisiloxane (DC704). This substance was chosen, first of all because it is van der Waals bonded end hence expected to be strongly correlating, and second because it is suited for the different linear response methods in terms of T_g, tendency to crystallize and reactiveness. Figure 6.2 shows the chemical structure of DC704. The glass transition temperature of DC704 (defined as the temperature where the dielectric loss peak is at 1mHz) is 210K. The liquid was used as received without any further purification (it is not hygroscopic). All measurements was performed on sample coming from the same bottle.

6.3 Dielectric measurements

6.3.1 Experimental

High pressure dielectric data were carried out at the Naval Research Institute in Washington DC. The setup can reach pressures up to 1.4 GPa. The sample is placed between two parallel capacitor plates and wrapped in teflon and rubber to prevent mixing of the sample and the pressure medium. The sample cell is then placed in a Manganin pressure cell from Harwood Engineering. The vessel is connected to an Enerpac manually operated pump in combination with a Harwood Engineering pressure intensifier

[Roland, Casalini & Paluch 2003]. Pressure is measured with a Sensotec tensometric transducer with a resolution of 150 kPa [Casalini & Roland 2004a]. A mixture of Dow Corning Spinnestic and heptane is used as pressure medium. The pressure vessel is placed inside a refrigerator for temperature control ($\pm$0.1 K [Casalini & Roland 2004a]). Two spectrometers are available for dielectric measurements, a Novocontrol Alpha (frequency range 10^{-2} Hz to 10^{7} Hz) and an IMass TDS (frequency range 10^{-4} Hz to 10^{4} Hz) [Roland et al. 2003].

The atmospheric dielectric measurements were carried out in the Roskilde University "Glass and Time" laboratory. The sample is placed in a multilayer parallel plate capacitor with an empty capacitance of approximately 70 pF. Temperature is controlled by a heater and coldfinger with a stability of a few milli kelvins [Igarashi et al. 2008a]. Dielectric measurements are conducted through a combination of a custom-build frequency generator and an Agilent 3458A multimeter for frequencies from 10^{-3} Hz to 100 Hz, and a commercial Agilent E4980A LCR meter for frequencies from 100 Hz to 10^{6} Hz. The setup, which is the same as the one used for bulk modulus measurements (chapter 3), is described in detail in [Igarashi et al. 2008a] and [Igarashi et al. 2008b]. The electronic part of the setup is identical also to the one used in the high pressure setup described in chapter 4.

Measuring protocol

For the high pressure measurements, dielectric spectra were obtained for varying pressures along four isotherms: 228.4K, 242.9 K, 260.0 K, and 296.9 K (from now on referred to as 228 K, 243 K, 260 K and 297 K). Measurements along isotherms are faster compared to measurements along isobars because pressure equilibration is much faster than temperature equilibration. A temperature equilibration time of at least 2 hours is taken at each temperature, while pressure equilibrium is reached after 15 minutes including the effect of the pressure induced temperature change.

Atmospheric measurements are done at varying temperatures after 2 hours of temperature equilibration.

6.3.2 Data

Figure 6.3 shows the imaginary part of the measured dielectric constant of DC704 for the four isotherms. Atmospheric data are not shown. Loss peaks were fitted with a second order polynomial in a log-log plot to the maximum 9 points of the peak.

6.4 PVT measurements

6.4.1 Experimental

PVT-measurements were also carried out at Naval Research Institute in Washington DC, with a commercial setup (Gnomix) with mercury as the confining fluid. The sample is immersed in the confining fluid inside the cell, and the change in dimension of the sample and confining fluid as a result of pressure and temperature changes is monitored magnetically. The volume of the sample is calculated by subtracting the volume of the confining fluid.

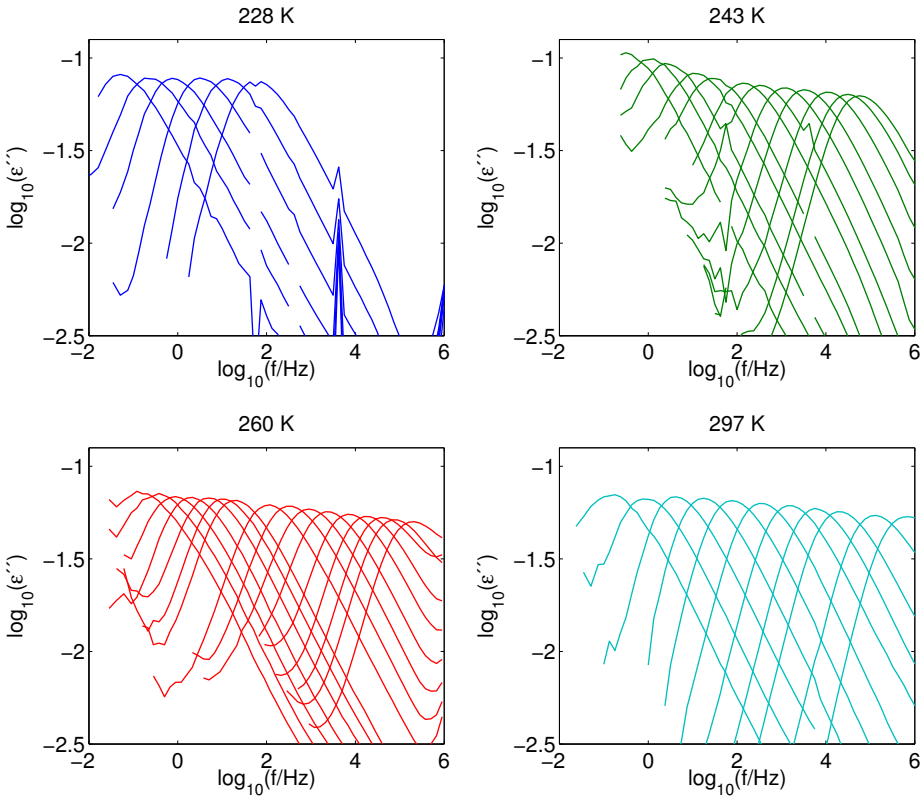

Figure 6.3 Imaginary part of the dielectric constant for DC704 measured along four isotherms: 228 K (from 18 to 60 MPa), 243 K (from 23 to 116 MPa), 260 K (from 74 to 199 MPa) and 297 K (from 200 to 383 MPa).

Measuring protocol

Volume as a function of pressure (10 MPa to 200 MPa) and temperature (20 ℃to 200 ℃) was measured both isobaricaly and isothermally. For the isobaric measurements, temperature steps of 0.5 K/min was performed along 5 isobars at 10 MPa, 50 MPa, 100 MPa, 150MPa and 200 MPa, and for the isotherms, pressure steps of 10 MPa was performed along 13 isotherms from 20 ℃to 80 ℃with 5 degrees interval.

6.4.2 Data

Results of measurements are shown in figure 6.4. The figure also shows a fit of an empirical expression, the Tait equation:

$$V_{sp}(T,p) = v_0 \exp(\alpha_0 T)\left\{1 - C\ln\left[1 + \frac{P}{b_0\exp(-b_1 T)}\right]\right\}. \tag{6.19}$$

V_{sp} is the specific volume (here in cm^3/g), P is pressure (in MPa) and T is temperature (in ℃). v_0, α_0, C, b_0 and b_1 are fitting parameters. Fitting is done for isotherms and

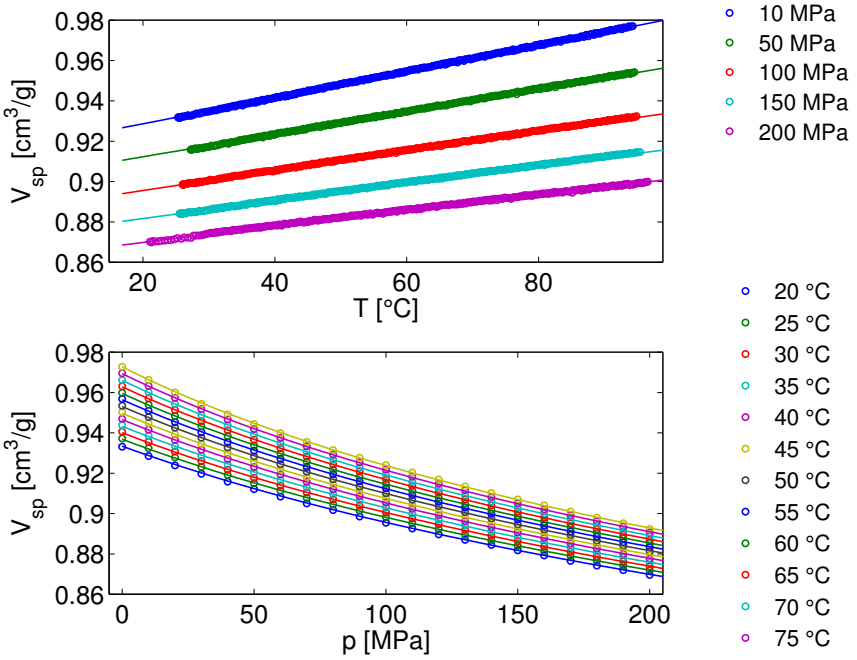

Figure 6.4 Measured PVT data for DC704. Top plot: specific volume V_{sp} as a function of temperature T along isobars. Bottom plot: specific volume V_{sp} as a function of pressure p along isotherms. Lines are fits of the Tait equation to data (fitting parameters from isotherms in both plots).

isobars seperately resulting in two sets of slightly different fitting parameters. The following values for the fitting parameters were used:

Parameter	Value
v_0	0.920
a_0	$7.1 \cdot 10^{-4}$
C	$8.8 \cdot 10^{-2}$
b_0	188
b_1	$4.8 \cdot 10^{-3}$

Which are the parameters resulting from the best fit to the isotherm data (plotted for both isotherms and isobars in figure 6.4).

6.5 Scaling

From equation 6.19, the specific volume $V_{sp}(T, p)$ is calculated at the relevant state points. Figure 6.5 shows relaxation time defined as the inverse angular frequency as a function of density $(1/V_{sp})$ for the four isotherms and the atmospheric isobar, and the reduced unit relaxation time ($\tilde{\tau} = \rho^{1/3}/\sqrt{m/k_B T}\tau$) as a function of the scaled data for a value of $\gamma_{scale} = 6.2$. The data falls nicely on a single curve when plotted as a

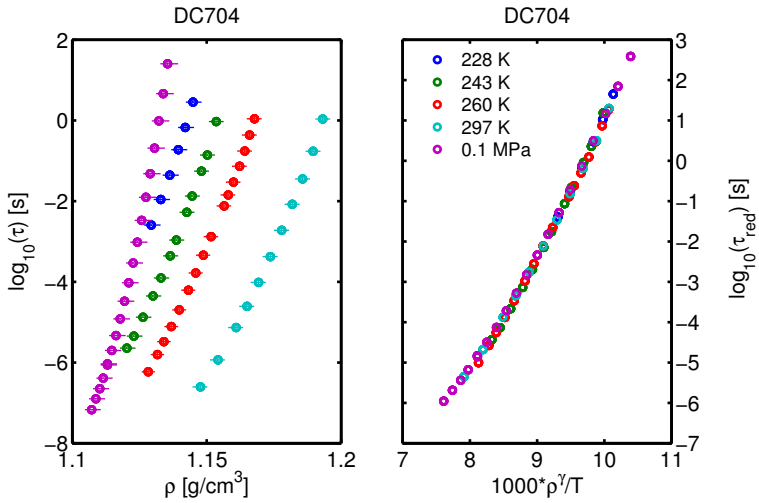

Figure 6.5 Relaxation time for DC704 measured along four different isotherms and the atmospheric pressure isobar. Left plot: Relaxation time (inverse angular frequency) as a function of density. Right plot: Reduced unit relaxation time, $\tau_{red} = \tilde{\tau}$ as a function of $1000\rho^{\gamma_{scale}}/T$, where $\gamma_{scale} = 6.2 \pm 0.2$

function of $\rho^{\gamma_{scale}}/T$.

6.5.1 Uncertainties

The total uncertainty on γ_{scale} is challenging to estimate due to the multiple origins of uncertainties and due to challenges in determining the propagation of the uncertainties. The data has been taken at three different setups (two different setups for dielectric measurements and one for PVT). This introduces a number of experimental uncertainties. The most significant source of experimental uncertainties are systematic errors in the measured quantities resulting from uncertainties in the absolute levels of temperature and pressure.

As mentioned in section 6.5, densities of the high pressure measurements are determined from the PVT data. Any uncertainty on the absolute level of temperature of the PVT setup compared to the dielectric setups results in an uncertainty in the calculated densities.

In addition to the experimental uncertainties, potential sources of uncertainties to the calculated densities results from the fitting and extrapolation of the PVT data. Figure 6.6 shows a map of the measured data points for both dielectric data and PVT data. While the PVT temperature and pressure range is limited by the experimental equipment, the temperature and pressure range of the dielectric data is mainly limited by the frequency window. The overlap between the two measurements hence depend on the sample. For DC704, the volumes calculated for the dielectric data are all outside the measured PVT range, which means that the calculation involves some extrapolation.

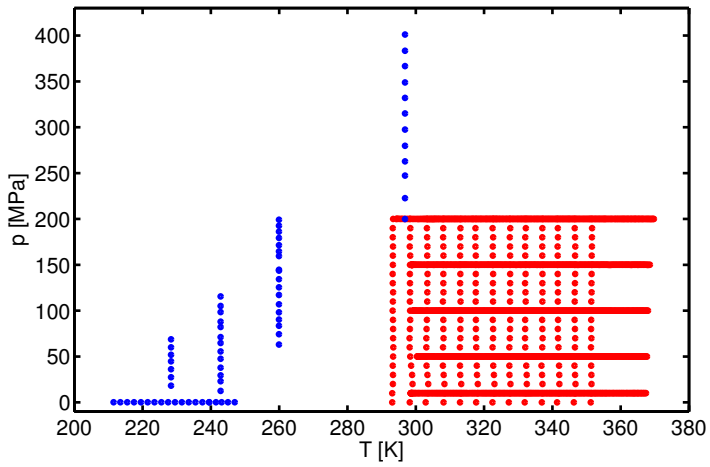

Figure 6.6 Map of measured data points for DC704. Blue dots are dielectric measurements, and red dots are PVT data.

Experimental uncertainties

The temperature of the atmospheric dielectric setup has been carefully calibrated yielding an uncertainty on the absolute temperature level of only 0.1 K [Igarashi et al. 2008a]. The temperature levels of the high pressure measurements can be compared to the atmospheric setup by comparing the loss peaks or relaxation times of the measurements in the overlaping area of the phase diagram. In order to do so, at least some of the high pressure measurements should be taken at (almost) atmospheric pressure. The isotherms should then agree with the atmospheric data temperatures. If this is not the case, a temperature correction of the high pressure data can be done. The temperature stability of the high pressure setup is 0.1 K [Casalini & Roland 2004a]. The uncertainty in the absolute level of pressure is assumed equal to the resolution of pressure measurements in the high pressure setup, 150 kPa. The effect of this uncertainty is small though, compared to the effect of a temperature uncertainty.

Zoller and Walsh [Zoller & Walsh 1995] reports the absolute accuracy of the GNOMIX PVT-setup on the measured specific volume as 0.002 cm^3/g in the relevant temperature range, while the resolution is 0.0002 cm^3/g [Zoller & Walsh 1995].

Uncertainty resulting from extrapolation of PVT data

The Tait equation, in some variation, is a commonly used expression for the temperature and pressure dependence of the volume of liquids, and it has been found to give a good fit to data above the glass transition (see for instance [Reiser, Kasper & Hunklinger 2005], [M. Paluch 2002]) and [Roland & Casalini 2005]. [Reiser et al. 2005] compairs the Tait expression for propylene carbonate found from PVT measurements at low temperatures and with a relatively wide pressure range with an expression obtained for the same liquid from PVT data at higher temperature and lower pressures [Pawlus, Casalini, Roland, Paluch, Rzoska & Ziolo 2004], and finds that the two expressions agree well.

Provided that the data can be described by the Tait equation also outside the measured pressure and temperature range, the uncertainty in the extrapolation is then determined by the quality of the fit. As seen from figure 6.4, the random uncertainty in the data is small, and the quality of the fit to data is good, meaning that the uncertainty in the fitting parameters is relatively small. As mentioned in section 6.4.2, fitting is done for isotherms and isobars seperately (a collected fitting would be an effective fitting of the isobars due to the much larger number of data points for isobars), yielding two sets of slightly different fitting parameters. Although the difference between the two fits is small, the difference in the fitting parameters is larger than the calculated uncertainties in the individual fitting parameters, so the uncertainty in the fitting is taken as the difference in the returned specific volume from the two fits. This amounts to less than 0.002 cm^3/g (0.4 percent), which corresponds to the uncertainties in the absolute value of the specific volume reported by Zoller and Walsh [Zoller & Walsh 1995].

Uncertainty in the scaling and γ_{scale}

In order to be able to see the relative effects of the different uncertainties in the density and in the scaling, and to minimize problems with propagation of uncertainties, the data in figure 6.5 has been given errorbars on both axes. The errorbars on density then reflects the uncertainty resulting from PVT-data, i.e. both the uncertainty in the measured specific volume and the uncertainty on the fit defined as the difference between isotherm and isobar fits. Errorbars on the relaxation time reflects experimental uncertainties in the dielectric data. The latter is determined by evaluating the change in loss peak position as a result of uncertainties in pressure and temperature from a fit of an Avramov-expression to data (see chapter 7). The uncertainties in temperature is estimated on the bases of the extrapolation of the isotherms to the atmospheric pressure isobar where the absolute temperature level is known within $\pm 0.1K$. This means that the highest isotherms have the largest uncertainty in absolute temperature level (op to 0.5 K). As mentioned, the uncertainty in pressure is insignificant in this connection since it is much smaller than the temperature uncertainty. As seen from figure 6.5, even the uncertainty in temperature gives rise only to a small errorbar on $log_{10}(\tau)$, which is just visual for the highest temperature.

Traditionally, the value of γ_{scale} is determined by manually adjusting the value to obtain the best possible scaling of data. Therefore, the uncertainty can not be calculated from a standard expression for propagation of errors. Adding errorbars to the right plot of figure 6.5 would be misleading and would suggest a larger uncertainty in γ_{scale} than nessecary. Furthermore, the size of the errorbars depends on the value of γ_{scale}. A substantial fraction of the errorbars reflects systematic errors which will be the same or at least affect the data in the same direction. This is the case with the experimental contribution to the uncertainty in density, which is more than 75 percent of the total uncertainty in density for the high pressure data. The temperature uncertainty of the dielectric data can in principle be independent, but is limited by the extrapolation of the high pressure data to the atmospheric data.

The uncertainty in γ_{scale} is found by adjusting the different variables within the given uncertainties and evaluating the effect on the scaling. The effect on the scaling of the three main origins of uncertainties: the uncertainty in the measured specific volume, the uncertainty on the fitting parameters of the Tait equation, and the uncertainty on the

temperature level of the dielectric data is tested both individually and in combination. For densities calculated from the Tait equation with isobar fitting parameters the best scaling is obtained with γ_{scale}=6.3. The uncertainty in the measured density (specific volume) gives rise to an uncertainty in γ_{scale} of ± 0.1, in the sence that the best scaling for the data shifted ± 0.002 cm^3/g in specific volume ($1/\rho$) is obtained with γ_{scale}=6.2±0.1. For a temperature shift of all data of 1 degree, the effect on γ_{scale} is likewise ± 0.1. The effect of the combined errors gives an uncertainty in γ_{scale} of ± 0.2.

6.6 Linear response measurements

As showed in section 6.1, γ_{isom} can be determined through linear response data of the isochoric specific heat $c_p(\omega)$ and isochoric pressure coefficient $\beta_V(\omega)$ measured at a single state point. It was also showed that it is possible to calculate γ_{isom} from data on the isobaric specific heat $c_p(\omega)$, the isobaric expansion coefficient $\alpha_p(\omega)$ and the adiabatic bulk modulus $K_S(\omega)$ through thermodynamic identities.

As mentioned even constant pressure conditions can be difficult to attain for viscous liquids near the glass transition [Christensen, Olsen & Dyre 2007]. The reason is that thermal expansion causes thermal stresses that relax on the experimental time scale, and hence the specific heat is not measured at isobaric conditions in most setups. As a result it is the frequency dependent longitudinal specific heat that is measured, a quantity that is in between $c_p(\omega)$ and $c_v(\omega)$, defined by

$$c_l(\omega) = \frac{1+\frac{4}{3}\frac{G(\omega)}{K_S(\omega)}}{1+\frac{4}{3}\frac{G(\omega)}{K_T(\omega)}} c_p(\omega), \tag{6.20}$$

where $G(\omega)$ is the frequency dependent shear modulus. Similarly, we do not measure the adiabatic expansion coefficient, but a quantity termed the longitudinal expansion coefficient, defined by

$$\alpha_l(\omega) = \frac{\alpha_p(\omega)}{1+\frac{4}{3}\frac{G(\omega)}{K_T(\omega)}}. \tag{6.21}$$

Luckily it is still possible to determine $c_V(\omega)$ and $\beta_V(\omega)$ from the longitudinal versions by measuring 4 frequency dependent response functions, namely the longitudinal specific heat $c_l(\omega)$, the longitudinal expansion coefficient $\alpha_l(\omega)$, the adiabatic bulk modulus $K_S(\omega)$ and the shear modulus $G(\omega)$. From equations 6.20 and 6.21 together with

$$c_V(\omega) = c_p(\omega) - T\alpha_p(\omega)^2 K_T(\omega) \tag{6.22}$$

and

$$K_T(\omega) = K_S(\omega)\frac{c_V(\omega)}{c_p(\omega)}. \tag{6.23}$$

we have four equations with four unknowns. From solving these equations, and by using $\beta_V(\omega) = \alpha_p(\omega)K_T(\omega)$, we can determine γ_{isom} (equation 6.12).

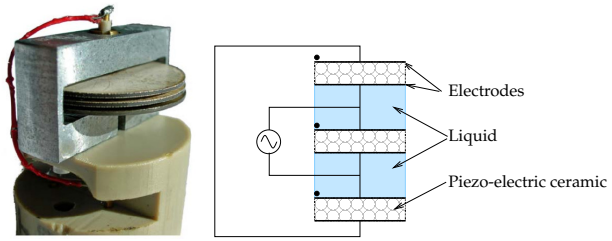

Figure 6.7 A photo and a scetch of the shear transducer. The radius of the discs are 10 mm, and the thickness and spacing are both 0.5 mm. The dots indicate the direction of the polarization. The electrical connection of the discs causes the middle plate to move in the opposite direction as the two outer discs.

6.6.1 Techniques

Adiabatic bulk modulus $K_S(\omega)$

The technique is described in chapter 3.

Shear modulus

The frequency dependent shear modulus is measured by the piezo-electric shear modulus gauge (PSG) technique [Christensen & Olsen 1995], which is a similar technique as the PBG-technique used to measure the adiabatic bulk modulus. The liquid is placed between three plates of silver coated piezo ceramic material with a spacing of 0.5 mm. When an oscillating voltage is applied, the piezo ceramic material will expand or contract in the radial direction depending on the polarization and the direction of the applied electric field, causing a shear deformation of the liquid between the plates. The measured capacitance of the plates depends on whether the plates are free to move or partially clamped by the stiffness of the liquid. The shear modulus can then be found from the change in capacitance of the liquid filled spectrum compared to a reference spectrum. Figure 6.7 shows a schematic of the principle of the shear transducer and a photo.

Longitudinal expansion coefficient $\alpha_l(\omega)$

The longitudinal expansion coefficient is measured in a home build setup [Niss, Gundermann, Christensen & Dyre 2012]. The method is based on capacitative scanning dilatometry [Bauer, Böhmer, Moreno-Flores, Richert, Sillescu & Neher 2000], but modified to work in the time domain. The sample is placed between two capacitor plates separated by thin spacers (50 μm). The upper plate is free to move as the liquid changes volume due to temperature changes. The volume change is determined from the capacitance of the capacitor. A microregulator allows for very fast temperature changes, and by using a high resolution capacitance bridge, responses to very small temperature steps can be measured. This ensures that the experiment is performed linearly. Figure 6.8 shows a sketch and a photo of the measuring cell.

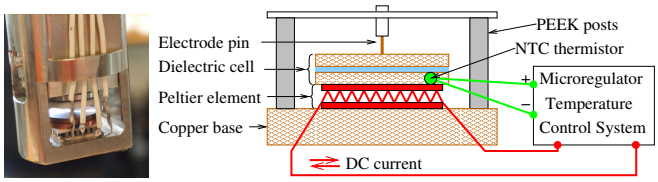

Figure 6.8 A photo and a scetch of the measuring cell for measuring the longitudinal expansion coefficient. The capacitor plates are seperated by 50 μm spacers. The upper plate is free to move as the liquid changes volume due to temperature changes. The microregulator allows for very fast temperatur changes. [Niss et al. 2012]

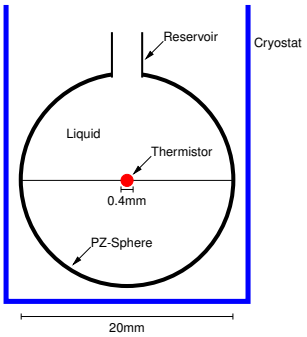

Figure 6.9 Schematic illustration of the measuring cell inside the cryostat. The thermistor acting as combined heater and thermometer is placed in a sphere filled with the liquid. The piezoelectric properties of the sphere is not important in this connection [Jakobsen et al. 2010].

Longitudinal specific heat $C_l(\omega)$

The longitudinal specific heat is measured using a newly developed technique [Jakobsen, Olsen & Christensen 2010] based on the so called 3ω-method by Birge and Nagel [Birge & Nagel 1985]. While the Birge and Nagel technique used a planar geometry, the present technique uses a spherical geometry. The advantage of this compared to the planar plate geometry is that the influence of the mechanical boundary conditions can be calculated analytically, and that the thermal conductivity and specific heat can be found independently. The thermal impedance of the liquid is measured using a small spherical thermister bead, which serves both as the heat generator and the thermometer. From the thermal impedance (knowing the geometry of the bead) the specific heat can be determined. As mentioned earlier, it is the longitudinal specific heat which is measured in this setup, which covers a frequency range from $10^{-2.5}$ Hz to $10^{0.5}$ Hz.

DC704	214K
$c_l^{liq}\left[10^6 J/(Km^3)\right]$	1.65 ± 0.15
$c_l^{sol}\left[10^6 J/(Km^3)\right]$	1.35 ± 0.05
$K_S^{liq}\left[10^9 Pa\right]$	4.0 ± 0.05
$K_S^{sol}\left[10^9 Pa\right]$	5.2 ± 0.05
$\alpha_l^{liq}\left[10^-3K^{-1}\right]$	0.46 ± 0.04
$\alpha_l^{sol}\left[10^-3K^{-1}\right]$	0.11 ± 0.01
$G^{liq}\left[10^9 Pa\right]$	0
$G^{sol}\left[10^9 Pa\right]$	1.1 ± 0.05
R	0.9 ± 0.2
Π_{VT}^{lin}	1.2 ± 0.6
γ_{isom}	6 ± 2
γ_{scale}	6.2 ± 0.2

Table 6.1 Measured high and low frequency plateau values and calculated γ_{isom}, correlation coefficient R and linear Prigogine-Defay ratio Π_{VT}^{lin}.

6.6.2 Results

Table 6.1 shows the measured high and low frequency (or short and long time) values of the measured response functions. Although it is only necessary to measure at a single state point, all the response functions have been measured at a number of state points. The different methods does not all cover the same temperature interval. The longitudinal expansion coefficient are measured from 204-210 K and the longitudinal heat capacity are measured from 214-218 K, i.e. both in a relatively narrow temperature interval, while the shear modulus and the adiabatic bulk modulus work from approximately 214 K and up. The temperature 214 K is chosen in order to make the required extrapolation of the longitudinal expansion coefficient data as limited as possible, but in principle any state point in the super cooled regime could be used.

Figure 6.10 shows examples of data for the different response functions.

6.6.3 Limitations and uncertainties

The different techniques are customized to work in the same cryostats with the same sample holders. $G(\omega)$, $c_l(\omega)$ and $K_S(\omega)$ were measured in the same cryostat while $\alpha_l(\omega)$ were measured in a similar cryostat which were carefully temperature calibrated with the other.

The large uncertainty on γ_{isom} reflects the large challenges involved in measuring the absolute levels of the frequency dependent response functions. Some of the methods are still under development. The fact that each response function was measured over several temperatures was also done to reduce the uncertainty on the absolute levels by obtaining a reliable temperature dependence of the levels.

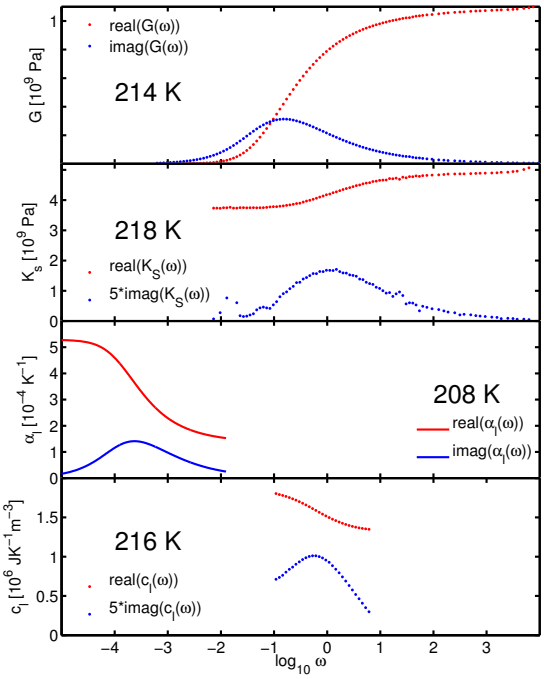

Figure 6.10 Example of measured real and imaginary part of linear response data. Data are shown for different state points to have the relaxation fall within the frequency window of the given technique. Top: shear modulus $G(\omega)$. Second: adiabatic bulk modulus $K_S(\omega)$. Third: longitudinal expansion coefficient $\alpha_l(\omega)$. Data was measured in the time domain and converted to the frequency representation by a numerical Laplace transfrom. Bottom: longitudinal specific heat $c_l(\omega)$.

6.7 Discussion

Table 6.1 also shows the calculated $\gamma_{isom} = 6 \pm 2$. This agrees well with the value of the density scaling exponent $\gamma_{scale} = 6.2 \pm 0.2$ even considering the large uncertainties on γ_{isom}. In the light of the fact that the density scaling exponent is obtained from data measured over many state points ranging from atmospheric to almost 400 MPa and a temperature range of 90 K, while the value predicted from linear response is measured at a single state point, it is quite striking that the two values agrees so well. This indicates that DC704 is a strongly correlating liquid. The correlation coefficient (equation 5.6) quantifies the degree of WU correlations in the NVT ensemble:

$$R = \frac{\langle \Delta W \Delta U \rangle}{\sqrt{\langle (\Delta W)^2 \rangle \langle (\Delta U)^2 \rangle}}. \tag{6.24}$$

Equivalent to γ_{isom}, the correlation coefficient can also be expressed in terms of linear response functions:

$$R_{lin} = \frac{\beta_V^{slow} - \beta_V^{fast}}{\sqrt{-(K_T^{slow} - K_T^{fast})(c_V^{slow} - c_V^{fast})/T}}. \tag{6.25}$$

Here the notion fast and slow refers to the high and low frequency limits of the dynamic linear response functions. Table 6.1 shows the correlation coefficient calculated from equation 6.25. The value of 0.9 ±0.2 confirms that DC704 is strongly correlating according to the original definition (section 5.1.2). It is seen from equation 6.25 that R_{lin} is given by the inverse square root of the linear Prigogine-Defay ratio [Ellegaard, Christensen, Christiansen, Olsen, Pedersen, Schrøder & Dyre 2007]:

$$R = \frac{1}{\sqrt{\Pi_{VT}^{lin}}}, \tag{6.26}$$

where

$$\Pi_{VT}^{lin} = \frac{-(K_T^{slow} - K_T^{fast})(c_V^{slow} - c_V^{fast})}{T(\beta_V^{slow} - \beta_V^{fast})^2}. \tag{6.27}$$

The linear Prigogine-Defay ratio is a linear version of the traditional Prigogine-Defay ratio. Like with the traditional Prigogine-Defay ratio, the linear Prigogine-Defay ratio equals unity if the liquid is a single-paramter liquid. This means, that a single parameter liquid has $R = 1$ and hence a perfectly correlating liquid corresponds to a single parameter liquid in the traditional meaning. While the traditional understanding of the Prigogine-Defay ratio did not include an interpretation of values different from but close to unity, the connection between R and Π_{VT} provides a new understanding of the PD-ratio as a measure of how strongly correlating a liquid is, where perfect correlations implies that the liquid is a single-prameter liquid. Table 6.1 also shows the calculated $\Pi_{VT}^{lin} = 1.2 \pm 0.6$ for DC704.

While the linear PD ratio is expressed in terms of plateau values of linear response functions measured on the equilibrium liquid at a single state point, the classical PD ratio is calculated from measured static glassy and liquid responses extrapolated to T_g. This makes the classical PD ratio less well defined, also because the glassy response is time dependent and depends on the history of the glass. However, no data on linear PD ratios can be found in literature, so in order to compare the results for DC704 with other systems and in lack of literature data on the linear Prigogine-Defay ratio, Pedersen [Pedersen 2009] collected values of classical PD ratios from literature. A table with these values is shown in Paper I (appendix A.1). The collection includes different systems, like polymers, a metallic alloy, and both hydrogen-bond rich and van der Waals bonded liquids. The liquids have been listed according to their PD ratio. The liquids with low PD ratios are van der Waals bonded polymers and liquids, while network-bonded and hydrogen-bonded liquids have larger PD ratios in accordance with the theory. The bottom of the table in Paper I shows the inverse square root of the PD ratio. This is here interpreted as an approximate correlation coefficient, and it is seen that liquids with low PD ratios have approximate correlation coefficients closest to 1 all in all supporting the understanding interpretation that strongly correlating liquids are approximate single parameter liquids.

7 Density dependence of γ

As showed in section 5.3.2, according to the isomorph theory γ_{isom} depends only on density. For strongly correlating liquids $\gamma_{isom} = \gamma_{scale}$, so we will simply refer to γ in the following. The density dependence of γ has been tested in computer liquids of strongly correlating liquids, which supports the theory, and also very recently by new experimental data on two liquids [Bøhling, Ingebrigtsen, Grzybowski, Paluch, Dyre & Schrøder 2012]. The results show that $\gamma = g(\rho)/T$, and that $g(\rho)$ is not a power law, although using a power law density dependence is a good approximation at moderate density changes [Bøhling et al. 2012]. This supports the original idea by Alba-Simionesco and co-workers [Alba-Simionesco et al. 2004] about how to scale dielectric relaxation times measured at different pressures and temperatures. This is also in line whith the findings of [Niss, Dalle-Ferrier, Tarjus & Alba-Simionesco 2007], who showed that the scaling for DBP was not possible using a power law.

7.1 Experimental evidence?

The density dependence of γ is here examined for two data sets on DC704 and 5PPE (polyphenylether). Both liquids are van der Waals bonded, and are hence expected to be strongly correlated. The chemical structure of 5PPE is shown in figure 7.1 (the chemical structure of DC704 is shown in figure 6.2). The DC704 data set is the same data set which was used to test the prediction in chapter 6. Like the DC704 data, the high pressure dielectric data and the PVT data for 5PPE was obtained at the Naval Research Institude in Washington DC. The atmospheric pressure dielectric data was obtained at the "glass and Time" facility in Roskilde.

Figure 7.2 shows reduced unit dielectric relaxation time (defined as the inverse angular frequency) for the two liquids. Densities are determined from PVT-measurements as described in chapter 6. Errorbars are created as described in section 6.5.1. The figure

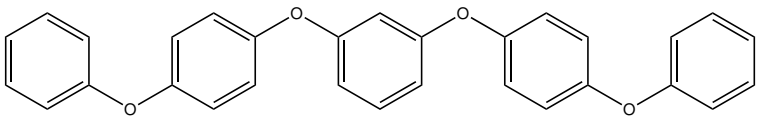

1,3-bis(4-phenoxyphenoxy)benzene
Chemical Formula: $C_{30}H_{22}O_4$
Molecular Weight: 446,49

Figure 7.1 Chemical structure of 5PPE.

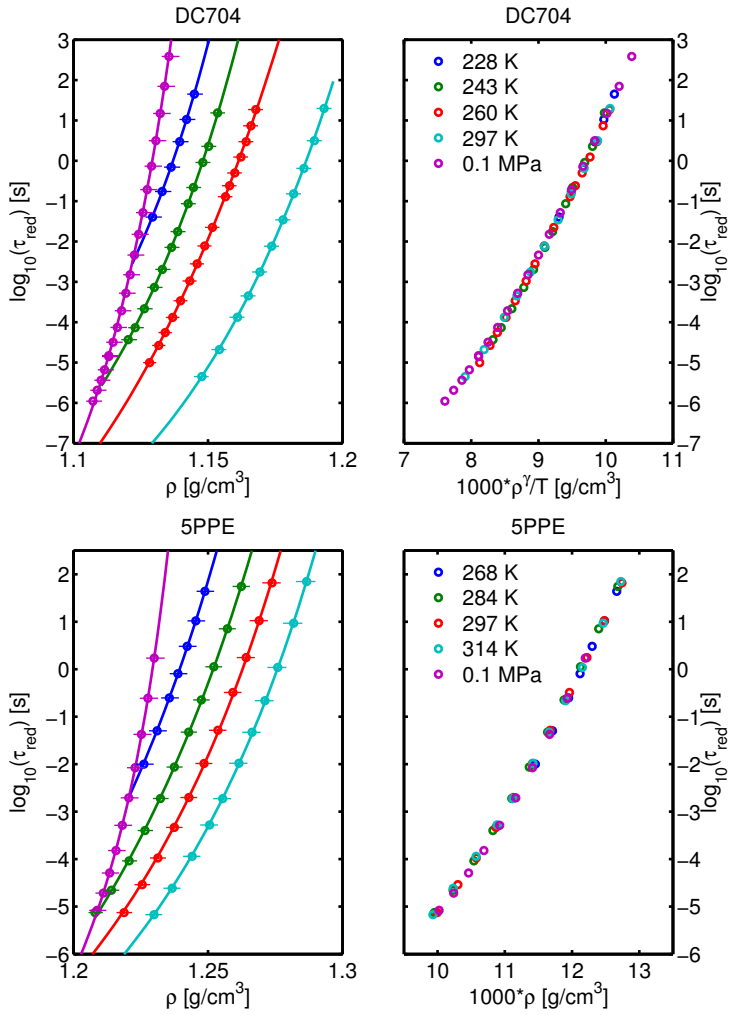

Figure 7.2 Left: reduced unit relaxation time, $\tau_{red} = \tilde{\tau} = C\rho^{1/3}T^{1/2}\tau$, as a function of density for four isotherms and the atmospheric pressure isobar for 5PPE and DC704. Symbols are data, lines are fits (an Avramov expression for DC704 and an extended VFT expression for 5PPE). Right: reduced unit relaxation time as a function of ρ^{γ}/T, with $\gamma = 5.5$ for 5PPE and $\gamma = 6.2$ for DC704.

also shows that both data sets scales nicely with $\gamma = 5.5$ for 5PPE and $\gamma = 6.2$ for DC704.

Recall that γ is given by (equation 5.13)

$$\gamma = \left(\frac{\partial \ln T}{\partial \ln \rho}\right)_{\tilde{\tau}}. \tag{7.1}$$

A change in γ with state point should then be seen in a plot of $\ln(\rho)$ vs $\ln(T)$. In figure 7.3, both data sets are plotted in such a plot (only for the high pressure data). Each

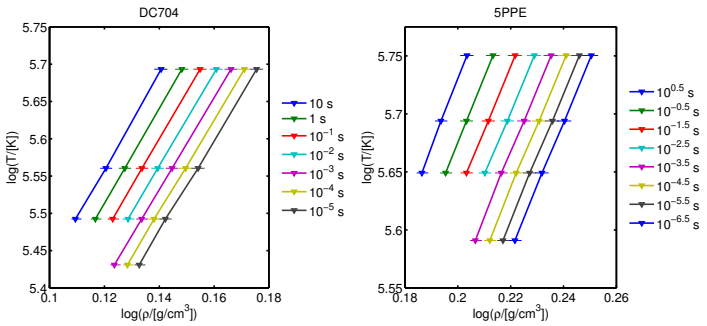

Figure 7.3 Isochrones at $10^{-6.5}$ s, $10^{-5.5}$ s, $10^{-4.5}$ s, $10^{-3.5}$ s, $10^{-2.5}$ s, $10^{-1.5}$ s, $10^{-0.5}$ s and $10^{0.5}$ s for 5PPE, and 10^{-5} s, 10^{-4} s, 10^{-3} s, 10^{-2} s, 10^{-1} s, 1 s and 10 s for DC704.

line in the plot is an isochrone and a change in γ will be seen as a change in slope with density. In order to create isochrones from the data, the data has been fitted with two different fitting functions.

For DC704 an Avramov expression was used [Roland et al. 2005]:

$$\tau(T,P) = \tau_0 \exp\left[30\left(\frac{T_r}{T}\right)^{a_{AV}}\left(1+\frac{P}{\Pi}\right)^{b_{AV}}\right], \tag{7.2}$$

where τ_0, T_r, a_{AV}, Π and b_{AV} are fitting parameters. The physical interpretation of the parameters is not important in this connection since the function was only used to get the best possible fit to data. For a given isotherm T, the first term in the exponential reduces to a single parameter

$$K = K_1\left(\frac{T_r}{T}\right)^{a_{AV}}, \tag{7.3}$$

which reduces the Avramov-expression to

$$\tau(T,P) = \tau_0 \exp\left[K\left(1+\frac{P}{\Pi}\right)^{b_{AV}}\right]. \tag{7.4}$$

With τ_0 set to $10^{-14}s$ this reduces the number of fitting paramters to three: K, Π and b_{AV}. The parameters were fitted to each isotherm seperately. For the atmospheric data equation 7.2 reduces to:

$$\tau(T) = \tau_0 \exp\left[\frac{K_2}{T^{a_{AV}}}\right], \tag{7.5}$$

which was fitted to the atmospheric data.

The 5PPE data set was fitted with a VFT expression [Roland et al. 2005]:

$$\tau(t,P) = \tau_0 \exp\left(\frac{B}{T-T_0}\right)\exp\left(\frac{D_P P}{P_0 - P}\right), \tag{7.6}$$

where τ_0, B, T_0, D_P and P_0 are fitting parameters. In this case the atmospheric term was first fitted to the atmospheric data to obtain τ_0, B and T_0, and the pressure dependent expression was then fitted to the high pressure data.

For each liquid, the corresponding pressures at each isotherm and for each selected relaxation time was then found from the fit. Isochrones was created for the following times: $10^{-6.5}$ s, $10^{-5.5}$ s, $10^{-4.5}$ s, $10^{-3.5}$ s, $10^{-2.5}$ s, $10^{-1.5}$ s, $10^{-0.5}$ s and $10^{0.5}$ s for 5PPE, and 10^{-6} s, 10^{-5} s, 10^{-4} s, 10^{-3} s, 10^{-2} s, 10^{-1} s, 1 s and 10 s for DC704.

The errorbars on γ in figure 7.4 are estimated on the basis of the errorbars in figure 7.3, which are created as described in section 6.5.1. As described in section 6.5.1, the most significant contribution to the errorbars on density in figure 7.3 is due to the experimental uncertainty on the measured specific volume. This means that all data are affected by the same amount, which will not change the slope significantly as long as this amount is small. On evaluation of the slopes in figure 7.3, the uncertainty in γ resulting from independent uncertainties is estimated to be around 5 percent.

A density dependence of γ will as mentioned be seen as a change of slope of the isochrones in figure 7.3 with density, and if γ is purely density dependent, it should be possible to make the lines collapse onto a single line when shifted in the vertical diraction. As seen from figure 7.4 this is not clearly the case, since there is some spread in γ when plotted as a function of density. For 5PPE there seems to be tendency of a decreasing $\gamma(\rho)$, but this is not seen for DC704. In order to put the density dependence into perspective, a comparrison of $\gamma(\rho)$ with $\gamma(T)$ is made in figure 7.4. Here it is seen that, although the spread in $\gamma(T)$ is larger for one temperature for both liquids, the overall picture for both liquids is that the temperature dependence is comparable to the density dependence.

7.2 Final remarks

The very resent experimental results [Bøhling et al. 2012] on the density dependence of γ that was mentioned in the beginning of this chapter relies on data with an unusually large density range (18-20 %) compared to typical scaling experiments. The DC704 and 5PPE data sets analysed here were taken with another purpose than to investigate the density dependence, and the density ranges are rather limited for this purpose. This could explain the inconclusive results.

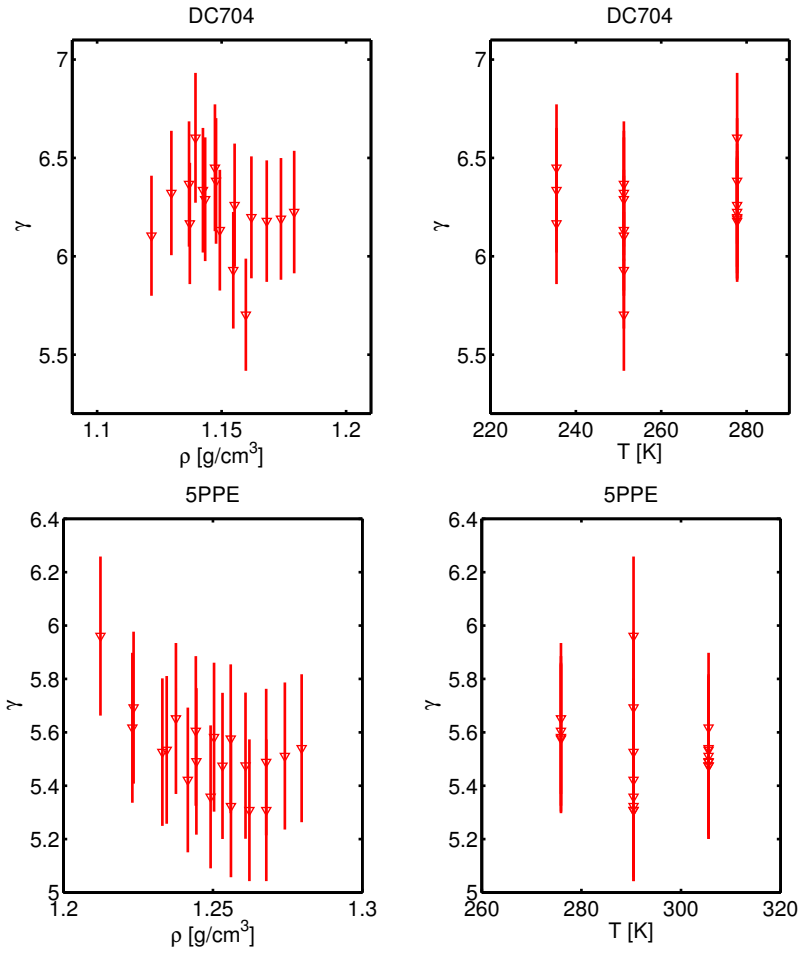

Figure 7.4 The density and temperature dependence of γ for DC704 and 5PPE. Left: γ as a function of density, right: γ as a function of temperature.

8 Prediction 2: Aging of strongly correlating liquids

As a consequence of the existence of isomorphs, a strongly correlating liquid has certain aging properties as described in chapter 5. For instance it is possible to change density and volume of the liquid instantaneously along an isomorph without the liquid falling out of equilibrium at any time. This was demonstrated in computer simulations [Gnan et al. 2009] (see section 5.3.3). An experimental test of these properties seems obvious and important, but so far no such experiment has been done. An ambition of the present PhD project has been to design and carry out such an experiment, but due to various mainly experimental challenges the experiment has not been performed yet. The following discusses the idea for the experiment, potential experimental challenges and suggestions for solutions to these challenges. Hopefully this will provide a useful starting point for future experiments along this line.

8.1 The idea

The idea is to do different jumps in state points following the procedure of Gnan and coworkers [Gnan et al. 2009]. While the computer simulations are performed with temperature and volume as control parameters, experiments are done with temperature and pressure as control parameters, but this is no problem since the aging behavior of the liquid will be the same [Gnan et al. 2009].

8.1.1 Experimental protocols

The following jumps would be of interest, and should be carried out for both a liquid expected to be strongly correlating and a counter example:

a) A jump along an isomorph. Changing temperature and pressure instantaneously along an isomorph should take the liquid instantaneously to equilibrium if the liquid is strongly correlating. If not, we will expect to observe slow relaxation towards equilibrium.

b) A jump from the same pressure as above but a different temperature to the same final point. This isobaric point is not isomorphic to the final point, and we will expect aging both for the strongly correlating liquid and the counterexample.

c) A jump from a point that is isomorphic to the initial point of b) to the same final point as in b) (or a point that is isomorphic to this point). For the strongly correlating liquid, this should show the same aging behavior as the jump in b) since jumps between

mutually isomorphic state points show the same aging pattern. For the counter example a different aging pattern from b) is expected.

8.1.2 Choice of liquids

The chosen sample should be a liquid expected to be strongly correlating. This means first of all that it should be a van der Waals bonded liquid. Moreover, indications for strongly correlating-ness is density scaling and isochronal super position. Due to the capabilities of the setup, the glass transition temperature and pressure should lie within the range of the setup. The sample should have no beta relaxation. For practical reasons it should be stable and easy to handle (non toxic, low viscosity at room temperature).

For the counter example we should choose a liquid not expected to be strongly correlating. Glycerol is a hydrogen bonded liquid with a suited dielectric constant. It has no beta relaxation and is non toxic.

8.2 Experimental challenges

8.2.1 Changing temperature and pressure

An experimental test is challenging first of all because it requires very fast changes in temperature and density (or pressure). This challenge can be overcome by choosing state points with a sufficiently long relaxation time that the change in temperature and pressure is much faster than the relaxation time. This means that the technical capabilities of the setup to a large extend determines the timescale of the experiment.

Two effects contribute to the time it takes to make a temperature step: the time it takes for the cooler to supply the new temperature, and the time it takes for the sample in the cell to reach this new temperature. In practice obviously these two effects overlap.

Regarding pressure, pressure equilibration in it self is fast, both regarding the pump speed and the time it takes for pressure to transmit through the liquid, but there will be an after effect due to the induced temperature change that a pressure change gives rise to. This effect also decreases relatively fast (minutes) because of the ability of the large mass of cell to take up (or release) extra heat. The resulting pressure equilibration time is then around 15 minutes if the pressure change is not too big (a couple of MPa).

Temperature changes are significantly slower than pressure changes. Cooling capacities (see table in section 4.3) is at most a few degrees per minute for the bath itself. In addition to this comes the cooling or heating of the pressure cell and medium. While pressure changes are relatively fast and independent of the location in the phase diagram and the direction (increase or decrease) of the change, none of these properties applies for temperature changes. A study of the total equilibration time in response to temperature steps of 5 and 10 degrees was done by Haargaard Olsen and Videnkjær [Olsen & Videnkjær 2010]. They found that cooling 10 degrees in the range 5℃ to −15℃ takes approximately 54 minutes, while heating 5 degrees in the range −20℃ to 5℃ takes around 20 minutes.

Therefore the choice of both initial and final state points of the experiment is to a large extend determined by the performance of the cooler.

Since temperature equilibration is fastest during heating, temperature up jumps are most suited for the experiment. For an isomorphic point this implies an up jump in pressure as well, which is fortunate because the two effects goes in the same direction, meaning that a pressure increase will give rise to a temperature increase. In addition, pressure up jumps are favorable because the pump has an automatic mode for pressure increases but not for pressure decreases, which must be done manually.

Choosing state points

Although an isomorph is characterized by $\rho^\gamma/T = constant$, we do not need PVT measurements to identify isomorphic state points. State points with the same relaxation time can be identified from measurements at different temperatures and pressures, choosing two temperatures and varying pressure until the right relaxation time is found. For the counter example we will also (attempt to) jump between state points with the same relaxation time, but these can be difficult to identify if they are outside the frequency window (see section 8.2.2).

8.2.2 Monitoring the relaxation

Strongly correlating liquids obey isochronal superposition, i.e. state points with the same average relaxation time have (almost) the same dielectric loss spectrum. It is hence possible to use the loss as identification of relaxation after an isomorphic jump. A measurement of the entire loss peak is not possible since the liquid will have relaxed during the measurement. In stead, one can use the method of Hecksher et al [Hecksher, Olsen, Niss & Dyre 2010] of measuring at a single frequency on the high frequency side of the loss peak frequency. A change in average relaxation time will be associated with a change in the value of the imaginary part. When using this method it is necessary that the measurement is done within the power law area of the peak. In order to be sure about this, a series of measurements is required at different state points (which we already needed for identifying state points with the same relaxation time for the jump.)

8.2.3 Timescales

As mentioned above, in order for the step in pressure and temperature to be instantaneous, it has to be very short compared to the relaxation time of the liquid. As mentioned also, temperature is the controlling factor when it comes to equilibration time. For the right choice of temperatures it takes 20 minutes to change state point. This means that we need a relaxation time of $100 \cdot 20 = 2000$ minutes, which is roughly 33 hours, corresponding to a loss peak frequency around 10^{-5} Hz. This implies the following challenges: 1) The loss peak is outside the frequency window. This is not a big problem as long as a sufficient part of the peak is inside the frequency window. 2) The measuring time is long. A measurement at 10^{-3} Hz takes around 17 minutes, which is still much shorter than the relaxation time. 3) The experimental timescale is long. In order to ensure that the liquid is in equilibrium at the first state point, several

days are needed, and in order to determine whether the liquid relaxes after a jump, several days are also needed.

8.2.4 The counter example

For the counter example it is a little less obvious how to monitor and interpret the relaxation. Since the loss peak is outside the frequency window, we can not unambiguously identify state points with the same relaxation time. But we can find two state points with the same value of the imaginary part. If the liquid is not strongly correlating, we will expect the liquid to show some relaxation after a jump in state point. Since the initial and final value of the measured loss is the same, the relaxation will not be a relaxation from one value to another, but a relaxation from one value to the same value, but with a change in between. Such a relaxation can have at least two origins: a change of shape and a change of average relaxation time. In any case, it will reflect that the liquid falls out of equilibrium during the change of state point. If the two state points have approximate time temperature pressure superposition (TTPS) within the range of temperatures and pressures of the experiment, a change in loss can be interpreted as relaxation.

9 Summary and conclusion

In chapter 3 data on the frequency dependent bulk modulus of two liquids, namely DC705 and DBP was presented. Bulk modulus measurements are interesting in them selves because only few exist in the litterature, and more knowledge can be obtained about the generic features of glass forming liquids by studying different responses. In addition, the bulk modulus is of interest in the present context since it is one of the four linear response functions used to determine γ_{isom} of chapter 6 and Paper I. The two liquids showed TTS within the accuracy of the data, and an extended Maxwell fit to data returned high frequency slopes of -0.5 for DC705 and -0.42 for DBP partly supporting the conjecture that a high frequency slope of -0.5 should be a generic feature of the alpha relaxation when this is not interfered by secondary relaxations. The method of the PBG has great potential, but both measurements and data analysis are rather time consuming and challenging. In order to obtain high quality data, the agreement between the liquid and reference measurement is essential.

Chapter 4 presented the newly acquired high pressure setup for dielectric measurements and some of the challenges connected to the implementation. Among the most significant was the low frequency signal due to conductivity.

After a description of the theory of strongly correlating liquids and isomorphs in chapter 5, chapter 6 presented the first experimental test of the predicted identity between the density scaling exponent γ_{scale} and the proportionality constant between virial and potential energy fluctuations in the NVT ensemble, γ_{isom}. It was showed how γ_{isom}, can be expressed in terms of frequency dependent response functions. The experimental test was based on the one hand on high pressure dielectric measurements, and on the other hand on a number of linear response measurements. The results showed a striking similarity between the two constants, supporting the theory and findings from computer simulations. The results furthermore suggests, also in the light of the Prigogine-Defay ratio interpretation, that contrary to the existing perception, simple liquids do exist, and strongly correlating liquids are simple liquids, which have a number of simple properties.

According to the isomorph theory, γ_{isom} is slightly state point dependent, but depends only on density. This was examined for high pressure dielectric data sets for two liquids, namely 5PPE and DC704. The results was inconclusive, mainly due to the relatively limited density variation in the data. Although a slight change in γ with state point was found, there was no clear sign that it should be more dependent on density than on temperature.

An ambition of this project was to test the predicted aging behavior of strongly correlating liquids in the newly implemented high pressure setup. An idea for the experiment and a recipe for carrying it out was described in chapter 8. Due to a number of exper-

imental challenges, among which the most important was the low frequency signal due to conductivity (chapter 4), the experiment has not been carried out yet.

In conclusion, this PhD has taken the first step towards showing that strongly correlating liquids exist as real liquids and not only in computer simulations. The existence of strongly correlating liquids has several implications for understanding the nature of viscous liquids.

Bibliography

Alba-Simionesco, C., Cailliaux, A., Alegria, A. & Tarjus, G. [2004]. Scaling out the density dependence of the α-relaxation in glass-forming polymers, *Europhysics Letters* **68 (1)**: 58–64.

Alba-Simionesco, C., Kivelson, D. & Tarjus, G. [2002]. Temperature, density, and pressure dependence of relaxation times in supercooled liquids, *Journal of Chemical Physics* **116**(12): 5033–5038.

Bailey, N. P., Pedersen, U. R., Gnan, N., Schrøder, T. B. & Dyre, J. C. [2008a]. Pressure-energy correlations in liquids. I. Results from computer simulations., *Journal of Chemical Physics* **129**: 184507.

Bailey, N. P., Pedersen, U. R., Gnan, N., Schrøder, T. B. & Dyre, J. C. [2008b]. Pressure-energy correlations in liquids. II. Analysis and consequences, *Journal of Chemical Physics* **129**(184508): 184508.

Bauer, C., Böhmer, R., Moreno-Flores, S., Richert, R., Sillescu, H. & Neher, D. [2000]. High-frequency elastic moduli of simple fluids., *Physical Review E* **61**(10): 1755–&.

Birge, N. O. & Nagel, S. R. [1985]. Specific-heat spectroscopy of the glass-transition., *Physical Review Letters* **54**: 2674–2677.

Bøhling, L., Ingebrigtsen, T. S., Grzybowski, A., Paluch, M., Dyre, J. C. & Schrøder, T. B. [2012]. Scaling of viscous dynamics in simple liquids: theory, simulation and experiment, *New Journal of Physics* **14**: 113035.

Böhmer, R., Ngai, K. L., Angell, C. A. & Plazek, D. J. [1993]. Nonexponential relaxation in strong and fragile glass-formers., *Journal of chemical physics* **99**: 4201.

Casalini, R. & Roland, C. M. [2004a]. Excess wing in the dielectric loss spectra of propylene glycol oligomers at elevated pressure, *Physical Review B* **69**: 094202.

Casalini, R. & Roland, C. M. [2004b]. Thermodynamical scaling of the glass transition dynamics, *Physical Review E* **69**: 062501.

Chamberlin, R. V. [1998]. Experiments and theory of the nonexponential relaxation in liquids, glasses, polymers and crystals, *Phase transitions* **65**: 169–209.

Christensen, T. & Olsen, N. B. [1994]. Determination of the frequency-dependent bulk modulus of glycerol using a piezoelectric spherical shell, *Physical review B* **49**(21): 15396–15399.

Christensen, T. & Olsen, N. B. [1995]. A rheometer for the measurement of high shear modulus covering more than seven decades of frequency below 50 khz., *Review of Scientific Instruments* **66**: 5019–5031.

Christensen, T., Olsen, N. B. & Dyre, J. C. [2007]. Conventional methods fail to measure $cp(\omega)$ of glass-forming liquids, *Physical Review E* **75**: 041502.

Coslovich, D. & Roland, C. M. [2008]. Thermodynamic scaling of diffusion in supercooled lennard-jones liquids., *Journal of Physical Chemistry B* **112**(5): 1329–1332.

Coslovich, D. & Roland, C. M. [2009]. Pressure-energy correlations and thermodynamic scaling in viscous lennard-jones liquids., *Journal of Chemical Physics* **130**(1): 014508.

Dixon, P. K., Wu, L., Nagel, S. R., Williams, B. D. & Carini, J. P. [1990]. Scaling in the relaxation of supercooled liquids, *Physical Review Letters* **65**: 1108–1111.

Doi, M. & Edwards, S. F. [1986]. *The theory of polymer dynamics*, Oxford university press inc., New York.

Dreyfus, C., Aouadi, A., Gapinski, J., Matos-Lopes, M., Steffen, W., Patkowski, A. & Pick, R. M. [2003]. Temperature and pressure study of brillouin transverse modes in the organic glass-forming liquid orthoterphenyl., *Physical Review E* **68**(1): 011204.

Dreyfus, C., Grand, A. L., Gapinski, J., Steffen, W. & Patkowski, A. [2004]. Scaling the α-relaxation time of supercooled fragile organic liquids, *European Physical Journal B: Condensed Matter Physics* **42**: 309–319.

Ellegaard, N. L., Christensen, T., Christiansen, P. V., Olsen, N. B., Pedersen, U. R., Schrøder, T. B. & Dyre, J. C. [2007]. Single-order-parameter description of glass-forming liquids: A one-frequency test, *Journal of Chemical Physics* **126**: 074502.

Gnan, N., Schrøder, T. B., Pedersen, U. R., Bailey, N. P. & Dyre, J. C. [2009]. Pressure-energy correlations in liquids. IV. Isomorphs in liquid phase diagrams, *Journal of Chemical Physics* **131**(234504): 234504.

Hansen, J.-P. & McDonald, I. R. [1991]. *Theory of simple liquids*, 2nd ed edn, Academic press.

Hecksher, T. [2011]. *Relaxation in supercooled liquids*, PhD thesis, Roskilde University.

Hecksher, T., Olsen, N. B., Niss, K. & Dyre, J. C. [2010]. Physical aging of molecular glasses studied by a device allowing for rapid thermal equilibration, *Journal of Chemical Physics* **133**: 174514.

Igarashi, B., Christensen, T., Larsen, E. H., Olsen, N. B., Pedersen, I. H., Rasmussen, T. & Dyre, J. [2008a]. A cryostat and temperature control system optimized for measuring relaxations of glass-forming liquids., *Review of Scientific Instruments* **79**: 045105.

Igarashi, B., Christensen, T., Larsen, E. H., Olsen, N. B., Pedersen, I. H., Rasmussen, T. & Dyre, J. [2008b]. An impedance-measurement setup optimized for measuring relaxations of glass-forming liquids., *Review of Scientific Instruments* **79**: 045106.

Ingebrigtsen, T. S., Bøhling, L., Schrøder, T. B. & J. C. Dyre, J. [2011]. Thermodynamics of condensed matter with strong pressure-energy correlations, *arXiv:1107.3130v2 [cond-mat.soft]* .

Jakobsen, B., Olsen, N. B. & Christensen, T. [2010]. Frequency-dependent specific heat from thermal effusion in spherical geometry, *Physical Review E* **81**: 061505.

Julabo, T. t. c. c. [2009]. Julabo Labortechnik GmbH, 77960 Seelbach, Germany.

Landau, L. D. & Lifshitz, E. M. [1986]. *Elasticity theory, Course of theoretical physics*, Vol. 7, 3rd ed edn, Pergamon, New York.

M. Paluch, C.M. Roland, A. B. [2002]. Dielectric and mechanical relaxation of cresolphthalein-dimethylether., *J. Chem. Phys.* **117**: 1188.

Maggi, C., Jakobsen, B., Christensen, T., Olsen, N. B. & Dyre, J. C. [2008]. Supercooled liquid dynamics studied via shear-mechanical spectroscopy, *Journal of Physical Chemistry B* **112**: 16320–16325.

Mazurin, O. V. [1977]. Relaxation phenomena in glass, *Journal of non-crystalline solids* **25**: 129–169.

Mossa, S., Nave, E. L., Stanley, H. E., Donati, C., Sciortino, F. & Tartaglia, P. [2002]. Dynamics and configurational entropy in the Lewis-Wahnstrom model for supercooled orthoterphenyl, *Physical Review E* **65**(4, Part 1): 041205.

Ngai, K. L., Casalini, R., Capaccioli, S., Paluch, M. & Roland., C. M. [2005]. Do theories of the glass transition, in which the structural relaxation time does not define the dispersion of the structural relaxation, need revision?, *Journal of Physical Chemistry B* **109**: 17356–17360.

Nielsen, A. I., Christensen, T., Jakobsen, B., Niss, K., Olsen, N. B., Richert, R. & Dyre, J. C. [2009]. Prevalence of approximate $\sqrt{t}$ relaxation for the dielectric α process in viscous organic liquids, *Journal of Chemical Physics* **130**: 154508.

Nielsen, J. K. & Dyre, J. C. [1996]. Fluctuation-dissipation theorem for frequency-dependent specific heat., *Physical Review B* **54**(22): 15754.

Niss, K., Dalle-Ferrier, C., Tarjus, G. & Alba-Simionesco, C. [2007]. On the correlation between fragility and stretching in glass-forming liquids, *Journal of Physics: Condensed Matter* **19**: 076102 (25pp).

Niss, K., Gundermann, D., Christensen, T. & Dyre, J. C. [2012]. Measuring the dynamic thermal expansivity of molecular liquids near the glass transition, *arXiv:1103.4104v4 [cond-mat.soft]* .

Olsen, C. H. & Videnkjær, C. [2010]. *Spring op og fald ned på isomorfer*, Master's thesis, IMFUFA, NSM, Roskilde University.

Olsen, N. B., Christensen, T. & Dyre, J. C. [2001]. Time-temperature superposition in viscous liquids, *Physical Review Letters* **86**(7): 1271–1274.

Pawlus, S., Casalini, R., Roland, C. M., Paluch, M., Rzoska, S. J. & Ziolo, J. [2004]. Temperature and volume effects on the change of dynamics in propylene carbonate., *Physical Review E* **70**: 061501.

Pedersen, U. R. [2009]. *Long-time simulation of viscous liquids, from strong correlations to crystallization*, PhD thesis, Roskilde University, DNRF Centre "Glass and Time", IMFUFA, NSM.

Pedersen, U. R., Bailey, N. P., Schrøder, T. B. & Dyre, J. C. [2008]. Strong pressure-energy correlations in van der Waals liquids., *Physical Review Letters* **100**: 015701.

Reiser, A., Kasper, G. & Hunklinger, S. [2005]. Pressure-induced isothermal glass transition of small organic molecules., *Physical Review B* **72**: 094204.

Roland, C. M. & Casalini, R. [2005]. Effect of chemical structure on the isobaric and isochoric fragility in polychlorinated biphenyls., *J. Chem. Phys.* **122**: 134505.

Roland, C. M., Casalini, R., Bergman, R. & Mattson, J. [2008]. Role of hydrogen bonds in the supercooled dynamics of glass-froming liquids at high pressures., *Physical Review B* **77**: 012201.

Roland, C. M., Casalini, R. & Paluch, M. [2003]. Isochronal temperature-pressure superpositioning of the $\alpha-$relaxation in type-A glass formers, *Chemical Physics Letters* **367**: 259.

Roland, C. M., Hensel-Bielowka, S., Paluch, M. & Casalini, R. [2005]. Supercooled dynamics of glass-forming liquids and polymers under hydrostatic pressure, *Reports on Progress in Physics* **68**: 1405–1478.

Schrøder, T. B., Pedersen, U. R., Bailey, N. P., Toxværd, S. & Dyre, J. C. [2009]. Hidden scale invariance in molecular van der waals liquids: A simulation study., *Physical Review E* **80**: 041502.

Schrøder, T., Gnan, N., Pedersen, U. R., Bailey, N. P. & Dyre, J. C. [2011]. Pressure-energy correlations in liquids. V. Isomorphs in generalized lennard-jones systems, *Journal of Chemical Physics* **134**(164505): 164505.

Schrøder, T. B., Bailey, N. P., Pedersen, U. R., Gnan, N. & Dyre, J. C. [2009]. Pressure-energy correlations in liquids. iii. statistical mechanics and thermodynamics of liquids with hidden scale invariance, *The Journal Of Chemical Physics* **131**: 234503.

Tarjus, G., Kivelson, D., Mossa, S. & Alba-Simionesco, C. [2004]. Disentangling density and temperature effects in the viscous slowing down of glassforming liquids, *Journal of Chemical Physics* **121**: 11503.

Tölle, A. [2001]. Neutron scattering studies of the model glass former orthoterphenyl, *Reports on Progress in Physics* **64**: 1473–1532.

Win, K. Z. & Menon, N. [2006]. Glass transition of glycerol in the volume-temperature plane, *Physical Review E* **73**: 040501(R).

Zoller, P. & Walsh, D. J. [1995]. *Standard pressure-volume-temperature data for polymers.*, Lancaster,Pa.: Technomic Publishing.

Zwanzig, R. & Mountain, R. D. [1965]. High-frequency elastic moduli of simple fluids., *Journal of Chemical Physics* **43**(12): 4464–&.

A Reprint of publications

ARTICLES
PUBLISHED ONLINE: 3 JULY 2011 | DOI: 10.1038/NPHYS2031
nature physics

Predicting the density-scaling exponent of a glass-forming liquid from Prigogine–Defay ratio measurements

Ditte Gundermann[1], Ulf R. Pedersen[2], Tina Hecksher[1], Nicholas P. Bailey[1], Bo Jakobsen[1], Tage Christensen[1], Niels B. Olsen[1], Thomas B. Schrøder[1], Daniel Fragiadakis[3], Riccardo Casalini[3], C. Michael Roland[3], Jeppe C. Dyre[1] and Kristine Niss[1]*

Understanding the origin of the dramatic temperature and density dependence of the relaxation time of glass-forming liquids is a fundamental challenge in glass science. The recently established 'density-scaling' relation quantifies the relative importance of temperature and density for the relaxation time in terms of a material-dependent exponent. We show that this exponent for approximate single-parameter liquids can be calculated from thermoviscoelastic linear-response data at a single state point, for instance an ambient-pressure state point. This prediction is confirmed for the van der Waals liquid tetramethyl-tetraphenyl-trisiloxane. Consistent with this, a compilation of literature data for the Prigogine–Defay ratio shows that van der Waals liquids and polymers are approximate single-parameter systems, whereas associated and network-forming liquids are not.

Many liquids are known to exhibit peculiar, sometimes even spectacular behaviour. Water is a notorious example with its many intriguing anomalies[1,2]. This raises the questions: Do liquids exist with 'simple' behaviour and what characterizes such behaviour? Based on theory and simulations, recent papers[3–5] proposed such a class of liquids, 'strongly correlating liquids', which are approximate single-parameter liquids[6]. The possible existence of approximate single-parameter liquids[7–15] has important implications, particularly for addressing long-standing fundamental questions related to the glass transition[16–20], but so far it has not been convincingly demonstrated in experiment.

In this paper we present an experimental test of a striking prediction for strongly correlating liquids, namely that the density-scaling exponent—characterizing how to scale density and temperature for different state points to have the relaxation times superpose onto a master curve[21–24]—may be calculated from the equilibrium fluctuations at a single state point[5]. The equilibrium fluctuations are probed using the fluctuation–dissipation theorem, which relates linear-response functions to fluctuations. The experiments were performed on the van der Waals glass-forming liquid, tetramethyl-tetraphenyl-trisiloxane, which is a commercial silicone oil (DC704). The paper further presents a reinterpretation of the classical Prigogine–Defay ratio, showing that many other systems are strongly correlating, that is, approximate single-parameter liquids. All together these results suggest that van der Waals liquids are strongly correlating, confirming the long-held, general view that these are simpler than associated liquids. In contrast, network-forming liquids such as water, glycerol, or silica are much more complex.

Temperature and volume both play important roles for the viscous slowing down as the glass transition is approached from above[25,26]. The first measurements of viscosity under high pressure were published in 1949 by Bridgman[27], but only during the past decade has a substantial amount of data become available on the dynamics of viscous liquids at different pressures. The information comes mainly from dielectric spectroscopy, but inelastic neutron scattering and other experiments have also been performed under pressure (ref. 24 reviews the dynamics of glass-forming liquids under hydrostatic pressure). The most important experimental finding from high-pressure studies of liquid dynamics is probably density scaling, that is, the fact that the temperature (T) and density (ρ) dependences of the relaxation time for many liquids can be described in terms of the single scaling variable $\rho^{\gamma_{\rm scale}}/T$ (refs 21–24), where $\gamma_{\rm scale}$ is the so-called density-scaling exponent. Density scaling applies, for example, for van der Waals liquids, but not for hydrogen-bonded liquids[28].

A simple explanation of density scaling can be given for strongly correlating liquids. These are characterized by near proportionality between the isochoric thermal equilibrium fluctuations of the virial W and the potential energy U (refs 3–5), the quantities that give the configurational parts of pressure and energy, respectively. That is, W and U are the terms resulting from the molecular interactions, which are added to the kinetic ideal gas terms. The total energy E is the kinetic energy K plus the potential energy U, and the pressure p is likewise an ideal gas term Nk_BT/V plus the configurational part W/V:

$$E = K + U$$
$$pV = Nk_BT + W$$

Here V is the volume and N the number of particles. Both the virial and the potential energy fluctuate around their equilibrium

[1]DNRF Centre 'Glass and Time', IMFUFA, Department of Sciences, Roskilde University, Postbox 260, DK-4000 Roskilde, Denmark, [2]Department of Chemistry, University of California, Berkeley, California 94720-1460, USA, [3]Chemistry Division, Naval Research Laboratory, Washington, District of Columbia 20375-5342, USA. *e-mail: kniss@ruc.dk.

© 2011 Macmillan Publishers Limited. All rights reserved.

NATURE PHYSICS DOI: 10.1038/NPHYS2031

values. At any given time the fluctuations are defined by $\Delta W(t) = W(t) - \langle W \rangle$ and $\Delta U(t) = U(t) - \langle U \rangle$ (Δ is here used in the standard meaning of statistical mechanics, whereas in the Prigogine–Defay ratio literature Δ denotes the difference between liquid and glass properties).

A strongly correlating liquid has 'isomorphs', which are curves in the phase diagram along which a number of properties in reduced units—including the dynamics—are invariant[5]. The isomorph concept implies density scaling: A strongly correlating liquid's isomorphs obey the equation $\rho^{\gamma_{\rm isom}}/T = \text{Const.}$, where $\gamma_{\rm isom}$ is determined from the near proportionality between virial and potential energy isochoric fluctuations, $\Delta W(t) \cong \gamma_{\rm isom} \Delta U(t)$ (ref. 5). In particular, the reduced-unit relaxation time is a function of $\rho^{\gamma_{\rm isom}}/T$. The predicted equality of the fluctuation exponent $\gamma_{\rm isom}$ and the density-scaling exponent $\gamma_{\rm scale}$ has been verified for a few computer-simulated liquids[29,30], but never tested experimentally. Such a test is very demanding, however, because it involves new and unique measurements of several frequency-dependent thermoviscoelastic response functions.

In this work we present the first test of this type. To do so we have chosen a liquid expected to be strongly correlating. It is known from computer simulations and theoretical considerations that liquids with simple Lennard-Jones-like interactions are strongly correlating, whereas liquids with directional bonds (for example, hydrogen bonds) are not[3–5]. This is consistent with the experimental finding that van der Waals bonded liquids obey density scaling, whereas hydrogen-bonded liquids do not. It is important to keep in mind that strong *WU* correlation implies density scaling, whereas the opposite is not necessarily true. Density scaling might well hold for a larger class of liquids. However, at this point there are only theoretical predictions for the density scaling exponent of strongly correlating liquids.

As our test sample we have chosen the van der Waals glass-forming liquid tetramethyl-tetraphenyl-trisiloxane (DC704). We expect it to be strongly correlating because it has a very low dipole moment, which means that it is truly van der Waals bonded, while the dipole moment is large enough to give a good signal in the high-pressure dielectric measurements. DC704 is moreover chemically very stable and an excellent glass former.

Figure 1a shows the dielectric relaxation time, defined as the inverse angular loss-peak frequency, for DC704 as a function of density for different isotherms, as well as data taken at atmospheric pressure. pVT-data were used to calculate the density at each state point. Density scaling is demonstrated in Fig. 1b, showing that all data collapse onto a master curve when the reduced-unit relaxation time is plotted as a function of the scaling variable $\rho^{\gamma_{\rm scale}}/T$. The $\gamma_{\rm scale} = 6.2 \pm 0.2$ is an empirical fit parameter and the reduced-unit relaxation time $\tilde{\tau}$ is given by $\tilde{\tau} = C\rho^{1/3}T^{1/2}\tau$, where C is an arbitrary constant with no influence on the scaling (it only changes the numbers on the y-axis). The use of reduced units is theoretically correct, but the actual difference between using reduced units or absolute values is minimal in the supercooled region because the relaxation times vary over many orders of magnitude, whereas T only changes 30% and ρ even less. In fact, when we perform the scaling using absolute values of τ we find $\gamma_{\rm scale} = 6.1 \pm 0.2$.

Turning now to the isomorph prediction, the near proportionality of the equilibrium fluctuations, $\Delta W(t) \cong \gamma_{\rm isom} \Delta U(t)$, is consistent with the theoretical expression for $\gamma_{\rm isom}$ (the sharp brackets denote NVT ensemble averages)[5]

$$\gamma_{\rm isom} = \frac{\langle \Delta W \Delta U \rangle}{\langle (\Delta U)^2 \rangle}$$

To calculate this quantity from linear thermoviscoelastic measurements we reason as follows. A characteristic feature of viscous liquids is timescale separation. Fluctuations of the kinetic terms decorrelate on a picosecond timescale. Consequently, if one averages the fluctuations in pressure and energy over a timescale much longer than picoseconds but much shorter than the liquid's relaxation time, one gets the fluctuations of the configurational terms. For such averages it follows that $\langle \Delta W \Delta U \rangle / \langle (\Delta U)^2 \rangle \cong V \langle \Delta p \Delta E \rangle / \langle (\Delta E)^2 \rangle$. This brings us closer to something that can be accessed experimentally, because fluctuations in pressure and energy determine the thermoviscoelastic linear-response functions through the fluctuation–dissipation theorem: $V \langle \Delta p \Delta E \rangle / \langle (\Delta E)^2 \rangle = (\beta_V^{\rm slow} - \beta_V^{\rm fast})/(c_V^{\rm slow} - c_V^{\rm fast})$, where $\beta_V = \left(\partial p/\partial T\right)_V$ is the pressure coefficient and c_V the isochoric specific heat per unit volume. Here 'slow' response means the long-time (low-frequency) liquid-like limit, and 'fast' response means the short-time (high-frequency) solid-like limit of the relevant (complex) frequency-dependent linear-response function of the equilibrium liquid, still probing the system at times much longer than phonon times. Thus

$$\gamma_{\rm isom} = \frac{\beta_V(\omega \to 0) - \beta_V(\omega \to \infty)}{c_V(\omega \to 0) - c_V(\omega \to \infty)} \qquad (1)$$

The high-frequency values ($\omega \to \infty$) correspond to solid-like responses, where the liquid has time to explore only one potential energy minimum, a so-called inherent state. This implies that $\gamma_{\rm isom}$, as discussed later, can be evaluated approximately using the much easier measured values for the glassy state instead of the high-frequency values[4,31].

The two linear thermoviscoelastic response functions $\beta_V(\omega)$ and $c_V(\omega)$ refer to constant-volume measurements; experiments are usually performed under constant pressure, however. This problem can be overcome by measuring three independent thermoviscoelastic response functions and subsequently calculating $\beta_V(\omega)$ and $c_V(\omega)$ using standard thermodynamic relations. These relations include dynamic versions of the Maxwell relations, which are the so-called generalized Onsager reciprocity relations reflecting the time reversibility of the underlying microscopic equations of motion[32]. Unfortunately, even constant-pressure conditions are difficult to attain for ultra-viscous liquids because thermal expansion is often

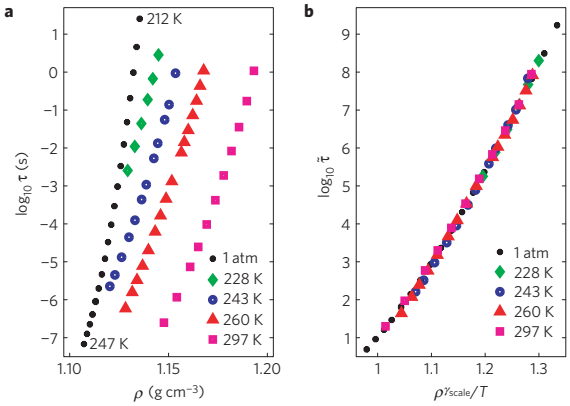

Figure 1 | The dielectric relaxation time τ measured along different isotherms and along the atmospheric pressure isobar for the silicone oil DC704. The points come from measured loss peaks and the relaxation times refer to inverse angular loss-peak frequencies. **a**, The relaxation times as functions of density (calculated from measured pVT-data). **b**, The reduced unit relaxation time, $\tilde{\tau} = C\rho^{1/3}T^{1/2}\tau$, as a function of $K\rho^{\gamma_{\rm scale}}/T$, where $\gamma_{\rm scale} = 6.2 \pm 0.2$ is a parameter adjusted to collapse the data of **a**. C and K are constants which have no influence on the quality of the scaling; they only shift the axes.

© 2011 Macmillan Publishers Limited. All rights reserved.

ARTICLES NATURE PHYSICS DOI: 10.1038/NPHYS2031

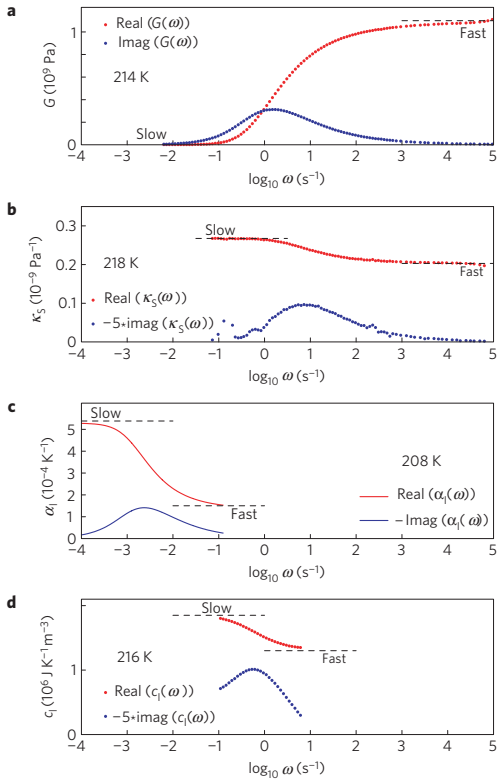

Figure 2 | Examples of frequency-dependent real and imaginary parts of the four required thermoviscoelastic response functions of DC704, illustrating the experimental challenges associated with checking the isomorph prediction $\gamma_{scale} = \gamma_{isom}$. The experimental techniques work in different frequency intervals (see the Methods section); to place the relaxation region central in the accessible frequency window for each technique we show data at temperatures that vary with response function. **a**, The shear modulus $G(\omega)$. **b**, The adiabatic compressibility $\kappa_S(\omega)$. **c**, The longitudinal expansion coefficient $\alpha_l(\omega)$, for which data were measured in the time domain and subsequently converted to the frequency representation by a numerical Laplace transform[34]. **d**, The longitudinal heat capacity $c_l(\omega)$.

limited in some directions, leading to significant shear stresses in the sample[33]. This implies that $c_p(\omega)$ is not measured directly; rather it is the 'longitudinal' dynamic heat capacity $c_l(\omega)$ that is measured in most experiments[33]. Similarly for thermal expansion we measure the dynamic longitudinal expansion coefficient $\alpha_l(\omega)$, rather than the dynamic isobaric expansion coefficient $\alpha_p(\omega)$ (ref. 34,39). Fortunately, knowledge of the shear modulus $G(\omega)$ allows one to calculate $c_p(\omega)$ and the isobaric expansion coefficient $\alpha_p(\omega)$ from data (see equation (2) below). In summary, to determine the predicted density-scaling exponent γ_{isom} we measured the following four complex linear thermoviscoelastic response functions: the dynamic adiabatic compressibility $\kappa_s(\omega)$, the dynamic longitudinal heat capacity $c_l(\omega)$, the dynamic longitudinal expansion coefficient $\alpha_l(\omega)$, and the dynamic shear modulus $G(\omega)$.

The dynamic shear modulus $G(\omega)$ was measured using a piezoceramic transducer[35], the dynamic adiabatic compressibility $\kappa_s(\omega)$ by a similar technique[36], and the dynamic longitudinal heat capacity $c_l(\omega)$ was measured using the 3ω-method[37] in a spherical geometry[38]. The dynamic longitudinal expansion coefficient $\alpha_l(\omega)$ was calculated by Laplace transformation of a signal measured in the time domain using capacitative dilatometry[34,39] (more details on the methods are given in the Methods section).

Examples of the measured complex, dynamic linear-response functions are shown in Fig. 2. In principle, we need only data at one state point to determine γ_{isom} from equation (1). In practice, we used several temperatures to estimate reliably the temperature dependence of the short-time and long-time levels. This was done to be able to extrapolate the DC704 expansion coefficient, which was obtained at lower temperatures than the other response functions (see the Methods section). The temperature 214 K is close to the calorimetric glass transition temperature of DC704, but it should be emphasized that all measurements refer to the linear response of the equilibrium liquid, a state that needs careful annealing to be reached, particularly at our lowest temperatures. The relevant values of $\beta_V(\omega)$ and $c_V(\omega)$ were calculated from the high- and low-frequency limits of the four measured thermoviscoelastic response functions, respectively, by solving the following four equations[33,34,38,39] with four unknowns:

$$c_l(\omega) = \frac{1+(4/3)G(\omega)\kappa_S(\omega)}{1+(4/3)G(\omega)\kappa_T(\omega)}c_p(\omega)$$

$$\alpha_l(\omega) = \frac{\alpha_p(\omega)}{1+(4/3)G(\omega)\kappa_T(\omega)}$$

$$c_V(\omega) = c_p(\omega) - \frac{T(\alpha_p(\omega))^2}{\kappa_T(\omega)} \qquad (2)$$

$$\kappa_S(\omega) = \frac{c_V(\omega)\kappa_T(\omega)}{c_p(\omega)}$$

and using the relation $\beta_V(\omega) = \alpha_p(\omega)/\kappa_T(\omega)$. The values of the measured short- and long-time levels at the reference temperature are reported in Table 1. When substituted into equation (1) we find that the isomorph prediction for the density-scaling exponent is $\gamma_{isom} = 6 \pm 2$, which is in good agreement with the experimental density-scaling exponent $\gamma_{scale} = 6.2 \pm 0.2$ (Fig. 1b). The large uncertainty of γ_{isom} derives from the fact that measuring the absolute values of the frequency-dependent thermoviscoelastic response functions is very challenging. Even considering the large uncertainty in the predicted γ_{isom}, it is striking that γ_{isom} agrees with the exponent from density scaling. This agreement shows that for DC704 thermoviscoelastic linear-response measurements at one ambient-pressure state point can be used to predict the density-scaling exponent, which describes the density and temperature dependence of relaxation times varying from micro- to kilo-seconds, measured at pressures up to 400 MPa over a 90 K temperature range. This is a main conclusion of the present paper.

The correlation coefficient between W and U in the NVT ensemble,

$$R = \frac{\langle \Delta W \Delta U \rangle}{\sqrt{\langle (\Delta U)^2 \rangle \langle (\Delta W)^2 \rangle}}$$

measures how strong the virial/potential energy correlations are in a liquid ($-1 \le R \le 1$; the closer R is to unity, the better correlation). It therefore provides a measure of how well a liquid is expected to follow the isomorph theory. Expressing R in terms of linear-response functions, it becomes clear that R is given directly by the linear NVT Prigogine–Defay (PD) ratio[6], Π_{VT}^{lin}:

$$R = \frac{\beta_V^{slow} - \beta_V^{fast}}{\sqrt{-(K_T^{slow} - K_T^{fast})(c_V^{slow} - c_V^{fast})/T}} = \frac{1}{\sqrt{\Pi_{VT}^{lin}}}$$

Here $K_T = 1/\kappa_T$ is the isothermal bulk modulus. The PD ratio equals unity if the liquid is a single-parameter liquid[7–15]. Thus, a perfectly correlating liquid is what was traditionally referred to as

© 2011 Macmillan Publishers Limited. All rights reserved.

NATURE PHYSICS DOI: 10.1038/NPHYS2031

Table 1 | Measured short-time ('fast') and long-time ('slow') levels of the four thermoviscoelastic response functions of DC704 at 214 K.

	DC704 (214 K)
c_l^{slow} [10^6 J (K m^3)$^{-1}$]	1.65±0.15
c_l^{fast} [10^6 J (K m^3)$^{-1}$]	1.35±0.05
κ_S^{slow} [10^{-9}Pa^{-1}]	0.25±0.03
κ_S^{fast} [10^{-9}Pa^{-1}]	0.19±0.03
α_l^{slow} [10^{-3}K^{-1}]	0.46±0.04
α_l^{fast} [10^{-3}K^{-1}]	0.11±0.01
G^{slow} [10^9Pa]	0
G^{fast} [10^9Pa]	1.1±0.05
$\Pi_{\text{pT}}^{\text{lin}}$	1.1±0.3
$\Pi_{\text{VT}}^{\text{lin}}$	1.2±0.6
R	0.9±0.2
γ_{isom}	6±2
γ_{scale}	6.2±0.2

These data were used to calculate the exponent γ_{isom} predicted to be equal to γ_{scale}. The error bars on the measured data reflect max–min values, the errors bars on the calculated values were identified using standard error propagation techniques.

a single-parameter liquid[6]. Earlier studies of the PD ratio gave no physical interpretation of values different from one, even if these were close to one. The above interpretation of the linear NVT PD ratio as given by the correlation coefficient shows that the PD ratio provides a measure of how strongly correlating a given liquid is.

When the linear NVT PD ratio is exactly unity, other linear PD ratios, for example, the experimentally relevant linear NpT PD ratio, are also unity[6]. When $\Pi_{\text{VT}}^{\text{lin}}$ is not strictly one, there is no such result, but by continuity we surmise that $\Pi_{\text{pT}}^{\text{lin}}$ is close to unity if and only if $\Pi_{\text{VT}}^{\text{lin}}$ is. For DC704 we find $\Pi_{\text{pT}}^{\text{lin}} = 1.1 \pm 0.3$ and $\Pi_{\text{VT}}^{\text{lin}} = 1.2 \pm 0.6$, which is consistent with this conjecture.

Whereas neither the linear NVT PD ratio nor the linear NpT PD ratio have been reported in the literature before this study, there are many reports on the classical (NpT) PD ratio. This quantity is calculated using temperature-extrapolated liquid and glassy static responses, where the glassy response is defined from the low-temperature ($T < T_g$) solid response:

$$\Pi_{\text{pT}}^{\text{classic}} \equiv \frac{(\kappa_T^{\text{liq}}(T_g) - \kappa_T^{\text{glass}}(T_g))(c_p^{\text{liq}}(T_g) - c_p^{\text{glass}}(T_g))}{T_g(\alpha_p^{\text{liq}}(T_g) - \alpha_p^{\text{glass}}(T_g))^2}$$

Here '(T_g)' indicates the extrapolation to the glass transition temperature. The classical PD ratio involves extrapolations and is therefore not rigorously well-defined[6,10,40,41]. Moreover, the glassy response depends on how the glass is made (for example, the cooling rate), which means that different protocols might well result in somewhat different values of the PD ratio. Nevertheless, the classical PD ratio provides an experimentally much easier route for estimating the degree of *WU* correlation than measuring the proper frequency-dependent linear thermoviscoelastic response functions at one temperature. In the absence of linear PD ratio data we compiled all the literature data we could find on the classical PD ratio.

Figure 3 shows the PD values for 22 glass formers, including polymers, a metallic alloy, inorganic and molecular liquids (both hydrogen-bond rich and van der Waals bonded). The systems have been sorted according to their PD ratio. In analogy with the NVT case, we define an approximate correlation coefficient of the NpT ensemble as the inverse square root of the NpT PD ratio. Network-bonded inorganic glass formers such as silica glasses and hydrogen-bond rich molecular liquids (for example, glycerol and glucose) have large PD ratios. In contrast, van der Waals systems, exemplified by the polymers and the two mixtures with o-terphenyl as the major constituent, have PD ratios close to one. This confirms the conjecture that van der Waals liquids are strongly correlating, whereas associated and network-forming liquids are not[4,5]. It is also interesting to compare propanol and glycerol, which have the same backbone of three carbon atoms, but one and three hydroxyl groups, respectively. Propanol, with only one hydroxyl group and therefore fewer hydrogen bonds, has a smaller PD ratio than glycerol. The pattern in Fig. 3 is consistent with computer simulation results, where liquids without directional bonding or competing interactions are generally found to be strongly correlating[4,5].

The glassy and liquid extrapolated response values used to calculate the classical PD ratio provide an alternative, but less well-defined way of calculating γ_{isom} (this type of expression for γ_{scale} was also found in ref. 31 by using an entropy-based model for the dynamics). We did the analysis on the data of a mixture of 67% o-terphenyl and 33% o-phenylphenol from a paper by Takahara and co-workers[42]. This mixture is a strongly correlating liquid with $\Pi_{\text{pT}}^{\text{classic}} = 1.20$ (ref. 42). We find $\gamma_{\text{isom}} = 5.4 \pm 1$, which is to be compared to the (absolute-unit) density scaling exponent for this liquid $\gamma_{\text{scale}} = 6.2 \pm 0.2$ (ref. 24). This is consistent with the isomorph prediction (see the Supplementary Information for details).

We have argued that the PD ratio of a large class of liquids should be regarded as essentially equal to unity. The general consensus, however, is that unity PD ratios are rare exceptions or not allowed (see, for example, refs 42–44). In recent years, several studies have been dedicated to understanding non-unity PD ratios. These approaches can be summarized as follows: (1) Linear-response theories of thermoviscoelasticity yielding non-unity ratios for systems with more than one internal state variable[6,13,45,46]. (2) A non-equilibrium thermodynamic theory explaining non-unity of the classical PD ratio as a non-equilibrium effect (even in the case of a single internal state variable)[43]. (3) A Landau theory using nano-thermodynamics where dynamical heterogeneity is the origin of non-unity PD ratios[47]. In this paper we adopted the first viewpoint, which is the original rigorous linear PD ratio interpretation going back to the seminal works by Moynihan and co-workers more than 30 years ago[10,48].

Our findings show that strongly correlating liquids exist not merely in computer simulations, but also as real liquids. These liquids are simpler than liquids in general, while still having all the hallmarks of viscous slowing down on supercooling, eventually leading to a glass transition. For strongly correlating liquids there is an 'isomorph filter'[5] according to which theories for the non-Arrhenius temperature dependence of the relaxation time can be sorted: only theories that express the relaxation time in terms of an isomorph invariant can be correct for strongly correlating liquids and thus be of general validity. Moreover, for strongly correlating liquids several phenomena can be explained in simple terms on the basis of the existence of isomorphs in the liquid's phase diagram[5]. Examples include isochronal superposition (that is, the finding that dielectric loss spectra under varying pressure and temperature are invariant for states with the same relaxation time), and ageing behaviour after temperature and density jumps[5,49]. These phenomena are well understood for perfectly correlating liquids, and liquids with strong correlations inherit the behaviour to a good approximation. The degree to which these phenomena survive as the correlation gets poorer is a cardinal point for further research; it is likely that some predictions are more sensitive to deviations from perfect correlation than others. We suggest that perfectly correlating liquids should be regarded as 'ideal gas' or 'Ising models'

© 2011 Macmillan Publishers Limited. All rights reserved.

ARTICLES NATURE PHYSICS DOI: 10.1038/NPHYS2031

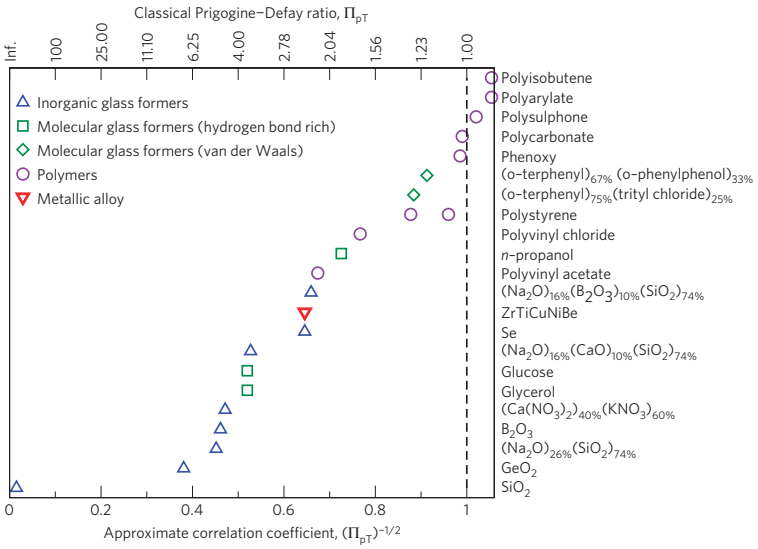

Figure 3 | Literature values of the classical (NpT) Prigogine–Defay (PD) ratios $\Pi_{pT}^{classic}$ of 22 glass formers. The liquids, which are sorted according to reported value of the PD ratio, include inorganic glass formers (triangles pointing up), hydrogen-bond-rich molecular liquids (squares), van der Waals molecular liquids (diamonds), polymers (circles), and a metallic alloy (triangle pointing down). The inverse square root of the classical NpT Prigogine–Defay ratio gives an estimate for the correlation coefficient (lower *x*-axis). Strong correlations are found in van der Waals bonded molecular liquids and polymers (the Supplementary Information provides the PD values shown in the figure and relevant references; note that each symbol in the figure corresponds to the liquid listed to the right).

of liquids—that is, simple systems for which a number of generic features of the glass transition phenomenology can be understood. In this way, the identification of what constitutes a 'simple' liquid will hopefully lead to a better general understanding of viscous liquids and the glass transition.

Methods

The liquid studied, the Dow Corning diffusion pump silicone oil tetramethyl-tetraphenyl-trisiloxane DC704, was used as received without further purification. The different measurements (in total six different experiments) were performed on a sample taken from the same bottle. DC704 is not hygroscopic so water contamination is not a problem. Moreover, the pVT measurements and the high pressure dielectric spectroscopy measurements used to determine γ_{scale} were performed in the same lab and by the same team. For all these reasons we are fairly confident by the γ_{scale} of DC704 reported in the paper; the uncertainties are much larger for γ_{isom}.

The four thermoviscoelastic linear-response techniques use a custom-built cryostat[50]. $G(\omega)$, $\kappa_S(\omega)$ and $c_l(\omega)$ were measured in the same cryostat; $\alpha_l(\omega)$ was obtained from measurements in the same type of cryostat and the temperatures were calibrated with dielectric spectra taken on the DC704 sample, ensuring that the absolute temperature calibration was the same for all types of measurements.

The shear modulus $G(\omega)$ is measured over the frequency range 10^{-3}–10^{4} Hz (ref. 35), and the adiabatic compressibility $\kappa_S(\omega)$ is measured over 10^{-2}–10^{4} Hz (ref. 36). Both methods are optimized for measurements on very stiff materials (modulus ranges of MPa–GPa) and are based on piezoceramic materials that act as converters of mechanical properties into electrical properties.

The measurements of specific heat were done using a 3ω thermal-effusion method in a spherical geometry[38], a technique which is equivalent to the planar plate 3ω technique of Birge and Nagel[37], however using a spherical thermistor bead instead of a thin planar metal film. It covers a frequency range of $10^{-2.5}$–$10^{0.5}$ Hz, limited by the intrinsic frequency dependence of the thermal impedance in this geometry. The isobaric specific heat, $c_p(\omega) = (\kappa_T(\omega)/\kappa_S(\omega))c_V(\omega)$ is not measured in this geometry; rather what is measured is the longitudinal specific heat, $c_l(\omega) = (M_S(\omega)/M_T(\omega))c_V(\omega)$ (where $M(\omega)$ represents longitudinal moduli)[38].

The measurements of the longitudinal thermal expansion coefficient in the time domain $\alpha_l(t)$ were carried out using a microregulator[34,50], allowing for fast temperature changes of a small planar capacitor. This technique is based on a temperature-step variant of 'capacitive scanning dilatometry'[39], which uses the fact that the capacitance of a capacitor is inversely proportional to the thickness of the liquid in the capacitor. What is measured in this geometry is the longitudinal thermal expansion coefficient[34,39] α_l (see equation (2); ref. 33 for a derivation). The dynamic longitudinal expansion coefficient $\alpha_l(\omega)$ shown in Fig. 2 was calculated by Laplace transformation of a signal measured in the time domain. However, equation (1) requires only knowledge of the high and low-frequency limits of the response functions and the required limits for $\alpha_l(\omega)$ were obtained directly from the data measured in the time domain (as short and long-time limits respectively), that is, without a Laplace transformation.

The heat capacity is the response function for which data are measured over the narrowest frequency (and therefore also temperature) range. The studied temperature range was 214–218 K, and within the experimental uncertainties there is no temperature dependence of the slow and fast values. We chose 214 K as the reference temperature to minimize the extrapolation required of the expansion coefficient data, which were measured in the 204–210 K range.

All data were taken in thermal equilibrium, a state it takes careful annealing to reach at low temperatures.

Received 20 December 2010; accepted 25 May 2011; published online 3 July 2011

References

1. Debenedetti, P. G. Supercooled glassy water. *J. Phys. Condens. Matter* **15,** R1669–R1726 (2003).
2. Angell, C. A. Insights into phases of liquid water from study of its unusual glass-forming properties. *Science* **319,** 582–587 (2008).
3. Pedersen, U. R., Bailey, N. P., Schrøder, T. B. & Dyre, J. C. Strong pressure–energy correlations in van der Waals liquids. *Phys. Rev. Lett.* **100,** 015701 (2008).
4. Schrøder, T. B., Bailey, N. P., Pedersen, U. R., Gnan, N. & Dyre, J. C. Pressure–energy correlations in liquids. III. Statistical mechanics and thermodynamics of liquids with hidden scale invariance. *J. Chem. Phys.* **131,** 234503 (2009).
5. Gnan, N., Schrøder, T. B., Pedersen, U. R., Bailey, N. P. & Dyre, J. C. Pressure–energy correlations in liquids. IV. "Isomorphs" in liquid phase diagrams. *J. Chem. Phys.* **131,** 234504 (2009).
6. Ellegaard, N. L. *et al.* Single-order-parameter description of glass-forming liquids: A one-frequency test. *J. Chem. Phys.* **126,** 074502 (2007).
7. Davies, R. O. & Jones, G. O. Thermodynamic and kinetic properties of glasses. *Adv. Phys.* **2,** 370–410 (1953).
8. Prigogine, I. & Defay, R. *Chemical Thermodynamics* (Longmans Green and Co., 1954).
9. Goldstein, M. Some thermodynamic aspects of the glass transition: Free volume, entropy, and enthalpy theories. *J. Chem. Phys.* **39,** 3369–3374 (1963).

© 2011 Macmillan Publishers Limited. All rights reserved.

10. Moynihan, C. T. & Gupta, P. K. Order parameter model for structural relaxation in glass. *J. Non-Cryst. Solids* **29,** 143–158 (1978).
11. Berg, J. I. & Cooper, A. R. Linear non-equilibrium thermodynamic theory of glass-transition kinetics. *J. Chem. Phys.* **68,** 4481–4485 (1978).
12. Hodge, I. M. Enthalpy relaxation and recovery in amorphous materials. *J. Non-Cryst. Solids* **169,** 211–266 (1994).
13. Nieuwenhuizen, Th. M. Ehrenfest relations at the glass transition: Solution to an old paradox. *Phys. Rev. Lett.* **79,** 1317–1320 (1997).
14. Wondraczek, L., Krolikowski, S. & Behrens, H. Relaxation and Prigogine–Defay ratio of compressed glasses with negative viscosity-pressure dependence. *J. Chem. Phys.* **130,** 204506 (2009).
15. Lion, A. & Peters, J. Coupling effects in dynamic calorimetry: Frequency-dependent relations for specific heat and thermomechanical responses—a one-dimensional approach based on thermodynamics with internal state variables. *Thermochim. Acta* **500,** 76–78 (2010).
16. Angell, C. A., Ngai, K. L., McKenna, G. B., McMillan, P. F. & Martin, S. W. Relaxation in glassforming liquids and amorphous solids. *J. Appl. Phys.* **88,** 3113–3157 (2000).
17. Dyre, J. C. The glass transition and elastic models of glass-forming liquids. *Rev. Mod. Phys.* **78,** 953–972 (2006).
18. Cavagna, A. Supercooled liquids for pedestrians. *Phys. Rep.* **476,** 51–124 (2009).
19. Floudas, G., Paluch, M., Grzybowski, A. & Ngai, K. L. *Molecular Dynamics of Glass-Forming Systems* (Advances in Dielectrics, Springer, 2010).
20. Berthier, L., Biroli, G., Bouchaud, J-P., Cipelletti, L. & van Saarloos, W. (eds). Dynamical heterogeneities in glasses, colloids, and granular media. Oxford Univ. Press (in the press).
21. Alba-Simionesco, C., Cailliaux, A., Alegria, A. & Tarjus, G. Scaling out the density dependence of the α relaxation in glass-forming polymers. *Europhys. Lett.* **68,** 58–64 (2004).
22. Dreyfus, C., Le Grand, A., Gapinski, J., Steffen, W. & Patkowski, A. Scaling the α-relaxation time of supercooled fragile organic liquids. *Eur. Phys. J. B* **42,** 309–319 (2004).
23. Casalini, R. & Roland, C. M. Thermodynamical scaling of the glass transition dynamics. *Phys. Rev. E* **69,** 062501 (2004).
24. Roland, C. M., Hensel-Bielowka, S., Paluch, M. & Casalini, R. Supercooled dynamics of glass-forming liquids and polymers under hydrostatic pressure. *Rep. Prog. Phys.* **68,** 1405–1478 (2005).
25. Ferrer, M. L. *et al.* Supercooled liquids and the glass transition: Temperature as the control variable. *J. Chem. Phys.* **109,** 8010–8015 (1998).
26. Roland, C. M. Relaxation phenomena in vitrifying polymers and molecular liquids. *Macromol* **43,** 7875–7890 (2010).
27. Bridgman, P. W. Viscosities to 30,000 kg/cm^2. *Proc. Am. Acad. Arts Sci.* **77,** 117–128 (1949).
28. Roland, C. M., Casalini, R., Bergman, R. & Mattsson, J. Role of hydrogen bonds in the supercooled dynamics of glass-forming liquids at high pressures. *Phys. Rev. B* **77,** 012201 (2008).
29. Coslovich, D. & Roland, C. M. Density scaling in viscous liquids: From relaxation times to four-point susceptibilities. *J. Chem. Phys.* **131,** 151103 (2009).
30. Schrøder, T. B., Pedersen, U. R., Bailey, N. P., Toxvaerd, S. & Dyre, J. C. Hidden scale invariance in molecular van der Waals liquids: A simulation study. *Phys. Rev. E* **80,** 041502 (2009).
31. Casalini, R., Mohanty, U. & Roland, C. M. Thermodynamic interpretation of the scaling of the dynamics of supercooled liquids. *J. Chem. Phys.* **125,** 014505 (2006).
32. de Groot, S. R. & Mazur, P. *Non-Equilibrium Thermodynamics* (North-Holland, Amsterdam, 1962).
33. Christensen, T., Olsen, N. B. & Dyre, J. C. Conventional methods fail to measure $c_p(\omega)$ of glass-forming liquids. *Phys. Rev. E* **75,** 041502 (2007).
34. Niss, K., Christensen, T. & Dyre, J. C. Measuring the dynamic thermal expansivity of molecular liquids near the glass transition. Preprint at http://arXiv.org/abs/1103.4104 (2011).
35. Christensen, T. & Olsen, N. B. A rheometer for the measurement of a high shear modulus covering more than seven decades of frequency below 50 kHz. *Rev. Sci. Instrum.* **66,** 5019–5031 (1995).
36. Christensen, T. & Olsen, N. B. Determination of the frequency-dependent bulk modulus of glycerol using a piezoelectric spherical shell. *Phys. Rev. B* **49,** 15396–15399 (1994).
37. Birge, N. O. & Nagel, S. R. Specific-heat spectroscopy of the glass-transition. *Phys. Rev. Lett.* **54,** 2674–2677 (1985).
38. Jakobsen, B., Olsen, N. B. & Christensen, T. Frequency-dependent specific heat from thermal effusion in spherical geometry. *Phys. Rev. E* **81,** 061505 (2010).
39. Bauer, C. *et al.* Capacitive scanning dilatometry and frequency-dependent thermal expansion of polymer films. *Phys. Rev. E* **61,** 1755–1764 (2000).
40. Roe, R. J. Thermodynamics of glassy state with multiple order parameters. *J. Appl. Phys.* **48,** 4085–4091 (1977).
41. Moynihan, C. T. & Lesikar, A. V. Comparison and analysis of relaxation processes at the glass-transition temperature. *Ann. N.Y. Acad. Sci.* **371,** 151–169 (1981).
42. Takahara, S., Ishikawa, M., Yamamuro, O. & Matsuo, T. Structural relaxations of glassy polystyrene and o-terphenyl studied by simultaneous measurement of enthalpy and volume under high pressure. *J. Phys. Chem. B* **103,** 792–796 (1999).
43. Schmelzer, J. W. P. & Gutzow, I. The Prigogine–Defay ratio revisited. *J. Chem. Phys.* **125,** 184511 (2006).
44. Banerjee, R., Modak, S. K. & Samanta, S. Glassy phase transition and stability in black holes. *Eur. Phys. J. C* **70,** 317–328 (2010).
45. Pick, R. M. The Prigogine–Defay ratio and the microscopic theory of supercooled liquids. *J. Chem. Phys.* **129,** 124115 (2008).
46. Liebl, C., Lion, A., Kolmeder, S. & Peters, J. Representation of the glass-transition in mechanical and thermal properties of glass-forming materials: A three-dimensional theory based on thermodynamics with internal state variables. *J. Mech. Phys. Solids* **58,** 1338–1360 (2010).
47. Javaheri, M. R. H & Chamberlin, R. V. A free-energy landscape picture and Landau theory for the dynamics of disordered materials. *J. Chem. Phys.* **125,** 154503 (2006).
48. Lesikar, A. V. & Moynihan, C. T. Some relations connecting volume and enthalpy relaxation in the order parameter model of liquids and glasses. *J. Chem. Phys.* **72,** 6422–6423 (1980).
49. Gnan, N., Maggi, C., Schrøder, T. B. & Dyre, J. C. Predicting the effective temperature of a glass. *Phys. Rev. Lett.* **104,** 125902 (2010).
50. Igarashi, B. *et al.* A cryostat and temperature control system optimized for measuring relaxations of glass-forming liquids. *Rev. Sci. Instrum.* **79,** 045105 (2008).

Acknowledgements

The Centre for Viscous Liquid Dynamics 'Glass and Time' is sponsored by the Danish National Research Foundation (DNRF). Work at NRL is supported by Office of Naval Research. URP is supported by The Danish Council for Independent Research in Natural Sciences.

Author contributions

U.R.P. and K.N. conceived the project. D.G., U.R.P., B.J., J.C.D. and K.N. wrote the paper with input from C.M.R. D.G., U.R.P., and K.N. did the main data analysis. T.H. measured the shear modulus and compressibility and did the raw data analysis. B.J. and T.C. measured the heat capacity and did the raw data analysis. K.N. measured the expansion coefficient and did the raw data analysis. T.C. and N.B.O. conceived and developed the four thermoviscoelastic measuring techniques used. D.G., D.F. and R.C. measured the high-pressure data and did the scaling data analysis. U.R.P., N.P.B., T.C., T.B.S. and J.C.D. supplied the theoretical background for the project, which was coordinated by K.N.

Additional information

The authors declare no competing financial interests. Supplementary information accompanies this paper on www.nature.com/naturephysics. Reprints and permissions information is available online at http://www.nature.com/reprints. Correspondence and requests for materials should be addressed to K.N.

© 2011 Macmillan Publishers Limited. All rights reserved.

PHYSICAL REVIEW E **85**, 041501 (2012)

Dynamic thermal expansivity of liquids near the glass transition

Kristine Niss, Ditte Gundermann, Tage Christensen, and Jeppe C. Dyre
DNRF Centre "Glass and Time", IMFUFA, Department of Sciences, Roskilde University, Postbox 260, DK-4000 Roskilde, Denmark
(Received 21 December 2011; published 9 April 2012)

Based on previous works on polymers by Bauer *et al*. [Phys. Rev. E **61**, 1755 (2000)], this paper describes a capacitative method for measuring the dynamical expansion coefficient of a viscous liquid. Data are presented for the glass-forming liquid tetramethyl tetraphenyl trisiloxane (DC704) in the ultraviscous regime. Compared to the method of Bauer *et al*., the dynamical range has been extended by making time-domain experiments and by making very small and fast temperature steps. The modeling of the experiment presented in this paper includes the situation in which the capacitor is not full because the liquid contracts when cooling from room temperature down to around the glass-transition temperature, which is relevant when measuring on a molecular liquid rather than a polymer.

DOI: 10.1103/PhysRevE.85.041501 PACS number(s): 64.70.pm, 65.60.+a

The glass transition occurs when the configurational degrees of freedom of a liquid are frozen in. Below the glass-transition temperature, T_g, only isostructural contraction takes place as temperature is decreased further. The measured thermal-expansion coefficient α_p (and heat capacity c_p) are therefore lower in the glass than in the equilibrium liquid. This change of the thermal-expansion coefficient (and the heat capacity) is probably the most classical signature of the glass transition, and a figure illustrating this change (see Fig. 1) is almost inevitably the starting point of introductory talks or texts on the glass transition (see, e.g., Refs. [1] and [2]).

The change in the heat capacity at the glass transition, $\Delta c_p = c_{p,\mathrm{liq}} - c_{p,\mathrm{glass}}$, has been studied extensively and is widely believed to play a role for the dynamics of liquids close to the glass transition. The change in expansion coefficient, $\Delta\alpha_p = \alpha_{p,\mathrm{liq}} - \alpha_{p,\mathrm{glass}}$, has received less attention but is of similar importance. This is seen, for instance, in the literature related to the Prigogine-Defay ratio, a dimensionless number characterizing the glass transition [3–7].

The glass is an out-of-equilibrium state and therefore the values of the thermodynamic derivatives are not rigorously well defined. They depend on cooling rate and also on the time spent in the glassy state. Contrary to this, the linear response of the metastable equilibrium liquid state is well-defined and history-independent [7]. The linear expansion coefficient of a viscous liquid close to its glass transition is dynamic, that is, time- (or frequency-) dependent, with short times giving a low (glasslike) value, $\alpha_{p,\mathrm{fast}}$, while long times give a higher liquid value, $\alpha_{p,\mathrm{slow}}$. The difference between these two levels, $\Delta\alpha_{p,\mathrm{lin}} = \alpha_{p,\mathrm{slow}} - \alpha_{p,\mathrm{fast}}$, thus gives well-defined information on the configurational part of the expansion coefficient. Likewise, $\Delta c_{p,\mathrm{lin}} = c_{p,\mathrm{slow}} - c_{p,\mathrm{fast}}$ is well-defined.

The relaxation between the fast and the slow response takes place on a certain time scale which is temperature-dependent. Considered in this way, the measurement of the expansion coefficient, just like the heat capacity [8,9], can be viewed as a type of spectroscopy, which gives both a relaxation time and a spectral shape analogous to other methods such as dielectric spectroscopy or mechanical spectroscopy. The study of the temperature dependence of relaxation times and of the spectral shape of different response functions is vital for understanding the viscous slowing down. There is a general belief that the liquid has a relaxation time that is fairly well-defined independent of probe, but there are also suggestions that different processes may decouple from each other at low temperatures [10].

There are good scientific reasons to study the dynamic linear expansion coefficient, but almost no data of this type are to be found in the literature. The time-dependent expansion coefficient can be found by studying the change in volume as a function of time after a temperature step. Such volume relaxation experiments are very classic in glass science and are still important [11–14]. However, volume relaxation experiments are traditionally performed as nonlinear aging experiments, i.e., with large amplitudes in the temperature jump. This type of experiment gives information on the relaxation of the configurational degrees of freedom, but the expansion coefficient and its characteristic time scale cannot be determined because the results depend on the amplitude and sign of the temperature jump. For sufficiently small temperature steps, this is not the case; this defines the linear-response regime.

The only linear dynamic data of which we are aware were reported about a decade ago by Bauer *et al*. [15,16] followed by a paper by Fukao and Miyamoto [17]. These papers reported frequency-domain measurements on thin polymer films, performed with temperature scans at a couple of fixed frequencies, covering 1.5 decades of the dynamics. The measurements were pioneering, but 1.5 decades is not very much for studying relaxation in viscous liquids because the relaxation is extremely temperature-dependent and quite "stretched," which means that even at one fixed temperature the relaxation covers several decades.

The technique developed by Bauer *et al*. is based on a principle by which the sample is placed in a parallel plate capacitor such that it is the sample that maintains the spacing between the plates. Thus a change in sample volume in response to temperature change leads to a change of the capacitance. This principle is also used in the present work. The advantage of this technique is that capacitance can be

Published by the American Physical Society under the terms of the Creative Commons Attribution 3.0 License. Further distribution of this work must maintain attribution to the author(s) and the published article's title, journal citation, and DOI.

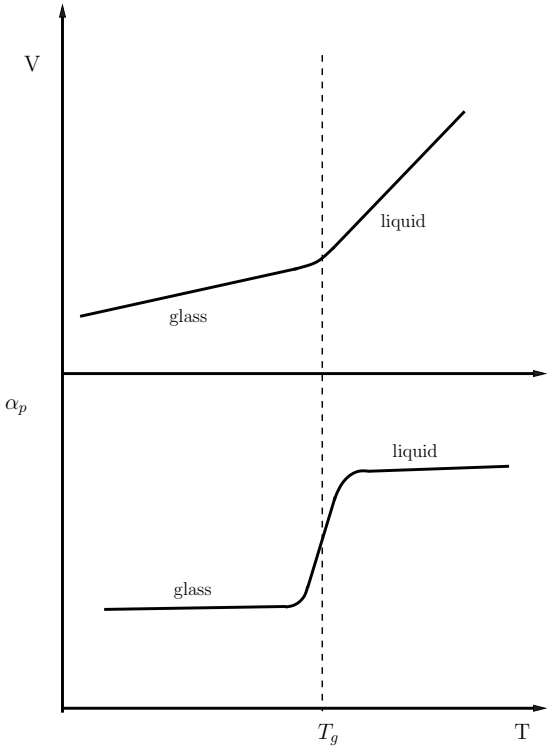

FIG. 1. Illustration of the temperature dependence of the volume and expansion coefficient of a liquid in the vicinity of the glass transition. Upon cooling, the expansivity decreases abruptly at the glass transition. This gives rise to a kink in the temperature dependence of the volume. These features are the original signatures of the glass transition.

measured with high accuracy, and it is this accuracy that makes linear experiments possible.

The use of sample-filled capacitors for measuring an expansion coefficient is not unique, and it has been done by others before and after Bauer *et al*. (see, e.g., Refs. [18–21]) in capacitative scanning dilatometry, i.e., working in a temperature ramping mode. To the best of our knowledge, capacitative scanning dilatometry has never been used on simple liquids. It is particularly useful for studying thin polymer films because the signal gets better with a thin sample. The technique has been used for determining the glass-transition temperature, for example as a function of film thickness [19,20] or as a function of cooling rate [18]. The main focus of these papers is on the temperature dependence of the expansion coefficient, while little attention is given to the absolute values. There have been no studies of the dynamics since the pioneering work of Bauer and no attempts to extend the dynamical range.

To the best of our knowledge, there are no measurements of the dynamic linear expansion coefficient of molecular liquids. The reported data from scanning dilatometry and nonlinear volume relaxation are also mainly for polymers, while data on molecular liquids are relatively scarce. This may be due to the higher technological importance of polymers. It is probably also related to the fact that working with molecular liquids requires other experimental conditions, meaning that techniques developed for polymers are not always directly applicable to liquids.

This paper gives a description of an experimental method developed for measuring the dynamical expansion coefficient of a viscous liquid. As mentioned, the principle is based on the capacitive technique by Bauer *et al*. [15,16]. The method is modified in three respects compared to the work of Bauer *et al*.: (i) The modeling takes into account the situation in which the capacitor is not full, which is relevant when measuring on a molecular liquid rather than on a polymer. (ii) The experiment is performed in the time domain using a very fast temperature regulation, which gives a dynamical range of more than four decades. (iii) The sensitivity is enhanced by using a capacitance bridge with a very high resolution. This makes it possible to measure the response following very small temperature steps, ensuring that the response is close to perfectly linear. As an application of the technique, the paper presents data on the glass-forming liquid tetramethyl tetraphenyl trisiloxane (DC704) in the ultraviscous regime.

I. RESPONSE FUNCTIONS WITH CONSISTENT DIMENSIONS

In a linear-response experiment, the response of a system to an external perturbation is studied. If the perturbation is small, the output is assumed to be linearly dependent on the input. The formalism to describe this is well known. However, different formulations can be used, and the version used in this work when converting the measured time-domain response to the frequency-domain response function may not be the most common one. The formalism used here has the advantage that the time-domain response function and the frequency-domain response function have the same dimension and there is no differentiation involved when transforming between the two. This section gives a summary of the response function formalism used, including a comparison to the standard formalism.

The fundamental assumption is that the output depends linearly on the input. The most general statement is that the change in input $dI(t')$ at time t' leads to a contribution in output $dO(t)$ at time t:

$$dO(t) = R(t - t')dI(t'). \tag{1}$$

It is assumed here that the change in output only depends on the time difference $(t - t')$. Causality implies that

$$R(t) = 0 \text{ for } t < 0. \tag{2}$$

Integrating on both sides of Eq. (1),

$$O(t) = \int_{-\infty}^{t} R(t - t')dI(t'),$$

and substituting $t'' = t - t'$ and writing $\dot{I}(t) = \dfrac{dI(t)}{dt}$,

$$O(t) = -\int_{\infty}^{0} R(t'')\dot{I}(t - t'')dt''.$$

Changing t'' to t',

$$O(t) = \int_0^\infty R(t')\dot{I}(t-t')dt'. \quad (3)$$

If the input is a Heaviside function,

$$I(t) = I_0 H(t) = I_0 \begin{cases} 0 & \text{for} \quad t \leqslant 0, \\ 1 & \text{for} \quad t > 0, \end{cases}$$

then

$$O(t) = I_0 \int_0^\infty R(t')\delta(t-t')dt' = I_0 R(t), \quad (4)$$

and it is seen that $R(t)$ is the output from a Heaviside step input.

Linear response can also be studied in the frequency domain. In the case of a harmonic-oscillating input $I(t) = I_0 e^{i(\omega t+\phi_I)}$, the output $O(t) = O_0 e^{i(\omega t+\phi_O)}$ will be a periodic signal with the same frequency ω, but there will be a phase shift of the output relative to the input. From Eq. (3), the output is

$$\begin{aligned} O(t) &= \int_0^\infty R(t')i\omega I_0 e^{i\phi_I} e^{i\omega(t-t')}dt' \\ &= I_0 e^{i\omega t} e^{i\phi_I} i\omega \int_0^\infty R(t')e^{-i\omega t'}dt' = I(t)R(\omega), \end{aligned}$$

where $R(\omega)$ is the frequency domain response function, which is given by the Laplace transform of $R(t)$ times $i\omega$:

$$R(\omega) = i\omega \int_0^\infty R(t')e^{-i\omega t'}dt'. \quad (5)$$

The linear-response relation is often expressed in an alternative formulation, where the linearity assumption is expressed by

$$O(t) = \int_{-\infty}^t \mu(t-t')I(t')dt',$$

where μ is sometimes called the memory function, but it is also sometimes called the response function. The use of the term "response function' for $\mu(t)$ is somewhat inconvenient because it has a different dimension compared to the frequency-domain response function $R(\omega)$. Substituting again $(t'' = t - t')$ and changing t'' to t',

$$O(t) = \int_0^\infty \mu(t')I(t-t')dt'.$$

Applying a Heaviside input again,

$$O(t) = \int_0^\infty \mu(t')I_o H(t-t')dt' = I_0 \int_0^t \mu(t')dt'. \quad (6)$$

From Eqs. (4) and (6), we have

$$R(t) = \int_0^t \mu(t')dt',$$

and therefore

$$\frac{dR(t)}{dt} = \mu(t). \quad (7)$$

In the memory function formalism, the frequency-domain response is again found by inserting a harmonic-oscillating input. In this case, the result becomes

$$R(\omega) = \int_0^\infty \mu(t')e^{-i\omega t'}dt' = \int_0^\infty \frac{dR(t')}{dt'}e^{-i\omega t'}dt',$$

where the last equality comes from inserting Eq. (7). This expression is formally equivalent to Eq. (5), which can be shown by integration by parts and by invoking $R(t=0)=0$. However, when converting data in practice, Eq. (5) has the advantages that differentiation of the time-domain data is avoided. It is always good to avoid differentiation of numerical data because it introduces increased noise. Moreover, if we introduce an "instantaneous" response in terms of $R(t \to 0) \neq 0$ corresponding to very short times where we cannot measure the time dependence of the response, then this information would be lost by differentiation.

II. PRINCIPLE, DESIGN, AND PROCEDURE

The method requires that there is a simple relation between sample density and dielectric constant. The dielectric constant in general has two contributions: atomic polarization and rotational polarization [22]. The atomic polarization is due to the displacement of the electron cloud upon application of a field. This contribution is governed by the microscopic polarizability of the molecule, x (usually called α, but α is reserved for the expansivity in this paper). The atomic polarizability can be assumed to be temperature- and density-independent in the relevant range. This means that the desired simple relation between density and dielectric constant can be obtained when the atomic polarization is the only contribution.

The rotational polarization is due to rotation of the permanent dipoles in the sample. This contribution is relevant when the liquid has a permanent dipole moment and mainly at frequencies lower than or comparable to the inverse relaxation time of the liquid. The rotational contribution gives the dielectric signal monitored in standard dielectric spectroscopy. The rotational polarization is temperature-, density-, and frequency-dependent, and it is therefore nontrivial to relate the density to the dielectric constant when rotational polarization is present. Therefore, in capacitative dilatometry it is a contribution one would like to avoid. It is sometimes assumed that the high-frequency plateau value of the dielectric constant measured in dielectric spectroscopy contains only atomic polarization and that it corresponds to the square of the refraction index n^2. However, there is also a fast ("glasslike") contribution to the rotational part of the polarization. The fast rotational contribution will dominate over the geometric effects even at high frequencies if the sample has a high dipole moment. This was demonstrated in Ref. [23]. To minimize the rotational contribution, two things are done: (i) Only liquids with very small dipole moment are studied, i.e., liquids in which the atomic polarization is dominant at all frequencies and temperatures. (ii) These liquids are only studied at frequencies much higher than the inverse relaxation time. In the data reported in this paper, the measuring frequency is 10 kHz and the relaxation time is 100 s or more.

The cell is a capacitor made of circular copper plates of 1 cm diameter and 1 mm thickness, with a 50-μm spacing. The separation is kept by four 0.5 mm $\times$ 0.5 mm and 50-μm-thick Kapton spacers. The spacing between the capacitor plates is filled with the sample liquid. The thin spacing results in a reasonably large dielectric signal (empty capacitance is 14 pF) despite the small size. The thin spacing moreover makes it possible to heat or cool the sample fast, even though the heat

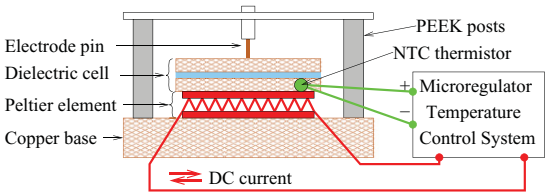

FIG. 2. (Color) Schematic drawing of the dielectric measuring cell with the microregulator. The liquid is deposited in the 50 μm gap between the disks of the dielectric cell. The Peltier element heats or cools the dielectric cell, depending on the direction of the electrical current powering the element. The current is controlled by an analog temperature-control system that receives temperature feedback information from an NTC thermistor embedded in one disc of the dielectric cell (reproduced from Ref. [25]).

diffusion in the sample liquid is slow compared to the heat diffusion in the copper plates.

The cell is integrated with a microregulator, which is a tiny temperature regulator based on an NTC thermistor (placed in the lower copper plate of the capacitor cell), a Peltier element acting as a local source of heating and cooling, and an analog proportional-integral-derivative (PID) control. The integrated cell and microregulator are placed in our main cryostat. With this setup, the temperature of the sample can be changed by steps of up to 2 K within less than 10 s and the temperature can be kept stable within a few micro Kelvin over days and weeks. The cell is shown in Fig. 2 and the whole system of the main cryostat and the microregulator is described in detail in Ref. [24].

The temperature of the microregulated cell is calibrated to the average temperature of the main cryostat. This is done by adjusting the microregulator's set point until the regulation power of the microregulator fluctuates around zero. The temperature is moreover measured with the thermistor bead both before and after turning on the microregulator, and finally the calibration is verified by checking that the dielectric response of the sample does not change by turning on the microregulator.

The principle of the experiment is to make an "instantaneous" step in temperature and subsequently measure the capacitance at a fixed frequency as a function of time. From the capacitance we calculate the time-dependent expansion coefficient. In order for the temperature step to be "instantaneous" compared to the time scale of the relaxation, we need the relaxation time to be 100 s or longer. This means that the measurements are performed at or below the conventional glass-transition temperature. Nevertheless, it is important to emphasize that the liquid is in equilibrium when the experiment is performed because we wait at least five relaxation times whenever stepping to a new temperature before making a measurement. The measurements themselves also must be carried out over five relaxation times in order to obtain the relaxation curve all the way to equilibrium. Altogether, it takes days and sometimes even weeks to take a spectrum at a given temperature. This means that the experiment would be impossible without the stable temperature control ensured by the microregulator.

The relaxation time of viscous liquids close to the glass transition is extremely temperature-dependent. We therefore need to make small temperature steps in order for the measured response to be linear. This means that the change in volume and thereby the measured capacitance is very small; the relative changes in capacitance dC/C are of order 10^{-4}. We use an AH2700A Andeen Hagerling ultraprecision capacitance bridge, which measures capacitance with an accuracy of 5 ppm and true resolution of 0.5 aF in the frequency range 50 Hz–20 kHz. The capacitance is measured every second at 10 kHz.

The sample used is liquid at room temperature and the capacitor is filled by letting the liquid imbibe using the capillary effect. Complete filling is checked by measuring the capacitance before and after filling, comparing to the measured dielectric constant measured at the same temperature with a larger capacitor (which is easy to fill).

III. GEOMETRY AND BOUNDARY CONDITIONS

In order to model the relation between the measured change in capacitance and the expansion coefficient, some assumptions must be made regarding the behavior of the liquid during the experiment. In this section, we describe these assumptions and the arguments on which they are based.

The capacitor is filled completely at room temperature with a low-viscosity molecular liquid. The measuring temperatures (close to and below the conventional glass-transition temperature) are typically around 100 degrees below room temperature for these types of liquids. The cooling makes the liquid contract in the radial direction because the distance between the plates is maintained by the spacers (which have a much smaller expansion coefficient). This has the consequence that the capacitor is not completely filled at the temperatures where the measurements take place. This gives rise to a difference compared to the measurements done on polymers in earlier work [15,16], a difference which is taken into account when calculating the relation between the expansion coefficient and the change in capacitance in the following section.

The liquid contracts (expands) radially as long as it has low viscosity, but the situation changes when the liquid becomes ultraviscous. At high viscosities, the liquid gets clamped between the plates due to the small distance between them. This has the consequence that the liquid can no longer contract (expand) upon cooling (heating) by flowing radially, but will contract (expand) vertically and pull (push) the plates, changing the distance between them. This effect is the basis for the measurement, because the vertical expansion makes the capacitance change, and we calculate the expansion from the change in capacitance.

The distance between the plates is kept by the Kapton spacers at high temperatures (and long times) when the sample liquid flows. However, at times when the sample cannot flow, it is the sample, not the Kapton spacers, that determines the distance. This is true because Kapton has a stiffness [26] of the same order of magnitude as the sample (in the GPa range), but only takes up approximately 1% of the area between the plates.

The temperature change gives rise to an internal pressure, which is released by pressure diffusion via viscous flow. The

characteristic time τ_{flow} of the radial flow between two plates of fixed distance l can be estimated by the following argument. A temperature step of ΔT initiates an internal pressure $\Delta p = K_T \alpha_p \Delta T$ in the liquid. This creates a radial flow that eventually discharges the surplus volume $\Delta V = \Delta T \alpha_p \pi R^2 l$. Although the volume flows in the radial direction, we may take as a crude estimation the volume velocity $\dot{V}$ of planar Pouiseuille flow [27], $\dot{V} = \frac{\Delta p}{12\eta L} W l^3$, where L (the dimension in the direction of the flow) can be taken as R, and W (the dimension perpendicular to the flow) can be taken as $2\pi R$. The characteristic discharge flow time then becomes $\tau_{\text{flow}} = \frac{\Delta V}{\dot{V}} = 6\frac{\eta}{K_T}(\frac{R}{l})^2$. The high-frequency shear modulus is of the same order of magnitude as the bulk modulus. It follows that the Maxwell relaxation time, τ_{M} is roughly given by $\tau_{\text{M}} = \eta/G_\infty \simeq \eta/K_T$ and that $\tau_{\text{flow}} \propto (R/l)^2 \tau_{\text{M}}$. In the experiment, we have $l = 50$ μm and $R = 5$ mm, from which it follows that the radial flow time is 10 000 times longer than the Maxwell time. The α relaxation time is roughly given by the Maxwell time; the flow time will be more than ten days when the α relaxation time is 100 s. This means that the liquid can be considered as radially clamped in the region we study (where all relaxation times are longer than 100 s). The transition between the radial flow and the clamped situation can be seen in the capacitance when it is measured as a function of temperature, and the observed behavior is consistent with the above estimate.

The expansion coefficient we study with the boundary conditions described above is not the conventional isobaric expansion coefficient, $\alpha_p = \frac{1}{V}\frac{\partial V}{\partial T}|_p$, because the liquid is clamped in two directions and only free to move in one direction. We call this expansion coefficient the longitudinal expansion coefficient, in analogy with the longitudinal modulus (another name for it could be the iso-area expansion coefficient). It is expressed by $\alpha_l = \frac{1}{V}\frac{\partial V}{\partial T}|_A = \frac{1}{l}\frac{\partial l}{\partial T}|_A$, where A is the constant area and l is the dimension, which is free to respond to the temperature change. The longitudinal expansion coefficient is related to the isobaric expansion coefficient α_p via the following relation:

$$\alpha_l(\omega) = \frac{1}{1 + \frac{4G(\omega)}{3K_T(\omega)}}\alpha_p(\omega),$$

where G is the shear modulus and K_T is the isothermal bulk modulus, which are both dynamic, i.e., frequency- or time-dependent, as are the thermal-expansion coefficients.

From this expression, we see that α_l is smaller than α_p, except at low frequencies (long times or high temperatures), where $G = 0$, which implies $\alpha_l = \alpha_p$. This expression for the longitudinal expansion coefficient is given (but not derived) in another equivalent form in terms of Poisson's ratio in Refs. [15,19,28] and can be derived from row 3 of Eq. (53) in Ref. [29]. Also note that there is a total lack of standard notation. Bauer *et al.* use α_p to note the linear expansion coefficient, which is the quantity often used to express the volume expansion of solids. That is, their α_p is 1/3 of our α_p. The linear expansion coefficient is called α_L by Wallace *et al.* [28], while Fukao *et al.* [19] call it α_∞. The quantity we call the longitudinal expansion coefficient α_l is denoted α_{CA} (CA denotes clamped area) by Bauer, α_N by Wallace, and α_n by Fukao (n denotes normal).

IV. RELATING THE MEASURED CHANGE IN CAPACITANCE TO α_l

A. Deriving the relation

In the measurement, we perform a small temperature step δT and subsequently measure the capacitance C_m as a function of time. From the measurements, we find the time-dependent quantity $\frac{1}{C_m}\frac{\Delta C_m}{\Delta T}(t)$. In this section, we show that this quantity is proportional to the expansion coefficient, $\alpha_l(t)$, with a proportionality consant, P, that depends on the high frequency dielectric constant, ϵ_∞, and the degree of filling of the capacitor, f, but not on the geometrical capacitance or the distance between the plates.

The starting point is that the only contribution to the high-frequency dielectric constant, ϵ_∞, is the atomic polarizability (Sec. II). Moreover, we use the Lorentz field [22] from which it follows that the dielectric constant is given by the Clausius-Mossotti relation:

$$\frac{\epsilon_\infty - 1}{\epsilon_\infty + 2} = \frac{n}{3\epsilon_0}x,$$

where x is the polarizability of a single molecule, n is the number density of molecules, and ϵ_0 is the vacuum permeability.

Moreover, we assume that we have a parallel plate capacitor which is partially filled with a dielectric liquid. The degree of filling is denoted by f and the measured capacitance is given by

$$C_m = f\epsilon_\infty \frac{A\epsilon_0}{l} + (1-f)\frac{A\epsilon_0}{l} = [f\epsilon_\infty + (1-f)]\,C_g, \quad (8)$$

where $C_g = \frac{A\epsilon_0}{l}$ is the geometrical capacitance of the empty capacitor at the given temperature.

The derivative with respect to temperature is now given by

$$\frac{\mathrm{d}C_m}{\mathrm{d}T} = [f\epsilon_\infty + (1-f)]\frac{\mathrm{d}C_g}{\mathrm{d}T} + C_g f \frac{\mathrm{d}\epsilon_\infty}{\mathrm{d}T}. \quad (9)$$

Here it is assumed that the liquid does not contract radially at the temperatures (and on the time scale) we consider (see Sec. III), thus $\mathrm{d}f/\mathrm{d}T = 0$. The next step is to calculate $\frac{\mathrm{d}C_g}{\mathrm{d}T}$ and $\frac{\mathrm{d}\epsilon_\infty}{\mathrm{d}T}$ under the assumption that the area is constant. This was done by Bauer [15,16]. For completeness, we include a detailed derivation as an Appendix. The result is

$$\frac{\mathrm{d}\epsilon_\infty}{\mathrm{d}T} = -K(\epsilon_\infty)\alpha_l, \quad (10)$$

where $K(\epsilon_\infty)$ is given by $K(\epsilon_\infty) = (\epsilon_\infty - 1)(\epsilon_\infty + 2)/3$ and

$$\frac{\mathrm{d}C_g}{\mathrm{d}T} = -C_g\alpha_l\,. \quad (11)$$

Inserting Eqs. (10) and (11) into Eq. (9) yields

$$\begin{aligned}\frac{\mathrm{d}C_m}{\mathrm{d}T} &= [f\epsilon_\infty + (1-f)](-C_g\alpha_l) - C_g f K(\epsilon_\infty)\alpha_l \\ &= -C_g[f\epsilon_\infty + (1-f) + fK(\epsilon_\infty)]\alpha_l\,.\end{aligned}$$

Inserting $C_g = C_m/[f\epsilon_\infty + (1-f)]$ and dividing by C_m leads to

$$\frac{1}{C_m}\frac{\mathrm{d}C_m}{\mathrm{d}T} = -\frac{f\epsilon_\infty + (1-f) + fK(\epsilon_\infty)}{f\epsilon_\infty + (1-f)}\alpha_l\,. \quad (12)$$

Finally, isolating α_l gives

$$\alpha_l = -\frac{f\epsilon_\infty + (1-f)}{f\epsilon_\infty + (1-f) + fK(\epsilon_\infty)} \frac{1}{C_m} \frac{dC_m}{dT}, \qquad \alpha_l = P(f,\epsilon_\infty) \frac{1}{C_m} \frac{dC_m}{dT}, \tag{13}$$

where

$$P(f,\epsilon_\infty) = -\frac{f\epsilon_\infty + (1-f)}{f\epsilon_\infty + (1-f) + fK(\epsilon_\infty)}.$$

B. The absolute value of α_l

The determination of α_l and also the uncertainties of the measured value depend on determining correctly the proportionality constant $P(f,\epsilon_\infty)$. In order to do so, we need to determine the relevant values of f and ϵ_∞. To find f we use the expansion coefficient, and to find the dielectric constant ϵ_∞ we use the measured empty capacitance along with the measured full capacitance.

The high-temperature expansion coefficient is found by standard dilatometry [30] to be 0.7×10^{-3} K^{-1}; at low temperatures we find [31] that it is around 0.5×10^{-3} K^{-1} in the long-time limit. We use 0.6×10^{-3} K^{-1} as an average value, and we find from this that the degree of filling is $f = 0.95$ if the liquid is assumed to contract radially down to 213 K, where the relaxation time is 100 s. The choice of expansion coefficient in the range (0.5–0.7)$\times 10^{-3}$ K^{-1} and final temperatures in the range 210–215 K makes f change with $\pm 1\%$. The effect of changing f within this range leads only to $\pm 0.5\%$ changes in $P(f,\epsilon_\infty)$.

Isolating the dielectric constant from Eq. (8) gives

$$\epsilon_\infty = \frac{C_m - C_g(1-f)}{fC_g}. \tag{14}$$

From this it is seen that the uncertainty in f also gives an uncertainty in ϵ_∞, and this actually has a greater impact on the uncertainty of P than the direct effect of the uncertainty on f. Including this effect, the uncertainty in P due to uncertain degree on filling is still only $\pm 1\%$.

In order to determine ϵ_∞ from Eq. (14) we need to know the geometric capacitance, C_g. This is found from measurements on the empty capacitor at the measuring temperature. We estimate that the uncertainty is $\pm 2\%$ on C_g. This estimate is made by comparing measurements made on the capacitor after assembling it anew. The total uncertainty on ϵ_∞ is roughly $\pm 3\%$, which leads to an uncertainty on P of $\pm 2\%$.

Altogether, the uncertainty on $P(f,\epsilon_\infty)$ and therefore on the absolute value of α_l is about $\pm 3\%$. It should be emphasized that this uncertainty has no effect on the shape or the time scale of the measured relaxation. This is so as long as we stick to linear experiments. For larger temperature steps, there will be (at least in principle) some second-order effects making $P(f,\epsilon_\infty)$ change during the relaxation because of the change in ϵ_∞.

In the modeling of the connection between measured change in capacitance to α_l, we have not considered the radial expansion of the electrode plates. Including this (in the simplest possible way) gives rise to an extra additive term $\frac{1}{C_m}\frac{\epsilon_0}{l}\frac{dA}{dT}$ in Eq. (12). The size of this term will be given by the linear expansion coefficient of the electrodes. In this case they are made of copper, which at the relevant temperature has a linear expansion of approximately 15×10^{-6} K^{-1}. The total measured change in the capacitance is about 50–100 times bigger, thus the effect is small. However, the time dependence is different, therefore it could be relevant to include this effect in the future. Alternatively, we also consider shifting to an electrode material with an even smaller expansion coefficient in order to avoid the effect altogether.

The parasite capacitance from the edge is not considered in the modeling described above. An upper bound on the parasite capacitance is estimated by using the expression for the edge effect of an empty circular capacitor (found in Ref. [32]), and assuming that the edge capacitance is unaffected by the dielectric liquid between the plates. The maximal effect of the edge on the measured $\frac{1}{C_m}\frac{\Delta C_m}{\Delta T}(t)$ is 1%, and it is something that should be considered if further refinements are made on the technique. This could be handled, for instance, by using different spacer thicknesses.

It should be kept in mind that we have used the Lorentz field. This is an important assumption, and the use of another local field when connecting the density with the dielectric constant will change the result. Using the macroscopic Maxwell field will yield the same everywhere, except for $K(\epsilon_\infty)$ in Eq. (10), which will be given by $K_{\mathrm{Max}}(\epsilon_\infty) = (\epsilon_\infty - 1)$ instead of $K_{\mathrm{Lor}}(\epsilon_\infty) = (\epsilon_\infty - 1)(\epsilon_\infty + 2)/3$. This leads to a 20% increase in P and the calculated numerical value of α_l. Again we stress that using another local field will change the absolute values, but it will not change the time scale or shape of the measured relaxation.

While none of the above-mentioned factors affect the time scale or the spectral shape of the measured relaxation, the temperature dependence of ϵ_∞ could in principle affect the temperature dependence of the calculated α_l. However, this effect is negligible over the 6 degree range studied in this work, and P will be considered constant.

To summarize, the problems discussed in this section can lead to an unknown temperature- and frequency-independent scaling of all the measured α_l values.

C. The shape of the relaxation curve

In the following, we describe the measuring protocol in detail and a correction made to the data. Moreover, we use this to give an estimate of the uncertainty on the shape of the relaxation curves reported.

A main issue is, of course, the first part of the measuring curve where the temperature reaches in equilibrium. Figure 3 shows details of a single temperature step. It is clearly seen how the target temperature is achieved within less than 10 s, corresponding to a characteristic time of 2 s.

Figure 4(a) shows a typical set of temperature steps: a series of up and down jumps are made at the same temperature, with variable amplitude.

Figure 4(b) shows the raw measured capacitance corresponding to the temperature steps in Fig. 4(a). Two things are worth noticing. First, we see the expected rise in capacitance when temperature is decreased. Secondly, we see a long-time drift of the equilibrium level. At low temperatures where the liquid cannot contract radially, it contracts vertically.

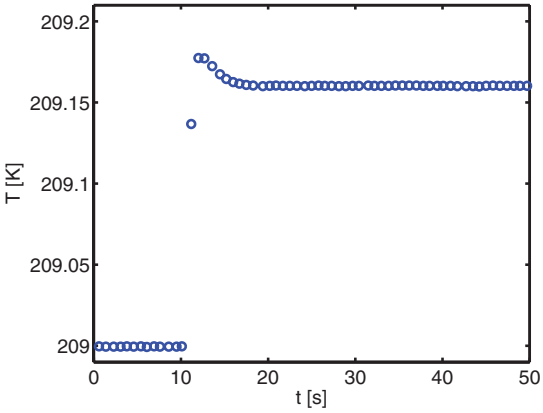

FIG. 3. (Color) Zoom on the temperature monitored in the NTC bead in the lower capacitor plate during the first 40 s of a temperature step.

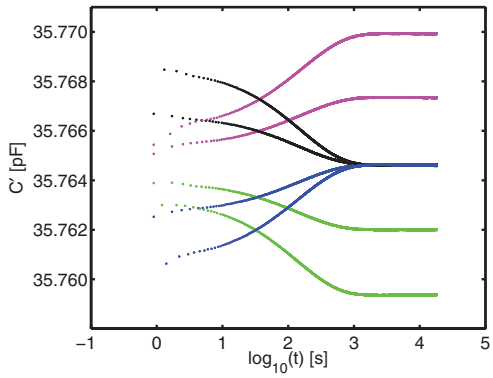

FIG. 5. (Color) The corrected measured capacitance shown on a logarithmic time scale with the temperature change as starting time. The temperature steps with the same final temperature (shown in black and blue) all have the same final value of the capacitance. The data shown here correspond to the last eight steps in Fig. 4.

Comparing measurements on the empty capacitor with liquid filled measurements, we estimate that the expansion coefficient of the liquid is roughly 10 times larger than that of the Kapton spacers. This means that the liquid compresses the Kapton. However, on very long times it will be the Kapton that dominates (because the liquid flows), and the Kapton will therefore slowly relax and press the electrodes apart. We believe that this effect is what leads to the long-time drift seen in Fig. 4(b). The drift is subtracted before treating the data, as illustrated in Figs. 4(c) and 5.

We make both up jumps and down jumps in temperature, and the subtraction of the drift has an opposite effect on the two. We can therefore check that the subtraction is made correctly by comparing up jumps and down jumps. This is illustrated in Fig. 6. The superposition of data obtained in up and down jumps also demonstrates that the experiment is linear and gives a general estimate of how precise the determination of the curve shape is.

The relaxation time is strongly temperature-dependent when the liquid is close to the glass transition, and therefore the steps have to be very small in order to maintain linear behavior. Smaller steps can be made as well, and the shape of the relaxation is maintained, but the curve starts to get noisy because the signal is very small. When we make larger temperature steps, we begin to get typical nonlinear aging behavior. That is, the relaxation is slower for down jumps than for up jumps when the final temperature is the same. The setup is actually well-suited for nonlinear experiments also; because of the extremely high resolution of the measured quantity, we get very well-defined curves and we can clearly see the nonlinear behavior already at steps of 1 degree. We plan to use the setup for these types of studies as well, but we focus in this paper on the linear results.

V. DATA

Figure 7 shows the expansion coefficient as a function of time at four different temperatures. The data are shown for steps made with ≈ 0.1 K, except the data at 211 K, which are

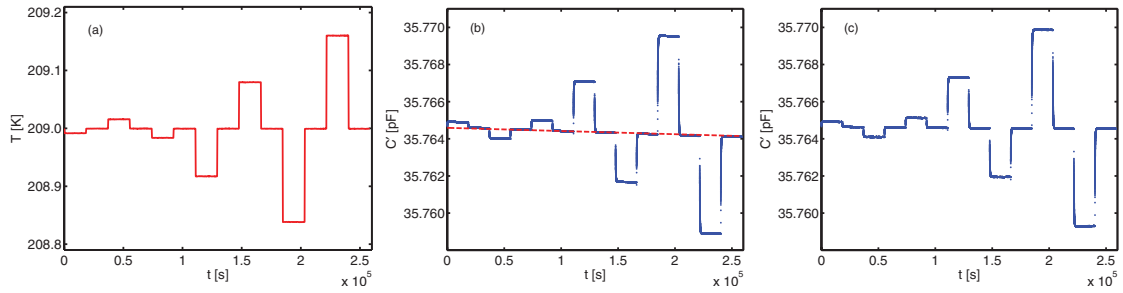

FIG. 4. (Color) (a) Example of a temperature protocol. A series of up and down jumps with different amplitudes are made at the same reference temperature. The temperatures shown are those measured with the NTC bead in the lower capacitor plate. Notice that the smallest jumps are 0.01 K. (b) The measured capacitance (blue points). Notice that the relative changes in capacitance (dC/C) for the small jumps are less than 10^{-4} and can still be measured precisely. There is a long time drift in the measured capacitance. The dashed line illustrates this background drift and this slope is subtracted from the data before further treatment. (c) The measured capacitance after subtraction of the drift.

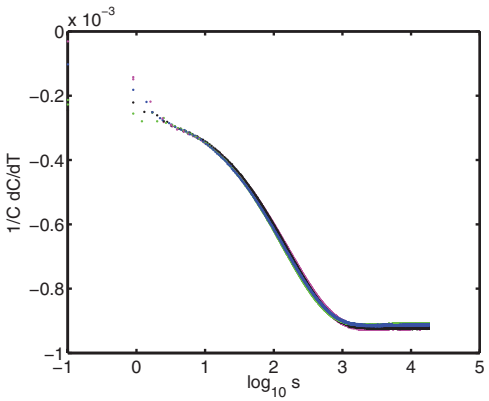

FIG. 6. (Color) The relative change in C divided by the size of the temperature step. The data shown are the same data as in Fig. 5, and the colors used for each curve are the same. All the curves superpose, which demonstrates that the experiment is linear. Moreover, it demonstrates that the subtraction of the background drift is successful.

taken with a temperature step of ≈ 0.01 K. This is why there is more noise on this data set.

Figure 8 shows all the data from Fig. 7 normalized and superimposed. This illustrates that the measured relaxation obeys time-temperature superposition (TTS) within the studied (relatively narrow) temperature range. The fit shown in Fig. 7 is a fit to the superimposed curve obtained from the data sets at $T = 205$ and 211 K.

The function used to fit the data is a modified stretched exponential [33] given by

$$\alpha_l(t) = \alpha_\infty + \Delta\alpha\left\{1 - \exp\left[-k\left(\frac{t}{\tau}\right)^\beta - \frac{t}{\tau}\right]\right\}. \qquad (15)$$

In the fit to the data, we get $\beta = 0.6$ and $k = 2.6$. The quality of the fit is so good that we have used it as an interpolation of the data and to calculate the frequency-domain response, which is given by the transformation in Eq. (5). The transformation is made by making a discrete Fourier transform (using the FFT procedure from MATLAB) on the fit of the normalized curve evaluated in a number of points. The transformed normalized curve is shown in Fig. 9. Here we also show an

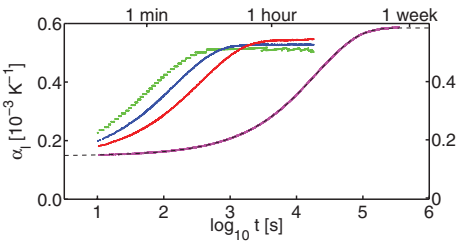

FIG. 7. (Color) The measured time-dependent expansion coefficient of tetramethyl tetraphenyl trisiloxane at $T = 205$, 209, 210, and 211 K. At the lowest temperature we also show a fit to the modified stretched exponential Eq. (15).

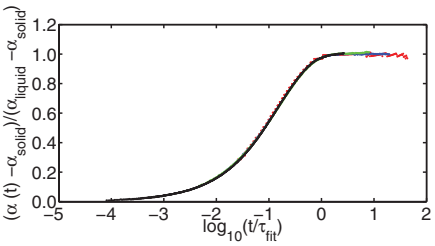

FIG. 8. (Color) The data from Fig. 7 normalized and plotted vs time scaled with the relaxation time (as defined from the fit to the modified stretched exponential). The figure demonstrates that the data obey time-temperature superposition (TTS).

exponential relaxation which has been transformed using the same algorithm along with the analytical Laplace transform. Moreover, the high-frequency power law, which corresponds to the exponent of the fit, is also shown.

In Fig. 10, we show the Laplace transformed fit rescaled with amplitudes and time scales in order to show the temperature dependence of the frequency-dependent thermal-expansion coefficient.

The expansion coefficient spectra have a behavior similar to that of other response functions measured in this sample. It is beyond the scope of this paper to go into a detailed analysis of the results. We use and discuss the data in relation to other response functions in Refs. [34] and [35]. The time scale is about half a decade slower than that of the dielectric response, but its temperature dependence is the same. The time scale of different response functions of this sample is discussed in detail in Ref. [34]. The shape of the relaxation curve appears to be a little more stretched than what we see in other response functions [36,37].

VI. SUMMARY AND OUTLOOK

We have presented a technique for measuring the dynamical expansion coefficient $\alpha(t)$ for a glass-forming liquid in the ultraviscous range. The experiment is performed on a setup which follows the capacitative principle suggested by Bauer

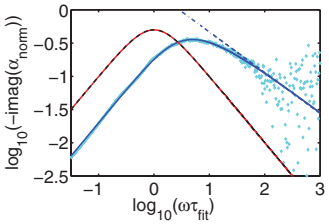

FIG. 9. (Color) Illustration of the Laplace transform. Cyan diamonds: Laplace transform of the normalized data (found by brute force numerical integration of the measured points). Blue: Laplace transform of the normalized fit (see text for details). Red: Exponential relaxation which has been transformed using the same algorithm as that used for the fit. Black dashed line: analytical Laplace transform of exponential relaxation. Blue dashed-dotted line: power law, which corresponds to the exponent of the fit.

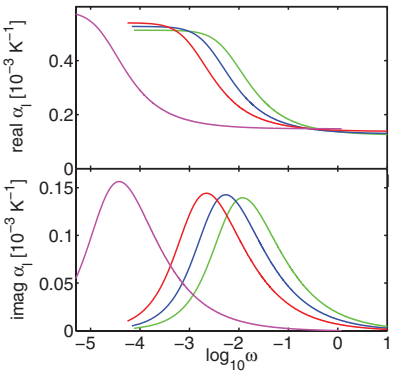

FIG. 10. (Color) Laplace transformed fits (see the text for details). The curves are shown in the dynamical range that roughly corresponds to the measurement.

et al. [15]. The dynamical range has been extended from 1.5 decades to more than 4 decades by making time-domain experiments, and by making very small and fast temperature steps. The modeling of the experiment has moreover been developed. Data are presented on the molecular glass-former tetramethyl tetraphenyl trisiloxane (DC704). This data set is, to the best of our knowledge, the first data on the dynamical expansion coefficient of a molecular liquid.

The technique presented in this paper is based on a principle by which the sample is placed in a parallel plate capacitor such that the sample maintains the spacing between the plates. Thus a change in sample volume in response to a temperature change leads to a change of the capacitance. The advantage of this technique is that capacitances can be measured with very high precision, and the small density changes associated with linear experiments can therefore be determined reliably. One limitation of the technique is that it only works on time scales larger than 10 s. This could possibly be overcome by smaller samples and thereby faster temperature control. A more intrinsic limitation is that the technique only works for samples with a very small dipole moment. For samples with a large dipole moment, therefore, we need a complementary technique.

The measurements of the thermal expansivity is part of a general ambition in the "Glass and Time" group to measure different response functions of viscous liquids. A unique feature of our techniques is that the measuring devices all fit into the same type of cryostat [24], ensuring that the absolute temperature of the liquid is the same for all measurements. The thermal-expansion measurements described in this paper are thus performed in the same cryostat as our shear mechanical spectroscopy [38], bulk mechanical spectroscopy [39], specific-heat spectroscopy [40], and dielectric spectroscopy [41]. The properties of liquids close to the glass transition are extremely temperature-dependent, and small differences in the temperature calibration can lead to rather large differences in the results. Measuring different response functions at the exact same conditions, therefore, makes it possible to analyze new aspects of the viscous slowing down and the glass transition. In recent papers, we used this to compare time scales of all the different response functions [34], to relate linear response to density scaling, and to determine the linear Prigogine Defay ratio [35].

ACKNOWLEDGMENTS

The center for viscous liquid dynamics "Glass and Time" is sponsored by the Danish National Research Foundation (DNRF). Ib Høst Pedersen, Torben Rasmussen, Ebbe Larsen, and Preben Larsen are thanked for their contribution to the development of the temperature control and the measuring cell. Niels Boye Olsen is thanked for sharing his experience and ideas. Tina Hecksher and Bo Jakobsen are thanked for fruitful discussions.

APPENDIX A

The relation between the temperature derivative of the dielectric constant and of the geometrical capacitance with the longitudinal expansion coefficient was derived by Bauer [15,16]. For completeness, we include a detailed derivation in this Appendix.

The longitudinal expansion coefficient is defined by

$$\alpha_l = \frac{1}{l}\left(\frac{\partial l}{\partial T}\right)_A . \tag{A1}$$

We start with the temperature derivative of ϵ_∞, which in this situation is given by

$$\frac{\partial \epsilon_\infty}{\partial T} = \left(\frac{\partial \epsilon_\infty}{\partial l}\right)_A \left(\frac{\partial l}{\partial T}\right)_A , \tag{A2}$$

so we need an expression for the first term, $(\frac{\partial \epsilon_\infty}{\partial l})_A$. The Clausius-Mossotti relation gives

$$\frac{xN}{3\epsilon_0 Al} = \frac{(\epsilon_\infty - 1)}{(\epsilon_\infty + 2)}, \tag{A3}$$

where N is the total number of molecules, A is the area, and l is the thickness, such that $N/(Al)$ is the number density of molecules and x is the microscopic polarizability of the molecule.

We rewrite this to get

$$\epsilon_\infty = \frac{xN}{3\epsilon_0 Al}(\epsilon_\infty + 2) + 1$$

and take the derivative with respect to l at constant A,

$$\left(\frac{\partial \epsilon_\infty}{\partial l}\right)_A = \frac{xN}{3\epsilon_0 Al}\left(\frac{\partial \epsilon_\infty}{\partial l}\right)_A - (\epsilon_\infty + 2)\frac{xN}{3\epsilon_0 Al^2},$$

which, by reinserting Eq. (A3), gives

$$\left(\frac{\partial \epsilon_\infty}{\partial l}\right)_A = \frac{(\epsilon_\infty - 1)}{(\epsilon_\infty + 2)}\left(\frac{\partial \epsilon_\infty}{\partial l}\right)_A - (\epsilon_\infty + 2)\frac{1}{l}\frac{(\epsilon_\infty - 1)}{(\epsilon_\infty + 2)}.$$

We now isolate $(\frac{\partial \epsilon_\infty}{\partial l})_A$ in this expression and get

$$\left(\frac{\partial \epsilon_\infty}{\partial l}\right)_A = -\frac{1}{l}\frac{(\epsilon_\infty - 1)(\epsilon_\infty + 2)}{3}.$$

Inserting this in Eq. (A2), we get

$$\left(\frac{\partial \epsilon_\infty}{\partial T}\right)_T = -\frac{(\epsilon_\infty - 1)(\epsilon_\infty + 2)}{3}\frac{1}{l}\left(\frac{\partial l}{\partial T}\right)_A ,$$

which, when comparing to the definition of the longitudinal expansion coefficient in Eq. (A1), can be rewritten as

$$\left(\frac{\partial \epsilon_\infty}{\partial T}\right)_T = -\frac{(\epsilon_\infty - 1)(\epsilon_\infty + 2)}{3}\alpha_l = -K(\epsilon_\infty)\alpha_l,$$

where the last equality comes from defining $K(\epsilon_\infty) = \frac{(\epsilon_\infty - 1)(\epsilon_\infty + 2)}{3}$.

Now we move on to the temperature derivative of the geometrical capacitance, C_g, which in this situation is given by

$$\frac{\partial C_g}{\partial T} = \left(\frac{\partial C_g}{\partial l}\right)_A \left(\frac{\partial l}{\partial T}\right)_A. \tag{A4}$$

The geometrical capacitance itself is given by

$$C_g = \frac{A\epsilon_0}{l},$$

giving

$$\left(\frac{\partial C_g}{\partial l}\right)_A = -\frac{A\epsilon_0}{l^2} = -\frac{1}{l}C_g,$$

which, when inserted in Eq. (A4) and combined with the definition of the longitudinal expansion coefficient, gives

$$\left(\frac{\partial C_g}{\partial T}\right)_A = -C_g\alpha_l. \tag{A5}$$

APPENDIX B: FD THEOREM AND THE EXPANSION COEFFICIENT

This appendix gives a formal definition of the dynamic expansion coefficient, including how it relates to fluctuations and how the frequency-domain response is related to the measured time-domain response. This is an extension of the presentation in Ref. [15]. However, Ref. [15] contains a typo as well as some definitions which are not precise regarding the absolute levels of the response functions. The precise definitions are important for our use of the data in Ref. [35].

The measured response to an external field, whether in the time domain or in the frequency domain, is directly related to the equilibrium thermal fluctuations of the system. This is expressed formally through the fluctuation dissipation theorem (FDT), which when expressed in the time domain is [42,43]

$$\frac{dR(t)}{dt} = -\frac{1}{k_B T}\frac{d}{dt}\langle \Delta A(t)\Delta B(0)\rangle. \tag{B1}$$

Here $R(t)$ is the response function (see Sec. I for a definition), and angular brackets denote ensemble averages. A is the measured physical quantity [that is, the output $O(t)$ in Sec. I] and B is conjugated to the applied input/field, which is called $I(t)$ in Sec. I. The function $\langle \Delta A(t)\Delta B(0)\rangle$ is the correlation function. In the simple case in which $A = B$, it reduces to the autocorrelation function.

Integrating on both sides of Eq. (B1) and inserting $R(t = 0) = 0$ gives the time-domain response function:

$$\int_0^t \frac{dR(t')}{dt}dt' = -\int_0^t \frac{1}{k_B T}\frac{d}{dt'}\langle \Delta A(t')\Delta B(0)\rangle dt',$$
$$R(t) = \frac{1}{k_B T}[\langle \Delta A(0)\Delta B(0)\rangle - \langle \Delta A(t)\Delta B(0)\rangle], \tag{B2}$$

from which it is seen that $R(t = 0) = 0$, as it should be. The frequency-domain response function is given by the Laplace transform of $R(t)$ times $i\omega$:

$$R(\omega) = i\omega\int_0^\infty R(t')e^{-i\omega t'}dt'. \tag{B3}$$

Combining this with Eq. (B2) gives the FDT in the frequency domain:

$$\begin{aligned} R(\omega) &= -\frac{i\omega}{k_B T}\int_0^\infty \langle \Delta A(t)\Delta B(0)\rangle - \langle \Delta A(0)\Delta B(0)\rangle e^{-i\omega t}dt \\ &= \frac{1}{k_B T}\langle \Delta A(0)\Delta B(0)\rangle - \frac{i\omega}{k_B T}\int_0^\infty \langle \Delta A(t)\Delta B(0)\rangle \\ &\quad \times e^{-i\omega t}dt. \end{aligned} \tag{B4}$$

Consider now a linear experiment in which a small temperature step δT is applied to a system at constant pressure at $t = 0$. Its volume response is subsequently measured as a function of time:

$$\delta V(t) = R(t - t')\delta T(t'). \tag{B5}$$

Then the response function $R(t)$ is given by $R(t) = \frac{\delta V(t)}{\delta T}$ (see Sec. I for more details on the linear-response formalism). The time-dependent isobaric expansion coefficient is defined by

$$\alpha_p(t) = \frac{1}{V}\frac{\delta V(t)}{\delta T} = \frac{R(t)}{V}. \tag{B6}$$

In terms of the FDT [Eq. (B2)], the relevant fluctuations for $\alpha_p(t)$ are volume and entropy, and the expansion coefficient can therefore be expressed in the following way:

$$\alpha_p(t) = \frac{1}{Vk_b T}[\langle \Delta V(0)\Delta S(0)\rangle - \langle \Delta V(t)\Delta S(0)\rangle]. \tag{B7}$$

The frequency-domain response function $\alpha_p(\omega)$ is then [from Eq. (B4)]

$$\begin{aligned} \alpha_P(\omega) &= \frac{1}{Vk_B T}\langle \Delta V(0)\Delta S(0)\rangle \\ &\quad -\frac{i\omega}{Vk_B T}\int_0^\infty \langle \Delta V(t)\Delta S(0)\rangle e^{-i\omega t}dt. \end{aligned} \tag{B8}$$

[1] C. A. Angell, K. L. Ngai, G. B. McKenna, P. F. McMillan, and S. W. Martin, J. Appl. Phys. **88**, 3113 (2000).
[2] J. C. Dyre, Rev. Mod. Phys. **78**, 953 (2006).
[3] R. O. Davies and G. O. Jones, Adv. Phys. **2**, 370 (1953).
[4] I. Prigogine and R. Defay, *Chemical Thermodynamics* (Longmans, London, 1954).
[5] M. Goldstein, J. Chem. Phys. **39**, 3369 (1963).
[6] C. T. Moynihan and P. K. Gupta, J. Non-Cryst. Solids **29**, 143 (1978).
[7] N. L. Ellegaard, T. Christensen, P. V. Christiansen, N. B. Olsen, U. R. Pedersen, T. B. Schrøder, and J. C. Dyre, J. Chem. Phys. **126**, 074502 (2007).
[8] T. Christensen, J. Phys. **46**, C8 (1985).
[9] N. O. Birge and S. R. Nagel, Phys. Rev. Lett. **54**, 2674 (1985).
[10] C. A. Angell, J. Non-Cryst. Solids **131–133**, 13 (1991).
[11] A. J. Kovacs, J. Polym. Sci. **30**, 131 (1958).
[12] R. Greiner and F. Schwarzl, Colloid Polym. Sci. **267**, 39 (1989).
[13] S. Kolla and S. L. Simon, Polymer **46**, 733 (2005).
[14] R. Svoboda, P. Pustkova, and J. Malek, J. Non-Cryst. Solids **352**, 42 (2006).
[15] C. Bauer, R. Böhmer, S. Moreno-Flores, R. Richert, H. Sillescu, and D. Neher, Phys. Rev. E **61**, 1755 (2000).
[16] C. Bauer, R. Richert, R. Böhmer, and T. Christensen, J. Non-Cryst. Solids **262**, 276 (2000).
[17] K. Fukao and Y. Miyamoto, Phys. Rev. E **64**, 011803 (2001).
[18] C. Meingast, M. Haluska, and H. Kuzmany, J. Non-Cryst. Solids **201**, 167 (1996).
[19] K. Fukao and Y. Miyamoto, Europhys. Lett. **46**, 649 (1999).
[20] A. Serghei, Y. Mikhailova, K. J. Eichhorn, B. Voit, and F. Kremer, J. Polym. Sci. B: Polym. Phys. **44**, 3006 (2006).
[21] H. Oh and P. F. Green, Nat. Mater. **8**, 139 (2009).
[22] C. J. F. Böttcher, *Theory of Electric Polarization*, 2nd ed., Vol. 1 (Elsevier, Amsterdam, 1973).
[23] K. Niss, B. Jakobsen, and N. B. Olsen, J. Chem. Phys. **123**, 234510 (2005).
[24] B. Igarashi, T. Christensen, E. H. Larsen, N. B. Olsen, I. H. Pedersen, T. Rasmussen, and J. C. Dyre, Rev. Sci. Instrum. **79**, 045105 (2008).
[25] T. Hecksher, N. B. Olsen, K. Niss, and J. C. Dyre, J. Chem. Phys. **133**, 174514 (2010).
[26] M. Davidson, S. Bastian, and F. Markley, in *FERMILAB-Conf-92/100* (Fermi National Accelerator Laboratory, 1992).
[27] B. Lautrup, *Physics of Continuous Matter* (IOP, Bristol, 2005).
[28] W. E. Wallace, J. H. van Zanten, and W. L. Wu, Phys. Rev. E **52**, 3329 (1995).
[29] T. Christensen, N. B. Olsen, and J. C. Dyre, Phys. Rev. E **75**, 041502 (2007).
[30] D. Gundermann, Ph.D. thesis, Roskilde University (2012).
[31] There is a small step of iteration involved in the data treatment here, since we use the expansion coefficient we find to get a more precise value of it.
[32] L. D. Landau, E. M. Lifhitz, and L. Pitaevskii, *Electrodynamics of Continuous Media*, 2nd ed. (Elsevier, Amsterdam, 1984).
[33] N. Sağlanmak, A. I. Nielsen, N. B. Olsen, J. C. Dyre, and K. Niss, J. Chem. Phys. **132**, 024503 (2010).
[34] B. Jakobsen, T. Hecksher, T. Christensen, N. B. Olsen, J. C. Dyre, and K. Niss, J. Chem. Phys. **136**, 081102 (2012).
[35] D. Gundermann, U. R. Pedersen, T. Hecksher, N. P. Bailey, B. Jakobsen, T. Christensen, N. B. Olsen, T. B. Schrøder, D. Fragiadakis, R. Casalini *et al.*, Nat. Phys. **7**, 816 (2011).
[36] B. Jakobsen, K. Niss, and N. B. Olsen, J. Chem. Phys. **123**, 234511 (2005).
[37] A. I. Nielsen, T. Christensen, B. Jakobsen, K. Niss, N. B. Olsen, R. Richert, and J. C. Dyre, J. Chem. Phys. **130**, 154508 (2009).
[38] T. Christensen and N. B. Olsen, Rev. Sci. Instrum. **66**, 5019 (1995).
[39] T. Christensen and N. B. Olsen, Phys. Rev. B **49**, 15396 (1994).
[40] B. Jakobsen, N. B. Olsen, and T. Christensen, Phys. Rev. E **81**, 061505 (2010).
[41] B. Igarashi, T. Christensen, E. H. Larsen, N. B. Olsen, I. H. Pedersen, T. Rasmussen, and J. C. Dyre, Rev. Sci. Instrum. **79**, 045106 (2008).
[42] M. Doi and S. F. Edwards, *The Theory of Polymer Dynamics* (Oxford University Press, Oxford, 1986).
[43] J. K. Nielsen and J. C. Dyre, Phys. Rev. B **54**, 15754 (1996).